THE ROLE OF TFE3 IN MEDIATING SKELETAL MUSCLE MITOCHONDRIAL ADAPTATIONS TO EXERCISE TRAINING

JENNA C. WONG

A THESIS SUBMITTED TO THE FACULTY OF GRADUATE STUDIES IN PARTIAL FULFILLMENT OF THE REQUIREMENTS FOR THE DEGREE OF

MASTER OF SCIENCE

GRADUATE PROGRAM IN KINESIOLOGY AND HEALTH SCIENCE

YORK UNIVERSITY
TORONTO, ONTARIO

JUNE 2023

ABSTRACT

Maintenance of a healthy mitochondrial pool is essential for skeletal muscle function. Mitophagy, the selective clearance of dysfunctional mitochondria, optimizes the mitochondrial network and heavily relies on lysosomal capacity within the tissue. The transcription factor E3 (TFE3) is a protein that activates the expression of lysosomal genes. With exercise, TFE3 is presumed to optimize the mitochondrial pool through the removal of organelles via lysosomes. However, the molecular mechanisms of the involved pathways remain unknown. Using WT and whole-body TFE3 KO mice, we sought to determine the role of TFE3 in regulating basal skeletal muscle mitochondrial function in response to acute and chronic endurance exercise. Our results suggest that the loss of TFE3 compromises beneficial training adaptations leading to improved muscle endurance and mitochondrial function and may induce a greater sensitivity to mitophagy induction in untrained muscle.

ACKNOWLEDGEMENTS

Firstly, I would like to thank my parents. I could never have accomplished any of this without your endless support. You gave me the opportunity to follow my passions, and for this, I am eternally grateful. Thank you to my brother, Jonathon, for being my trailblazer and role model. It is impossible to fully encapsulate how much you all mean to me. I hope I make you proud.

Thank you to my supervisor, Dr. David Hood. I am so grateful that you welcomed me into your lab and the world of mitochondria. Thank you for your diligence, guidance, and care as a mentor. You have helped me become a more curious and capable learner. I look forward to our paths crossing again soon.

I would like to thank my labmates for all your help during my time at York. To Ashley, thank you for being so patient with me and guiding me through the mysteries of TFE3. To Victoria, thank you for the much-needed coffees and learning by my side the past 2 years. To Neushaw and Mikhaela, thank you for your generosity and invaluable advice. To Priyanka and Sabrina, thank you for enthusiasm and support in the lab. It's been an absolute privilege working alongside such incredible women.

Thank you to my friends in the city and around the world. From impromptu dinners to calls from different time zones, you have always been there for me and kept me grounded. I deeply cherish the compassion you have shown me.

I am lucky to be surrounded by so many extraordinary people, and I appreciate everything you have all taught me. Thank you.

TABLE OF CONTENTS

ABSTRACT ..... **II**

ACKNOWLEDGEMENTS ..... **III**

TABLE OF CONTENTS ..... **IV**

LIST OF FIGURES ..... **VI**

LIST OF TABLES ..... **VII**

LIST OF ABBREVIATIONS ..... **VIII**

CHAPTER 1: REVIEW OF LITERATURE **1**

1.0. SKELETAL MUSCLE PHYSIOLOGY 2
- 1.1.Skeletal Muscle Composition and Fiber Types 2
- 1.2.Mitochondria in Skeletal Muscle 3
  - 1.2.1. Mitochondrial Quality Control 5
- 1.3.Skeletal Muscle and Exercise 8
  - 1.3.1. Exercise Adaptations 9
  - 1.3.2. In Situ Stimulation 10
  - 1.3.3. Voluntary Wheel Running 10

2.0. MITOPHAGY-LYSOSOME SYSTEM 11
- 2.1. Role of Lysosomes 12
- 2.2. Mechanism of Mitophagy 13
- 2.3. Mitophagy with Exercise 16

3.0. TFE3 PATHWAY 17
- 3.1. TFE3 Structure and Activation 17
- 3.2. Metabolic Regulation and TFE3 18
- 3.3. TFE3 Effects on Mitochondrial Function and Dynamics 20
- 3.4. Other MiT/TFE Family Members 21

RESEARCH OBJECTIVES 24

HYPOTHESES 24

REFERENCES 25

CHAPTER 2: MANUSCRIPT **36**

MANUSCRIPT AUTHOR CONTRIBUTIONS 36

ABSTRACT 38

INTRODUCTION 39

METHODS 41

RESULTS 45

DISCUSSION 55

ACKNOWLEDGEMENTS 59
REFERENCES 60
FUTURE DIRECTIONS 63

APPENDIX A: SAMPLE DATA AND STATISTICAL ANALYSES 64

APPENDIX B: SUPPLEMENTAL DATA 72

APPENDIX C: LABORATORY METHODS AND PROTOCOLS 77

DNA GENOTYPING 77
ISOLATING WHOLE MUSCLE PROTEIN EXTRACTS 78
ISOLATING MITOCHONDRIAL FRACTIONS 79
WESTERN/IMMUNOBLOTTING PROCEDURE 80
MITOCHONDRIAL RESPIRATION AND ROS EMISSION IN PERMEABILIZED FIBERS 84
COX ENZYME ACTIVITY ASSAY 86
RNA ISOLATION 87
FIRST-STRAND CDNA SYNTHESIS (REVERSE TRANSCRIPTION) 88

APPENDIX D: OTHER CONTRIBUTIONS TO THE LITERATURE 89

PEER-REVIEWED PUBLICATIONS 89
ORAL PRESENTATIONS AND PUBLISHED ABSTRACTS 89

LIST OF FIGURES

CHAPTER 1: REVIEW OF LITERATURE

Fig 1. Mitochondrial function, life cycle, and quality control processes……...6

Fig 2. The process of mitophagy……14

Fig 3. Lysosomal function and TFE3 mechanism of action……19

CHAPTER 2: MANUSCRIPT

Fig 1. Phenotypic characteristics of WT and TFE3 KO mice……46

Fig 2. Twitch kinetics and fatigability of hindlimb muscles with acute contractile activity……..48

Fig 3. Mitochondrial adaptations to endurance training in WT and TFE3 KO animals……..50

Fig 4. Lysosomal content adaptations to endurance training in WT and TFE3 KO animals……...52

Fig 5. Autophagic adaptations of WT and KO animals with endurance exercise and acute electrical stimulation……..54

APPENDIX A: SAMPLE DATA AND STATISTICAL ANALYSES

Image A1. Example Force Tracing of the *In Situ* Protocol……66

APPENDIX B: SUPPLEMENTAL DATA

Fig B1. Epididymal fat and raw muscle weights……72

Fig B2. Effects of colchicine on muscle performance *in situ*……..73

Fig B3. mRNA analysis of WT and TFE3 KO animals with endurance exercise and acute electrical stimulation……..74

LIST OF TABLES

APPENDIX A: SAMPLE DATA AND STATISTICAL ANALYSES

Table A1. TFE3 Protein Expression……...……...64

Table A2. Voluntary Wheel Running Distances……...…….....64

Table A3. Animal Body Weights……...……65

Table A4. GA/Body Weights…….65

Table A5. Fatigue at 5 mins……...……66

Table A6. Fatigue at 10 mins……...……..67

Table A7. Fatigue at 30 mins……...……..67

Table A8. Complex I+II Active Oxygen Consumption……..68

Table A9. Complex I+II Active ROS Consumption……...……...68

Table A10. COX Activity……...……...68

Table A11. Corresponding Fold-Above-Control for COX Activity……...……...69

Table A12. COX I Protein Expression……...……69

Table A13. Corresponding Fold-Above-Control for COX I Protein Expression……...……69

Table A14. v-ATPase Protein Expression……..70

Table A15. TFEB Protein Expression……..…..70

Table A16. Mitophagy Flux Data for p62……...……..70

Table A17. Mitophagy Flux Data for LC3-II……...…….……71

APPENDIX B: SUPPLEMENTAL DATA

Table B1. List of antibodies used for western blotting……...……...…….……..75

Table B2. List of primer oligonucleotide sequences in real-time qPCR analysis for *Mus musculus*……...……..76

LIST OF ABBREVIATIONS

ΔΨ	Mitochondrial membrane potential
AA	Amino acid
Ach	Acetylcholine
ADP	Adenosine diphosphate
AMBRA1	Autophagy and beclin 1 regulator 1
AMP	Adenosine monophosphate
AMPK	AMP-activated protein kinase
ANOVA	Analysis of variance
ATG	Autophagy-related protein
ATP	Adenosine triphosphate
bHLH	Basic helix loop helix
BECN1	Beclin 1
BNIP3L	BCL2/adenovirus E1B 19-kDa protein-interacting protein 3-like
CaMK	Ca2+/calmodulin-dependent protein kinase
CLEAR	Coordinated lysosomal expression and regulation
COL	Colchicine
COX	Cytochrome c oxidase
COX I/IV	Cytochrome oxidase subunit I and IV
CtsB	Cathepsin B
CtsD	Cathepsin D
Cyto C	Cytochrome c
DNA	Deoxyribonucleic acid
Drp1	Dynamin-related protein 1
EDL	Extensor digitorum longus
ETC	Electron transport chain
FAD+	Flavin adenine dinucleotide
$FADH_2$	Flavin adenine dinucleotide (reduced)
Fis1	Mitochondrial fission 1
FUNDC1	Fun14 domain containing 1
GABARAP	Gamma-aminobutyric acid receptor-associated protein
GAPDH	Glyceraldehyde-3-Phosphate Dehydrogenase
GATE16	Golgi-associated ATPase enhancer of 16kDa
Gsk3	Glycogen synthase kinase 3
GTPase	Guanosine triphosphatase
H^+	Hydrogen ion
H_2O_2	Hydrogen peroxide
HFD	High-fat diet
IMF	Intermyofibrillar
IMM	Inner mitochondrial membrane
IMS	Intermembrane space
KO	Knockout
kDa	Kilodaltons
LAMP	Lysosomal-associated membrane protein
LC3	Microtubule-associated proteins 1A/1B light chain 3A

LSD	Lysosomal storage disease
MCOLN1	Mucolipin1
Mff	Mitochondrial fission factor
Mfn1/2	Mitofusin-1/2
MHC	Myosin heavy chain
MiT	Micropthalmia family of bHLH transcription factors
MITF	Melanocyte inducing transcription factor
MPP	Mitochondrial processing peptidase
MQC	Mitochondrial quality control
Mt	Mitochondria(l)
mtDNA	Mitochondrial DNA
mTORC1	Mammalian/mechanistic target of rapamycin complex 1
NAD+	Nicotinamide adenine dinucleotide
NADH	Nicotinamide adenine dinucleotide (reduced)
NMJ	Neuromuscular junction
NuGEMPs	Nuclear gene-encoded mitochondrial proteins
OMM	Outer mitochondrial membrane
OPA1	Optic atrophy 1
OXPHOS	Oxidative phosphorylation
P38 MAPK	Mitogen-activated protein kinase
p62	Sequestosome-1 (SQSTM1)
PARL	Presenilin-associated rhomboid-like protein
PGC-1α	Peroxisome proliferator activator receptor (PPAR) γ coactivator 1 alpha
Pi	Inorganic phosphate
PI(3)P	Phosphatidylinositol 3-phosphate
PI3K	Phosphatidylinositol-4,5-bisphosphate 3-kinase
PIM	Protein import machinery
PINK1	PTEN-induced putative kinase 1
PMF	Proton motive force
PTEN	Phosphatase and tensin homolog
qPCR	Quantitative polymerase chain reaction
RER	Respiratory exchange ratio
RNA	Ribonucleic acid
ROS	Reactive oxygen species
RyR	Ryanodine receptor
SDS-PAGE	Sodium dodecyl sulfate polyacrylamide gel electrophoresis
SERCA	Sarco/endoplasmic reticulum Ca^{2+}-ATPase
SNARE	SNAP receptor
SR	Sarcoplasmic reticulum
SS	Subsarcolemmal
TA	Tibialis anterior
TCA	Tricarboxylic acid cycle
TD	Transactivation domain
Tfam	Mitochondrial transcription factor A
TFEB	Transcription factor EB
TFEC	Transcription factor EC

TFE3	Transcription factor E3
ULK1	Serine/threonine protein kinase ULK1
Ub	Ubiquitin
UPR	Unfolded protein response
UQCRC2	Ubiquinol-cytochrome c reductase core protein 2
vATPase	Vacuolar-type ATPase
VDAC1	Voltage-dependent anion channel 1
VEH	Vehicle
WT	Wild-type

CHAPTER 1: REVIEW OF LITERATURE

1.0. SKELETAL MUSCLE PHYSIOLOGY

The human body relies on skeletal muscle for basic functions, such as locomotion, and comprises approximately 40% of total body mass in humans (1). Skeletal muscle is composed of not only muscle fibers, but also other tissues including motor neurons, vasculature, and connective tissue. Importantly, it is responsible for a number of metabolic processes, including energy storage/usage, blood glucose, fatty acid oxidation, and temperature regulation (2). Skeletal muscle is highly sensitive to environmental stimuli, such as exercise, lending to the highly plastic nature of the tissue. Physiological adaptations of skeletal muscle have been well characterized over the years, however various aspects of molecular mechanisms have yet to be elucidated. This review of literature will focus on characteristics of mammalian skeletal muscle.

1.1. Skeletal Muscle Composition and Fiber Types

Skeletal muscle is composed of individual multinucleated muscle cells, named myofibers, each with their own membrane referred to as the sarcolemma. Within a myofiber are myofibril subunits composed of repeating sections, called sarcomeres (3). A sarcomere contains the highly organized contraction machinery, such as myosin and actin filaments. Contraction of the muscle begins with the depolarization of a motor neuron, innervating hundreds of fibers, which causes the release of the neurotransmitter acetylcholine (ACh) at the neuromuscular junction (NMJ) (4). Na^+ channels propagate the action potential along transverse tubules to stimulate the release of Ca^{2+} from the sarcoplasmic reticulum (SR) through ryanodine receptors (RyR). Ca^{2+} binds to troponin C, clearing the myosin-binding site on actin, and myosin and actin interact via cross-bridge cycling to generate a contraction. Ca^{2+} reuptake into the SR by the sarco/endoplasmic reticulum Ca^{2+}-ATPase pump (SERCA) allows for relaxation (5).

There are three main classes of fiber types within skeletal muscle that are designated by the myosin heavy chain (MHC) isoform present. The groups are as follows: 1) type I (slow-twitch red, STR) containing predominantly of MHC type I isoform, 2) type IIa (fast-twitch red, FTR) comprised mainly of MHC type IIa isoform, and 3) type IIb/x (fast-twitch white, FTW) involving MHC type IIb or IIx isoforms (6). Type I fibers display the smallest cross-sectional area, are easily recruited, possess slow shortening velocities, and demonstrate the most fatigue-resistance (7). Type IIb/x have the largest cross-sectional area, require a large stimulus for recruitment, produce fast twitch kinetics and high force production, but are quickly fatigable. Type IIa fibers exhibit an intermediate phenotype. Generally, fiber types dictate the metabolic profile of the muscle. Slow twitch fibers (type I) have a greater oxidative capacity with a higher mitochondrial abundance of ~5-7% (8). Fast twitch muscles (type II) are more glycolytic in nature with low mitochondrial content (~2-3%). Though these classifications exist, muscle groups are often heterogeneous in fiber type composition (9).

1.2. Mitochondria in Skeletal Muscle

Mitochondria make up 3-8% of skeletal muscle mass in humans (10). Pools of these organelles are distributed in distinct areas within skeletal muscle. The two main subpopulations are the subsarcolemmal (SS) mitochondria, residing below the sarcolemmal membrane near the capillary and nuclei, and the intermyofibrillar (IMF) mitochondria that lay adjacent to Z-line of the sarcomere. SS mitochondria provide energy for membrane active transport and gene transcription, whereas IMF mitochondria provide energy molecules to contractile filaments for muscle contraction (8,11-13). The mitochondrion contains several regions due to its double-membraned nature: the outer mitochondrial membrane (OMM), the intermembrane space (IMS), the inner mitochondrial membrane (IMM), and the mitochondrial matrix. The OMM is fairly

porous and allows small molecules of less than 10 kDa to pass through, but also contains receptors and channels for protein import from the nuclear genome (14). The IMM is much more selective and highly regulates the proteins that enters the matrix via protein import machinery (PIM) channels (15). The mitochondrial matrix contains a plethora of proteins required for its various functions, including mitochondrial DNA (mtDNA), transcriptional and translational machinery, antioxidants, ATP production enzymes, and chaperones and proteases.

Mitochondria are crucial organelles in the maintenance of skeletal muscle health. They are involved in Ca^{2+} signaling, antioxidant responses, and cellular apoptosis with dysfunction. Importantly, they also provide much of the cellular energy required for skeletal muscle function in the form of adenosine triphosphate (ATP) (16). The process of energy production via the mitochondrion begins with acetyl coenzyme-A that enters the tricarboxylic acid (TCA) cycle in the matrix. The TCA cycle produces a small number of ATP molecules, as well as nicotinamide adenine dinucleotide (NADH) and flavin adenine dinucleotide ($FADH_2$) for use in the electron transport chain (ETC). The ETC, comprising the machinery responsible for the bulk generation of ATP, is found on the IMM. Complex I oxidizes NADH into NAD^+, which pumps protons into the IMS and shuttles electrons to Complex III via Coenzyme Q. Complex II oxidizes $FADH_2$ into FAD^+ and also shuttles electrons to Complex III. Complex III further pumps protons into the IMS and continues the shuttling of electrons to Complex IV through Cytochrome c. Complex IV oxidizes Cytochrome c, pumps H^+ into the IMS, and donates the free electron to oxygen, the final electron acceptor, to produce water. Given the role of oxygen in this process, oxygen consumption is used as a measure of mitochondrial respiration and function (17,18). Protons pumped into the IMS by Complexes I, III, and IV create a proton motive force that can be utilized by Complex V, or ATP synthase. Complex V dissipates the gradient and produces ATP from ADP and P_i (19,20).

Tied to oxygen consumption is the production of free radicals, called reactive oxygen species (ROS), formed by electron slippage from back pressure on the ETC without ADP. ROS can be converted into less harmful H_2O_2 by antioxidant machinery present within the mitochondria. H_2O_2 as a measure of ROS emission (21,22). A baseline level of ROS is beneficial for mitochondrial function but can be detrimental to the health of the mitochondria and cell when present in high quantities (23).

1.2.1. Mitochondrial Quality Control

It is generally understood that skeletal muscle mitochondria do not exist as individual organelles but are organized in a reticular structure to efficiently carry out their functions (11). The life cycle of a mitochondrial reticulum is in constant flux of synthesis, degradation, and recycling. This dynamic network is remodeled through a system of processes collectively known as mitochondrial quality control (Figure 1). The primary processes that contribute to the maintenance of an optimally functioning pool of mitochondria include mitochondrial biogenesis and mitochondrial autophagy (hereafter referred to as mitophagy).

Building a healthy muscle involves the synthesis of new and functional organelles to work in conjunction with the existing network. Peroxisome proliferator-activated receptor-gamma coactivator 1 alpha (PGC-1α) is often described as the master regulator of mitochondrial biogenesis, coactivating transcription factors that drive the transcription of nuclear genes encoding mitochondrial proteins (NuGEMPs), such as mitochondrial transcription factor A (Tfam) (24). Proteins are then translated and imported into the mitochondria to contribute to the maintenance of mitochondrial structure and function. Newly synthesized mitochondria can undergo fusion with the existing network. Mitofusin (Mfn) 1/2 join the OMM of adjacent mitochondria, while optical atrophy 1 (Opa1) connects the IMMs (25,26). The integration of mitochondrial populations

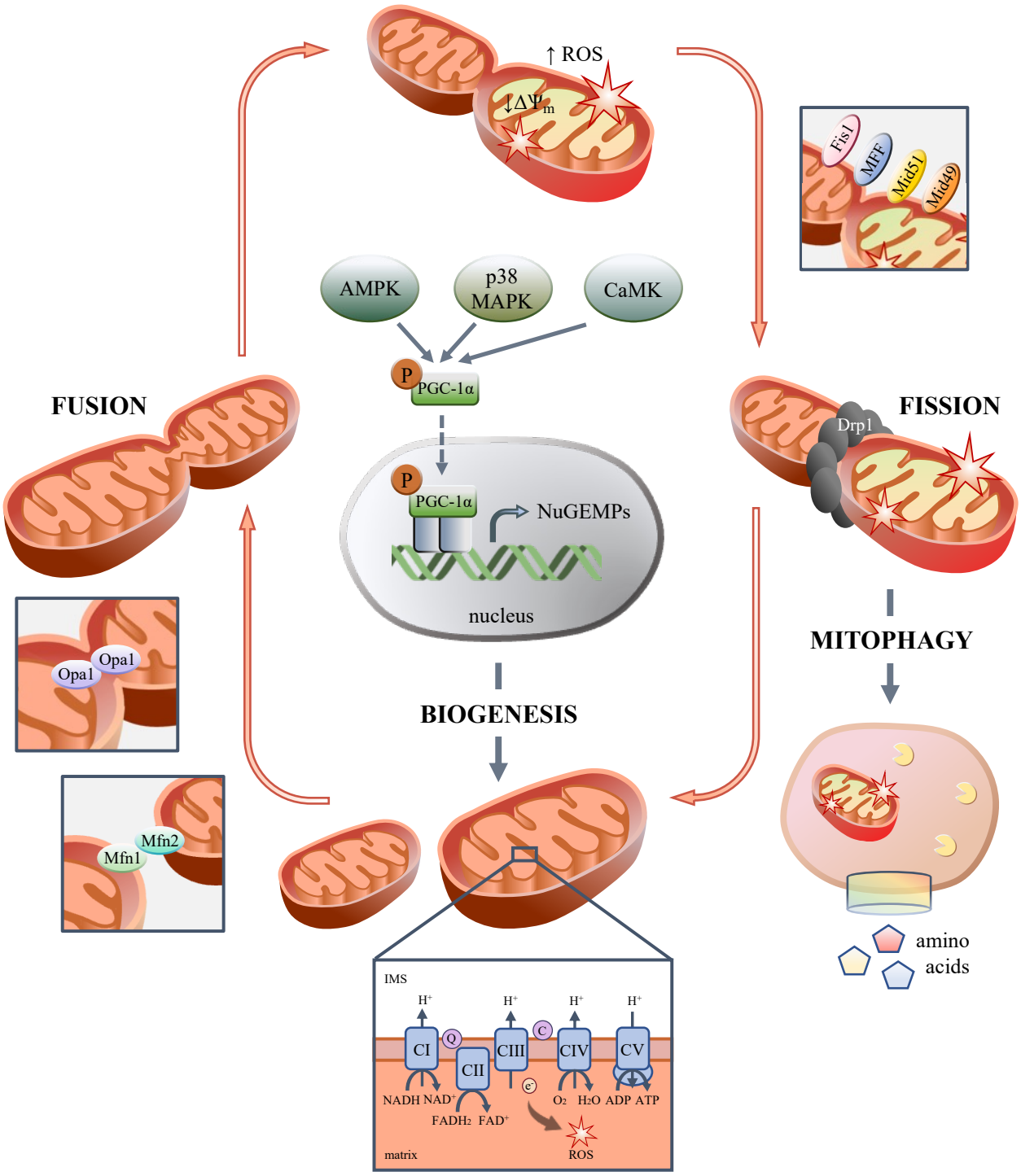
↑ ROS
↓ΔΨm
Fis1
MFF
Mid51
Mid49
AMPK
p38 MAPK
CaMK
P
PGC-1α
FUSION
FISSION
Drp1
P
PGC-1α
NuGEMPs
nucleus
MITOPHAGY
Opa1
Opa1
BIOGENESIS
Mfn2
Mfn1
amino acids
IMS
H+
CI
Q
CII
CIII
C
CIV
CV
e-
NADH NAD+
FADH2 FAD+
O2 H2O ADP ATP
matrix
ROS

Figure 1. Mitochondrial function, life cycle, and quality control processes. A primary function of mitochondria is to provide energy molecules in the form of ATP for skeletal muscle function. The electron transport chain (ETC), comprising the machinery responsible for the bulk generation of ATP, is found on the inner mitochondrial membrane (IMM). Electron carriers, NADH and $FADH_2$, are produced by the tricarboxylic acid cycle for use in the ETC. Complex I (CI) oxidizes NADH into NAD^+, which pumps protons into the intermembrane space (IMS) and shuttles electrons to Complex III (CIII) via Coenzyme Q (Q). Complex II (CII) oxidizes $FADH_2$ into FAD^+ and also shuttles electrons to CIII. CIII further pumps protons into the IMS and continues the shuttling of electrons to Complex IV (CIV) through Cytochrome c (C). CIV oxidizes Cytochrome c, pumps H^+ into the IMS, and donates the free electron to oxygen, the final electron acceptor, to produce water. Protons pumped into the IMS by CI, III, and IV create a proton motive force that can be utilized by Complex V (CV), or ATP synthase. CV dissipates the gradient and produces ATP from ADP and P_i. Reactive oxygen species (ROS) are natural by-products of mitochondrial respiration, created by electron slippage from back pressure on the ETC without ADP. Mitochondria exist as a reticulum and undergo constant remodeling via mitochondrial quality control mechanisms. Mitochondrial biogenesis is primarily driven by peroxisome proliferator-activated receptor-gamma coactivator 1 alpha (PGC-1α). Its activation is regulated by three signaling cascades involving AMP-activated protein kinase (AMPK), p38 mitogen-activated protein kinase (MAPK), and calcium calmodulin kinase (CaMK) activation that phosphorylates PGC-1α. Activated PGC-1α coactivates transcription factors that drive the transcription of nuclear genes encoding mitochondrial proteins (NuGEMPs) to add to mitochondrial structures and function. Mitochondria can be fused to the existing network to enable sharing of substrates and mitochondrial DNA. Mitofusin 1/2 (Mfn1/2) joins the OMM of adjacent mitochondria, while optical atrophy 1 (Opa1) connects the IMMs. When mitochondria become dysfunctional, exhibiting elevated levels of ROS and a loss of membrane potential ($\Delta\psi$), the organelles are subjected to removal to maintain the integrity of the adjoining network. The dysfunctional mitochondrion must first be separated via fission. Fis1, Mff, Mid49, and Mid51 recruit Drp1which then pinches off the organelle. The fragmented mitochondrion is targeted for degradation via a selective form of cellular recycling, termed mitophagy. This process terminates in the breakdown of the organelle into amino acid building blocks.

facilitate the sharing of substrates and mtDNA that can enable more rapid energy distribution throughout muscle cells (27).

Just as important to the health of the mitochondrial pool is the clearance of poorly operating organelles. When mitochondria become dysfunctional, as seen by a decrease in oxidative phosphorylation and an increase in harmful reactive oxygen species, the organelle is separated from the reticulum through mitochondrial fission (28,29). Adaptor proteins that reside on the OMM, such as fission protein 1 (Fis1), mitochondrial fission factor (Mff), Mid49, and Mid51, recruit dynamin-related protein 1 (Drp1). Drp1 wraps around and pinches off the dysfunctional mitochondrion, and the organelle is targeted for degradation. The process of mitochondrial recycling, termed mitophagy, where the organelle is engulfed by a phagophore, joins with a lysosome, the organelle ultimately responsible for recycling the mitochondria. As the focus of my thesis pertains to the mechanisms of this facet of MQC, a more detailed description is found in a later section (See Section 2.2).

1.3. Skeletal Muscle and Exercise

Skeletal muscle is an extremely adaptable tissue, changing size and composition, and its mitochondria are major contributors to its plasticity. They are sensitive responders to various stimuli and conditions that drive changes in their morphology and function. With disuse and aging, there is a loss of mitochondrial content and oxidative capacity (30). This is often accompanied with loss of strength, endurance, and muscle mass. Mitochondrial dysfunction has also been linked to the onset of diseases and disorders, such as muscular dystrophies, diabetes, and atrophy (31). Therefore, the maintenance of these organelles contribute to the overall health of individuals and their quality of life.

Exercise has been shown to impart considerable benefits in skeletal muscle through the enhancement of the mitochondrial network (32). Therefore, exercise as a model for disease prevention and health improvement is a promising avenue for research. The characteristics and degree of muscle transformation is dependent on the type and intensity of exercise. The following section will focus on endurance exercise. However, other types, such as resistance and high-intensity conditioning, are also being studied.

1.3.1. Exercise Adaptations

Acute exercise has been shown to have effects on cellular signaling in skeletal muscle. A single bout of endurance exercise induces an increase in PGC-1α (33,34). This increase in PGC-1α with exercise is driven by three main signaling cascades involving AMP-activated protein kinase (AMPK), p38 mitogen-activated protein kinase (MAPK), and calcium calmodulin kinase (CaMK) activation which cause downstream phosphorylation and activation of PGC-1α. During exercise, ATP is continuously synthesized and broken down into ADP and AMP, which can bind to and activate AMPK which then phosphorylates PGC-1α (35-37). The production of ROS with exercise has been shown to stimulate p38 MAPK, leading to PGC-1α activation (38,39). Muscle contraction also causes Ca^{2+} release and activation of CaMK which activates PGC-1α (40,41). Additionally, unfolded protein response (UPR) pathways, essential for cellular homeostasis, may be implicated in exercise adaptations as they have been shown to be activated following an acute bout of exercise (42,43).

With chronic exercise, the sustained signaling events lead to more drastic outcomes and considerable phenotypic changes are observed. Endurance training elicits improved oxidative capacity of the muscle, owing to an increase in mitochondrial content (32, 44-47). The expanded mitochondrial pool is concurrent with an increased expression of fusion proteins, Opa1 and Mfn2,

and a decrease in fission proteins Drp1 that are indications of a more reticular structure (48,49). Finally, a reduction in ROS emission is observed with acute exercise in trained animals (50). Evidently, exercise and endurance training are effective drivers for enhanced mitochondrial function and overall muscle health. Skeletal muscle also presents mitophagic adaptations. This area of research has become an emerging focus for mitochondrial adaptations and will be discussed in detail later as a key topic of this thesis (See Section 2.3).

1.3.2. In Situ Stimulation

In situ stimulation refers to the isolation and electrical stimulation of a nerve *in vivo* to trigger and measure muscle contractions. It is commonly used in rodents, and isolation of the sciatic nerve innervates the entire hindlimb, including the gastrocnemius, tibialis anterior (TA), extensor digitorum longus (EDL), and soleus muscle groups. As *in situ* stimulation intensity and duration is controlled by the experimenter, this method standardizes the exercise volume across all animals. It allows for measurement of skeletal muscle contractile properties under physiological conditions and rate of muscle fatigue (51-53). With this protocol, the effect of exercise is limited to muscle capacity of the groups stimulated, and outcomes are not influenced by whole-body effects that may be present with other models of acute exercise.

1.3.3. Voluntary Wheel Running

To measure physical activity in rodents, the running wheel has long been used as an instrument by researchers. Most rodents readily run when provided with wheels, therefore this method presents a simple and easily quantifiable measure for exercise. Rats and mice have been observed to run up to 43 and 16 km per day, respectively (54). As a result of this behaviour, running wheels have been used to study several physiological adaptations with endurance training. For example, voluntary wheel running was employed to study the involvement of proteins, such as

p53, Nrf2, and Parkin, in endurance training adaptations (55,56). Although the amount of physical activity is reliant on the animal's genetic and environmental dispositions to run, voluntary wheel running is still a useful model for the induction of a moderately-exercised state.

2.0. MITOPHAGY-LYSOSOME SYSTEM

The process of autophagy is a ubiquitous cellular mechanism that culminates in the recycling of dysfunctional components. It is regulated by mammalian target of rapamycin (mTOR) and AMP-activated kinase (AMPK) (57,58). There are five main steps of autophagy: initiation, nucleation, elongation, fusion, and degradation. The first step begins with the activation of the Unc-51 like autophagy activating kinase (ULK1) complex, which then activates the class III phosphatidylinositol 3-kinase (PI3K III)/Beclin-1 complex (59,60). During nucleation, phosphatidylinositol phosphate (PI(3)P) is produced, which constitutes a major component of the lipid membrane of the growing phagophore (61,62). The phagophore is then elongated through a series of autophagy-related gene (ATG)-mediated steps to lipidate microtubule-associated proteins 1A/B light chain (LC3) into the active LC3-II form, as well as gamma-aminobutyric acid receptor-associated protein (GABARAP) and golgi-associated ATPase enhancer of 16kDa (GATE16) (63-66). The fully engulfed autophagic cargo, or autophagosome, is transported along microtubule tracks towards the lysosome (67). The autophagosome and lysosome fuse to become an autolysosome, a process mediated by SNARE proteins and lysosomal-associated membrane proteins (LAMP) 1/2 (68,69). Finally, the contents of the autolysosome are degraded and released into the cytosol as amino acids.

It has become increasingly apparent that the regulation of autophagic function is vital to overall cellular health. Impairments in autophagy have been linked to several physiological and pathological issues. With aging, studies have shown a reduction in autophagy gene transcripts,

such as ULK1 and Beclin1 (BECN1), and subsequent drive for autophagy (70,71). Autophagy is also implicated in cancer cachexia, where its activation contributes to muscle wasting (72). Conversely, muscle-specific deletion of Atg7, which caused an inhibition of autophagy, promoted muscle atrophy (73). Studies have also shown that upregulation of autophagy through the overexpression of relevant proteins, such as Atg5 and Atg7, can extend lifespan (71,74). Additionally, exercise training can stimulate autophagy and improve muscle structure with sarcopenia (75). Evidently, cellular homeostasis via autophagy is required for muscle health. This places importance on the continued study of the autophagy-lysosome system.

2.1. Role of Lysosomes

Lysosomes are tightly associated with autophagy as they are required for the final step of cellular recycling. They are membrane-bound organelles with a highly acidic pH of 4.5-5.0 that is required for its function to degrade macromolecules (76). The acidic environment is created and maintained by vacuolar-type ATPase (v-ATPase) which hydrolyzes ATP to pump protons against their gradient into the lysosomal lumen (77,78). The organelle is also a store for calcium that further acidifies the lysosome, which is key for signaling processes (79,80). Hydrolases, such as Cathepsin B and D, enable the breakdown of proteins, lipids, carbohydrates, and nucleic acids within the organelle (81). Lysosomal biogenesis in response to stimuli is regulated by several transcription factors. The role of some of these factors will be later described in detail (See Section 3.0). Deficiencies in lysosomal capacity and organellar clearance can be extremely detrimental to health. Mutations of key enzymes result in lysosomal storage disorders (LSDs), such as Pompe disease and Danon disease, that are often characterized by skeletal muscle dysfunction (82,83). Therefore, the maintenance of a healthy lysosomal pool is essential for autophagy and optimal muscle conditions.

2.2. Mechanism of Mitophagy

Mitophagy, a selective form of autophagy, describes the degradation of dysfunctional mitochondria within the cell. It is an emerging focus for health maintenance as the cell's inability to efficiently clear these organelles is implicated in skeletal muscle disorders and diseases. With increased oxidative stress, mitochondria may accumulate toxic levels of ROS and present a loss of membrane potential that impair the organelles' functions. Under these conditions, the activation of mitophagy to clear the poorly functioning mitochondria is key to maintaining the health of the muscle. At least two mitophagy pathways have been established (Figure 2). The following section will describe the mechanisms pertaining to this process.

The first pathway is mediated by PTEN-induced kinase-1 (PINK1) and Parkin. Under unstressed conditions, PINK1 is imported into the mitochondria, translocating across mitochondrial membranes, and is cleaved in the matrix by mitochondrial processing peptidase (MPP) and presenilin-associated rhomboid-like protein (PARL) in the inner mitochondrial membrane (84,85). The cleaved PINK1 dissociates from the mitochondrion and is targeted for degradation by the ubiquitin-protease system. With the loss of membrane potential ($\Delta\mathbf{\Psi}$), a signal of organelle dysfunction, PINK1 import is impaired and it accumulates on the OMM (86,87). Proteotoxic stress featuring a buildup of misfolded proteins can also be sensed by PINK1, which leads to the activation of this pathway (88). PINK1 homodimerizes and autophosphorylates to recruit Parkin, an E3 ubiquitin ligase, and ubiquitin (Ub), a mitochondrial tag (89,90). The constructed Ub chains guide the phagophore to the mitochondrion and they are linked by adaptor proteins, such as p62 and Optineurin, that possess both a ubiquitin-binding motif and an LC3-interacting region (91,92). As the autophagosome is formed, the mitochondrion is transported to the lysosome for degradation.

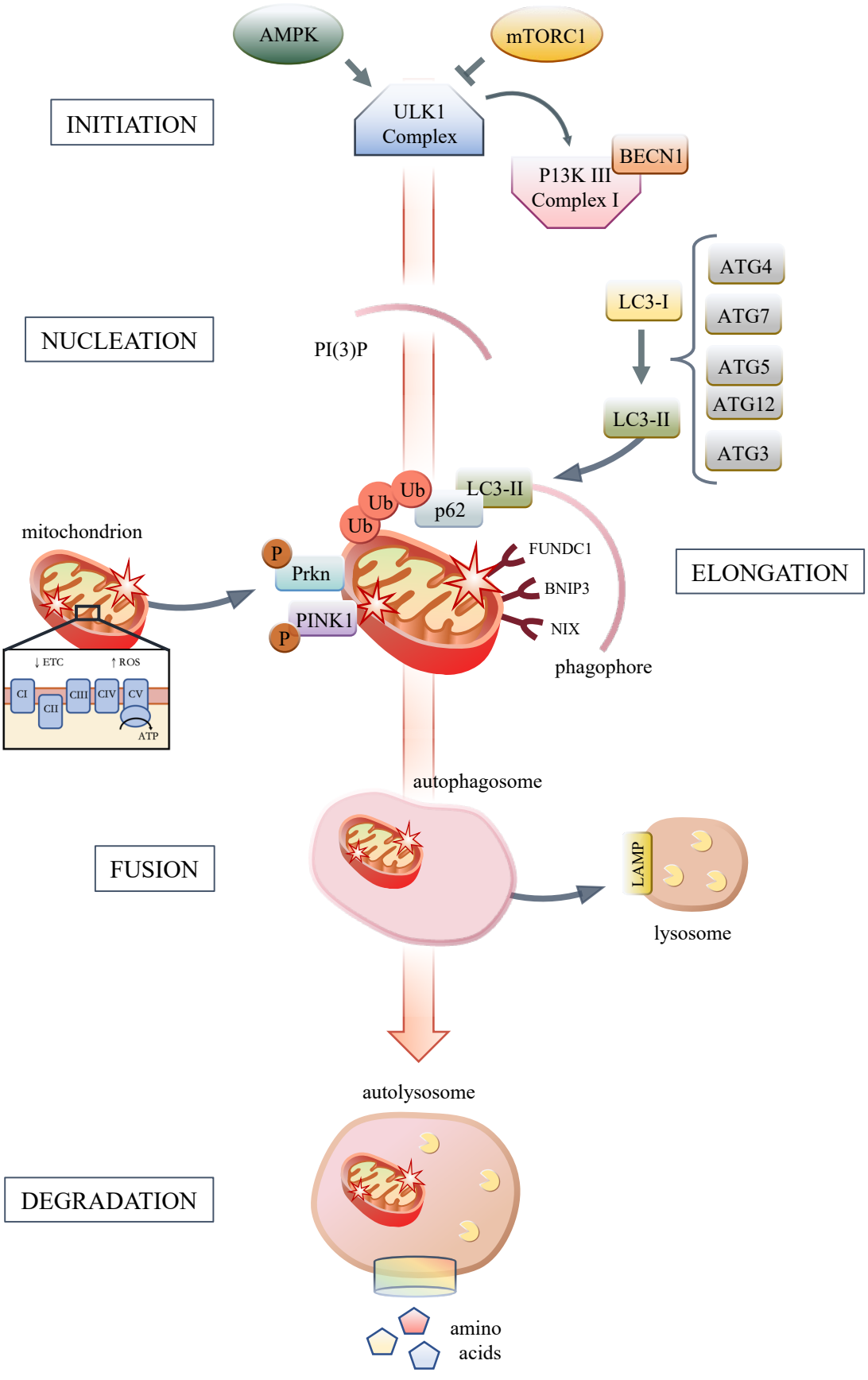
AMPK
mTORC1
INITIATION
ULK1
Complex
BECN1
P13K III
Complex I
NUCLEATION
PI(3)P
LC3-I
ATG4
ATG7
ATG5
ATG12
ATG3
LC3-II
Ub
Ub
Ub
p62
LC3-II
mitochondrion
P
Prkn
PINK1
P
FUNDC1
BNIP3
NIX
ELONGATION
phagophore
↓ ETC
↑ ROS
CI
CII
CIII
CIV
CV
ATP
autophagosome
FUSION
LAMP
lysosome
autolysosome
DEGRADATION
amino
acids

Figure 2. The process of mitophagy. Mitophagy is required to effectively degrade dysfunctional mitochondria. It involves five main steps: initiation, nucleation, elongation, fusion, and degradation. During, initiation. Unc-51 like autophagy activating kinase (ULK1) complex is activated by AMPK, which activates class III phosphatidylinositol 3-kinase (PI3K III) Complex. The lipid membrane is constructed by PI(3)P, a major component of the phagophore, during nucleation. The phagophore continues to elongate through a series of autophagy-related gene (ATG)-mediated steps to lipidate microtubule-associated proteins 1A/B light chain (LC3) into the active LC3-II form. Dysfunctional mitochondria, characterized by a reduction in electron transport chain (ETC) efficiency and an elevation in ROS, are targeted to the phagophore. PTEN-induced kinase-1 (PINK1) accumulates on the surface of the mitochondrion and undergoes autophosphorylation to recruit and phosphorylate Parkin (Prkn) and Ubiquitin (Ub). Ub chains guide the phagophore to the mitochondrion and they are linked by adaptor proteins, such as p62, that possess both a ubiquitin-binding motif and an LC3-interacting region. Receptor proteins FUNDC1, BNIP3, and NIX possessing LC3 binding domains may also guide the mitochondrion to the phagophore. The fully engulfed organelle, termed autophagosome, is transported to the lysosome via microtubule tracks to undergo fusion, aided by via lysosomal-associated membrane proteins (LAMP). Once fused, the contents of the autolysosome are degraded into amino acids.

The second mechanism of mitophagy is receptor mediated. The activation of several receptors on the OMM triggered by various stressors flag mitochondria for degradation. BCL2/adenovirus E1B interacting protein (BNIP3), BNIP3-like protein (NIX), and FUNDC1 are among a group of proteins implicated in mitophagic activity (93-100). These proteins have LC3 interacting domains, which allow for the engulfment of the damaged organelle by the growing phagophore. There still exists uncertainty about the dependence of mechanisms on one another. It is presumed that distinct stimuli, from membrane depolarization to hypoxia, determine the induced mitophagic pathway.

Given that the accumulation of dysfunctional mitochondria is a hallmark of several myopathies, it has been suggested that a decline in mitophagy contributes to the progress of their negative outcomes (101). However, there has also been conflicting evidence that enhanced autophagy impairs mitochondrial function (102), and much uncertainty still surrounds the

implications of mitophagy on muscle health. In general, it is recognized as an essential process, and it remains a compelling topic for investigation.

2.3. Mitophagy with Exercise

As evidenced previously, exercise is an effective driver for physiological adaptations. A single bout of treadmill running is sufficient to induce a mitophagic response 6 hours post-exercise in mice (103). This response is AMPK-dependent, leading to downstream ULK1 phosphorylation and activation. Parkin was also found to localize to mitochondria after acute treadmill exercise (104,105). Mitophagy flux increased accordingly, measured via p62, LC3-II, and ubiquitin (104-106). Mitophagy induction may be Parkin dependent as Parkin-knockout animals did not exhibit the same increase in mitophagy flux with acute exercise (56). Altogether, the process of mitophagy is sensitive to the physiological stress of exercise.

Research has also investigated mitophagic adaptations with chronic exercise. Five weeks of swimming increased the LC3-II/LC3-I ratio, decreased p62 levels, and increased BNIP3, signifying an increase in basal mitophagy in mice (106). Endurance-trained mice via four weeks of voluntary wheel running led to similar findings of LC3-II/LC3-I, p62, and BNIP3 in oxidative fibers only (107). Mitophagic responses may thereby be dependent on fiber type. In contrast, another study employing a swim training model showed that mitophagy levels were unaffected while whole muscle autophagy flux was upregulated (108). Chen et al. found that endurance-trained animals expressed higher levels of Parkin and increased mitochondrial localization in skeletal muscle (105). Mitophagy flux, however, was blunted following acute exercise. Though mitophagy flux was not able to be measured, a human study observed increased phosphorylation of PINK1 and Parkin, suggesting increased mitophagic targeting with endurance running (109).

These reports exhibit some variability in results, perhaps due to differences in exercise and mitophagy quantification models. Overall, these studies suggest that exercise can enhance the mitophagic system in skeletal muscle and mitophagy plays a role in the adaptations seen with exercise.

3.0. TFE3 PATHWAY

The transcription factor E3 (TFE3) belongs to a family of microphthalmia (MiT/TFE) transcription factors containing a basic helix-loop-helix leucine zipper (bHLH-Zip) motif (110,111). It holds several functions but is most well-understood to regulate lysosomal biogenesis and autophagy induction. Basally, the loss of TFE3 does not result in functional impairments. However, it is required for stress-induced lysosomal and autophagic responses, and overexpression of TFE3 is sufficient to stimulate autophagy and lysosomal biogenesis (112). TFE3 has also been implicated in whole-body metabolism and mitochondrial function. Overall, literature has established TFE3 as an important player in cellular processes, and the following section will describe its known functions in mammalian tissue.

3.1. TFE3 Structure and Activation

TFE3 possesses a transactivation domain (TD) close in proximity to the bHLH motif which allows for its transcriptional regulation (113). The homodimerization of TFE3 or heterodimerization with another member of its family is required for the recognition of palindromic E-box elements (CANNTG) (114-116). TFE3 binds directly to specific E-boxes: 10-base pair motif (GTCACGTGAC) coordinated lysosomal enhancement and regulation (CLEAR) elements (117). The CLEAR site is present in the promoter region of a network of genes related to lysosomal biogenesis and autophagy.

Under basal conditions, TFE3 remains inactive in the cytosol but is sensitized to various stimuli to promote its nuclear translocation (Figure 3). In a nutrient-rich environment, Rag GTPases recruit TFE3 to the lysosomal surface and activate mechanistic target of rapamycin complex 1 (mTORC1) (118). Activated mTORC1 phosphorylates TFE3 on the Ser321 residue and the transcription factor is bound to chaperone 14-3-3 and tethered to the lysosome, thereby inhibiting the signal for nuclear localization (112,119-121). With cellular starvation, mT1 and Rag GTPases are inhibited and TFE3 is released from the lysosome. Calcium levels also influence TFE3 activity. An increase in ROS can trigger Ca^{2+} release from the lysosome via mucolipin-1 (MCOLN1) (122-124). This activates Calcineurin, a Ca^{2+}-dependent phosphatase, which dephosphorylates TFE3 and allows for TFE3 to translocate to the nucleus (125). Ca^{2+} release from the SR is also mediated by ROS, further activating TFE3 (126,127). Transcriptional activation of TFE3 has been shown to be dependent on AMPK phosphorylation of three serine residues by the C-terminus (128). Additionally, TFE3 may translocate to the nucleus during mitophagy via a Parkin- and Atg5- dependent mechanism (129). Therefore, TFE3 is involved in the cellular response to various stress conditions, ranging from nutrient deprivation to oxidative stress.

3.2. Metabolic Regulation and TFE3

TFE3 has been shown to activate genes involved in energy metabolism, and several studies have explored TFE3's involvement in whole-body metabolic processes (130-132). Firstly, TFE3 contributes to lipid metabolism regulation. Pastore et al. found increased adiposity with greater fat mass relative to lean mass in whole-body TFE3 knock-out (KO) mice compared to wild-type (WT) animals. On a high-fat diet (HFD), KO mice were further susceptible to obesity with an increase in lipid droplet content in skeletal muscle (133). KO animals showed an increase in RER, indicating a preferential utilization of carbohydrates over lipid catabolism which rationalizes the

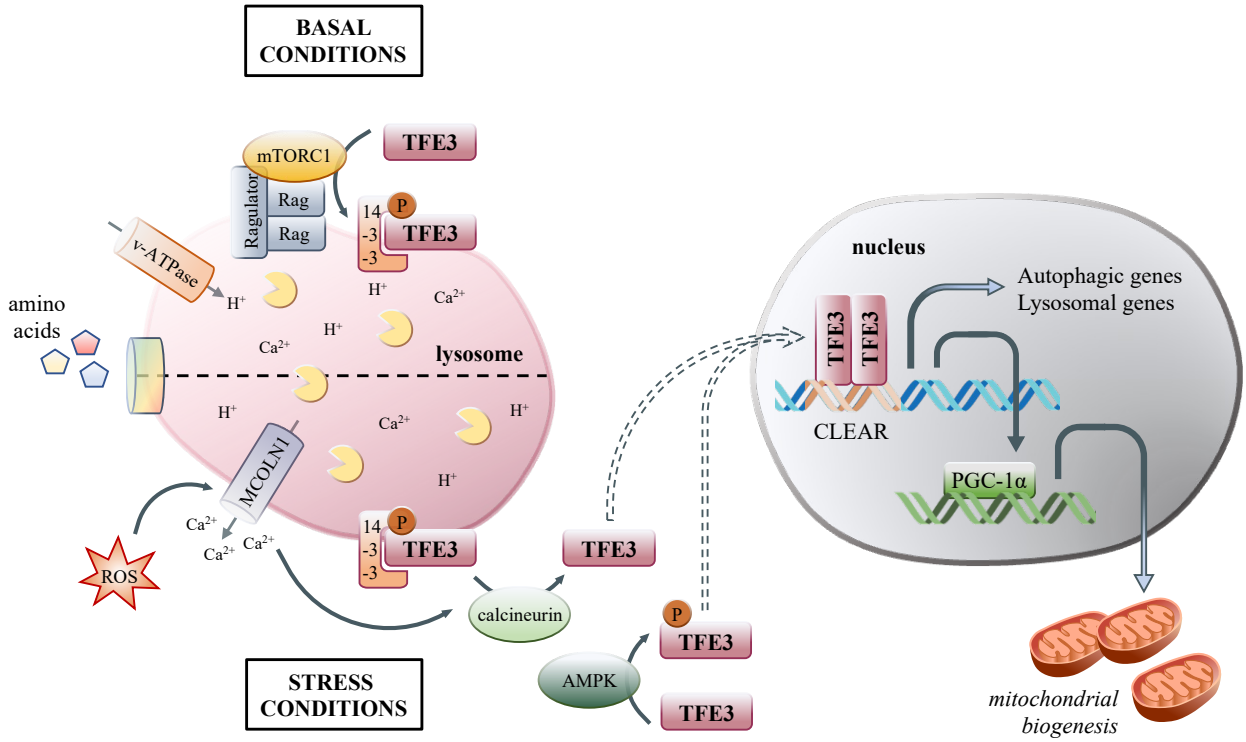

Figure 3. Lysosomal function and TFE3 mechanism of action. Lysosomes are key organelles for cellular recycling. Vacuolar-type ATPase (v-ATPase) pumps protons into the lysosomal lumen to maintain a highly acidic pH of 4.5-5.0, enabling the breakdown of macromolecules into amino acids. Transcription factor E3 (TFE3) is understood to be a regulator of lysosomal biogenesis and autophagic pathways. Under basal conditions, TFE3 is inactive via mTORC1 phosphorylation on the Ser321 residue. The transcription factor is then bound to chaperone 14-3-3 and tethered to the lysosome, thereby inhibiting the signal for nuclear localization. With cellular stress, mTORC1 and Rag GTPases are inhibited and TFE3 is released from the lysosome. Ca^{2+} release from the calcium channel mucolipin-1 (MCOLN1) is triggered by elevated ROS levels and activates calcineurin to dephosphorylate TFE3. AMPK can also phosphorylate TFE3 on three specific serine residues by the C-terminus to promote its transcriptional activation. TFE3 then translocates to the nucleus and homodimerizes (or heterodimerizes with other members of the MiT family), binding to CLEAR sites on lysosomal and autophagic genes and transcribing for proteins related to these pathways. TFE3 has also been shown to bind directly to PGC-1α, the master regulator for mitochondrial biogenesis.

obesity-prone phenotype. TFE3 has also been shown to regulate lipases (Atg1 and Hsl) in adipose tissue and PGC-1α, the master regulator of mitochondrial biogenesis, in adipocytes (134,135).

Glucose homeostasis is another metabolic mechanism subject to TFE3 activity. Global TFE3 KO animals presented glucose intolerance and a reduction in glycogen stores in both liver and skeletal muscle (133). Gsk3 expression was also reduced, potentially signifying a reduction in glycogen synthesis in the absence of TFE3 (133). Conversely, TFE3 overexpression in the liver improved glucose tolerance and body weight. A study done by Iwasaki et al. showed that mice overexpressing TFE3 in skeletal muscle had increased insulin sensitivity and mRNA expression of glucose metabolism-related genes (GLUT4, HKII and glycogen synthase) (136). These studies have strongly suggested a role for TFE3 in the regulation of glucose metabolism.

TFE3 appears to mediate exercise-induced adaptations. TFE3 KO mice presented reduced endurance capacity during an exhaustive treadmill test (133). Additionally, endurance training benefits seen in WT mice, including improved body weight and endurance performance, were not seen in KO mice. TFE3 overexpression in skeletal muscle increased distance and time to exhaustion with acute exercise (136). Evidently, TFE3 is a significant regulator of various metabolic pathways.

3.3. TFE3 Effects on Mitochondrial Function and Dynamics

As previously discussed, mitochondria are important organelles for metabolic function and TFE3 has now been implicated in the control of select mitochondrial processes. The global absence of TFE3 in a mouse model had pronounced effects on skeletal muscle and liver mitochondrial morphology (133). Abnormally large organelles with uneven cristae were seen in the tissue, and it also presented an increased number of mitochondria. Correspondingly, mitochondrial function was found to be modulated by TFE3 in hepatocytes. TFE3 KO liver cells had decreased OXPHOS

protein expression accompanied by reduced basal and uncoupled respiration compared to WT liver cells. Gene ontology analysis in the same study further revealed a potential role for TFE3 in mitochondrial dynamics. Mitochondria-related genes targeted by TFE3 were found to be highly enriched in the fission pathway. Notably, TFE3 was found to directly bind to the promoter of Fis1, a key mitochondrial fission receptor. TFE3 overexpression in the liver also increased expression of several mitochondrial dynamics-related genes, including Fis1, Drp1, OPA1, Mfn1, and Mfn2. Interestingly, TFE3 may interact with PGC-1α, a principal factor controlling mitochondrial biogenesis. A study using C2C12 myotubes observed that TFE3 binds directly to the PGC-1α promoter and induces PGC-1α transcription and mRNA expression (137). There exists clear evidence that TFE3 is partially responsible for mitochondrial operations. Given its role in the maintenance of lysosomal structure and its recent implications in mitochondrial function, TFE3 may coordinate these processes via the clearance of mitochondria via lysosomes. However, the influence of TFE3 on mitophagy has yet to be elucidated.

3.4. Other MiT/TFE Family Members

The four members of the MiT/TFE family are evolutionarily conserved and closely related. The following section describes the involvement of the other MiT/TFE proteins: TFEB, MITF, and TFEC. As members exhibit similar activity to TFE3, there exists an idea of compensatory mechanisms within the family (112,125,138).

Transcription factor EB (TFEB) is the most well-studied of the MiT/TFE proteins and is known as the master regulator of autophagy and lysosomal biogenesis (139). Like TFE3, TFEB is inactive during basal conditions, phosphorylated at Ser211 by mTORC1 (140). It is also activated by similar mechanisms, including via calcineurin with lysosomal Ca^{2+} release (141). When activated, TFEB homodimerizes or heterodimerizes with TFE3 to activate autophagic pathways

(142). TFEB also shares many functional similarities with TFE3 (111). In ARPE-19 cells, overexpression of TFEB increased mRNA and protein expression of v-ATPase subunits, and transmembrane proteins, and lysosomal hydrolases, as was seen in TFE3 overexpression cells (112). As TFEB is required for the vascularization of the placenta, whole-body KO models are embryonically lethal by day 10 and tissue-specific knockouts are required to study its effects *in vivo* (143). A study by Mansueto et al. showed that muscle-specific KO of TFEB caused a downregulation of genes involved in lipid and glucose homeostasis (144). This was accompanied by a decreased glucose uptake, a greater reliance on glycolysis, and a decrease in exercise tolerance. Expression of genes related to mitochondrial function were also decreased, leading to mitochondria malformations. Conversely, TFEB overexpression in muscle increased muscle glycogen content and exercise capacity, as well as the size and number of mitochondria and mitochondrial respiration. Further supporting a role for TFEB in exercise adaptations, acute exercise enhanced TFEB transcription and increased TFEB localization to the nucleus in both C2C12 myotubes and mice (145). The same study established that this response is PGC-1α-dependent. Endurance training via 7 weeks of treadmill running was found to increase TFEB expression in myonuclei (144). The overlap in function between TFEB and TFE3 led to the discovery of their cooperation to regulate energy metabolism (133). However, more analysis is needed to better understand the individual contributions of the two transcription factors to skeletal muscle function.

Microphthalmia-associated transcription factor (MITF) is the third major member of the MiT/TFE family. MITF is similarly regulated by mTORC1 activity and promotes upregulation of autophagic proteins (146). However, its role in lysosomal biogenesis is primarily linked to melanocytes (147). Mutations of this transcription factor is associated with Waardenburg

syndrome type II, a disease presenting hearing loss and pigmentation disturbances (148). TFEC is most structurally different from the other member of the family as it lacks a transactivation domain (149). It also acts in opposition to TFE3 as a transcriptional repressor of its dimerization partner (150). MITF and TFEC are less studied in the context of skeletal muscle and not much is known about their role in this tissue.

RESEARCH OBJECTIVES

Our research objectives are to:

- Assess basal muscle function, including twitch kinetics and fatigability, using an acute electrical stimulation protocol in the absence of TFE3;
- Measure the role of TFE3 in maintaining lysosomal content and mitochondrial content and function;
- Determine whether TFE3 plays a role in mitophagy and autophagy flux induction following acute stimulation;
- Compare skeletal muscle adaptations in WT and TFE3 KO mice with endurance training;

HYPOTHESES

We hypothesize that:

1. The absence of TFE3 will result in increased fatigability during *in situ* stimulation;
2. TFE3 KO animals will present muscle with reduced mitochondrial and lysosomal content and respiratory capacity;
3. Mitophagy flux will be attenuated during acute stimulation in the absence of TFE3;
4. TFE3 is required for the beneficial endurance training-mediated adaptations of these measures in skeletal muscle.

REFERENCES

1. Janssen I, Heymsfield SB, Wang Z, Ross R. Skeletal muscle mass and distribution in 468 men and women aged 18–88 yr. *J Appl Physiol* 89:81–88, 2000. doi: 10.1152/jappl.2000.89.1.81.
2. Argilés JM, Campos N, Lopez-Pedrosa JM, Rueda R, Rodriguez-Ma.as L. Skeletal Muscle Regulates Metabolism via Interorgan Crosstalk: Roles in Health and Disease. *J Am Med Dir Assoc* 17:789–796, 2016. doi: 10.1016/j.jamda.2016.04.019.
3. Gotti C, Sensini A, Zucchelli A, Carloni R, Focarete ML. Hierarchical fibrous structures for muscle-inspired soft-actuators: A review. *Appl Mater Today* 20:100772, 2020. doi.org/10.1016/j.apmt.2020.100772.
4. Shishmarev D. Excitation-contraction coupling in skeletal muscle: recent progress and unanswered questions. *Biophys Rev* 121(2020);12:143–153, 2020. doi: 10.1007/s12551-020-00610-x.
5. Tupling AR. The decay phase of Ca2+ transients in skeletal muscle: regulation and physiology. *Appl Physiol Nutr Metab* 34:373–376, 2009. doi: 10.1139/H09-033.
6. Pette D SR. Myosin isoform, muscle fiber types and transition. *Microsc Res Tech* 50:500–509, 2000. doi: 10.1002/1097-0029(20000915)50:6<500::AID-JEMT7>3.0.CO;2-7.
7. Mendell LM. The size principle: a rule describing the recruitment of motoneurons. *J Neurophysiol* 93:3024–3026, 2005. doi: 10.1152/classicessays.00025.2005.
8. Ogata T, Yamasaki Y. Scanning electron-microscopic studies on the three-dimensional structure of mitochondria in the mammalian red, white and intermediate muscle fibres. *Cell Tissue Res* 241:251, 1985. doi: 10.1007/BF00217168.
9. Schiaffino S. Muscle fiber type diversity revealed by anti-myosin heavy chain antibodies. *The FEBS Journal* 285(20):3688-3694, 2018. doi: 10.1111/febs.14502.
10. Larsen S, Nielsen J, Hansen CN, Nielsen LB, Wibrand F, Stride N, Schroder HD, Boushel R, Helge JW, Dela F, Hey-Mogensen M. Biomarkers of mitochondrial content in skeletal muscle of healthy young human subjects. *J Physiol* 590: 3349–3360, 2012. doi: 10.1113/jphysiol.2012.230185.
11. Kirkwood SP, Munn EA, Brooks, GA. Mitochondrial reticulum in limb skeletal muscle. *Am J Physiol* 251:C395-C402, 1986. doi: 10.1152/ajpcell.1986.251.3.C395.
12. Hoppeler H. Exercise-induced ultrastructural changes in skeletal muscle. *Integ J Sport Med* 7(4):187-204, 1986. doi: 10.1055/s-2008-1025758.
13. Ferreira R, Vitorino R, Alves RMP, Appell HJ, Power SK, Duarte JA, Amado F. Subsarcolemmal and intermyofibrillar mitochondria proteome differences disclose functional specializations in skeletal muscle. *Proteomics* 10(17):3142-54, 2010. doi: 10.1002/pmic.201000173.
14. Gupta A, Becker T. Mechanisms and pathways of mitochondrial outer membrane protein biogenesis. B*iochim Biophys Acta Bioenerg* 1862(1):148323, 2021. doi: 10.1016/j.bbabio.2020.148323.
15. Wiedemann N, Pfanner N. Mitochondrial Machineries for Protein Import and Assembly. *Annu Rev Biochem* 86:685-714, 2017. doi: 10.1146/annurev-biochem-060815-014352.
16. Gnaiger E. Capacity of oxidative phosphorylation in human skeletal muscle: New perspectives of mitochondrial physiology. *Int J Biochem* 41(10):1837–1845, 2009. doi: 10.1016/j.biocel.2009.03.013.

17. Silva AM, Oliveira PJ. Evaluation of respiration with clark type electrode in isolated mitochondria and permeabilized animal cells. *Methods Mol Biol* 810:7–24, 2012. doi: 10.1007/978-1-61779-382-0_2.
18. Clark Jr LC, Wolf R, Granger D, Taylor Z. Continuous recording of blood oxygen tension by polarography. *J Appl Physiol* 6:189–93, 1953. doi: 10.1152/jappl.1953.6.3.189.
19. Mitchell P. Coupling of phosphorylation to electron and hydrogen transfer by a chemiosmotic type of mechanism. *Nature* 191:144–148, 1961. doi: 10.1038/191144a0.
20. Lowell BB, Spiegelman BM. Towards a molecular understanding of adaptive thermogenesis. *Nature* 404:652–660, 2000. doi: 10.1038/35007527.
21. Mailloux RJ. Mitochondrial antioxidants and the maintenance of cellular hydrogen peroxide levels. *Oxid Med Cell Longev* 2018, 2018. doi: 10.1155/2018/7857251.
22. Murphy MP. How mitochondria produce reactive oxygen species. *Biochem J* 417:1, 2009. doi: 10.1042/BJ20081386.
23. Powers SK, Deminice R, Ozdemir M, Yoshihara T, Bomkamp MP, Hyatt H. Exercise-induced oxidative stress: Friend or foe? *J Sport Health Sci* 9(5):415-425, 2020. doi: 10.1016/j.jshs.2020.04.001.
24. Scarpulla RC. Metabolic control of mitochondrial biogenesis through the PGC-1 family regulatory network. *Biochem Biophys Acta* 1813:1269–78, 2011. doi: 10.1016/j.bbamcr.2010.09.019.
25. Giacomello M, Pyakurel A, Glytsou C, Scorrano L. The cell biology of mitochondrial membrane dynamics. *Nat Rev Mol Cell Biol* 214(2020);21:204–224, 2020. doi: 10.1038/s41580-020-0210-7.
26. Cipolat S, De Brito OM, Dal Zilio B, Scorrano L. OPA1 requires mitofusin 1 to promote mitochondrial fusion. *Proc Natl Acad Sci USA* 101:15927–15932, 2004. doi: 10.1073/pnas.0407043101.
27. Glancy B, Hartnell LM, Combs CA, Femnou A, Sun J, Murphy E, Subramaniam S, Balaban RS. Power Grid Protection of the Muscle Mitochondrial Reticulum. *Cell Rep* 19(3):487-496, 2017. doi: 10.1016/j.celrep.2017.03.063.
28. Twig G, Elorza A, Molina AJA, Mohamed H, Wikstrom JD, Walzer G, Stiles L, Haigh SE, Katz S, Las G, Alroy J, Wu M, Py BF, Yuan J, Deeney JT, Corkey BE, Shirihai OS. Fission and selective fusion govern mitochondrial segregation and elimination by autophagy. *EMBO J* 27:433–46, 2008. doi: 10.1038/sj.emboj.7601963.
29. Kleele T, Rey T, Winter J, Zaganelli S, Mahecic D, Perreten Lambert H, Ruberto FP, Nemir M, Wai T, Pedrazzini T, Manley S. Distinct fission signatures predict mitochondrial degradation or biogenesis. *Nature* 593:435–439, 2021. doi: 10.1038/s41586-021-03510-6.
30. Carter HN, Chen CCW, Hood DA. Mitochondria, muscle health, and exercise with advancing age. *Physiology* 30(3):208–23, 2015. doi: 10.1152/physiol.00039.2014.
31. De Mario A, Gherardi G, Rizzuto R, Mammucari C. Skeletal muscle mitochondria in health and disease. *Cell Calcium* 94:102357, 2021. doi: 10.1016/j.ceca.2021.102357.
32. Holloszy JO. Biochemical adaptations in muscle. Effects of exercise on mitochondrial oxygen uptake and respiratory enzyme activity in skeletal muscle. *J Biol Chem* 242(9):2278-82, 1967.
33. Mathai AS, Bonen A, Benton CR, Robinson DL, Graham TE. Rapid exercise-induced changes in PGC-1α mRNA and protein in human skeletal muscle. *J Appl Physiol* 105(4):1098–1105, 2008. doi: 10.1152/japplphysiol.00847.2007.

34. Pilegaard H, Saltin B, Neufer DP, Neufer PD. Exercise induces transient transcriptional activation of the PGC-1α gene in human skeletal muscle. *J Physiol* 546:851–858, 2003. doi: 10.1113/jphysiol.2002.034850.
35. Gowans GJ, Hawley SA, Ross FA, Hardie DG. AMP is a true physiological regulator of AMP-activated protein kinase by both allosteric activation and enhancing net phosphorylation. *Cell Metab* 18(4):556-66, 2013. doi: 10.1016/j.cmet.2013.08.019.
36. Winder WW, Holmes BF, Rubink DS, Jensen EB, Chen M, Holloszy JO. Activation of AMP-activated protein kinase increases mitochondrial enzymes in skeletal muscle. *J Appl Physiol* 88(6):2219–26, 2000. doi: 10.1152/jappl.2000.88.6.2219.
37. Jäger S, Handschin C, St-Pierre J, Spiegelman BM. AMP-activated protein kinase (AMPK) action in skeletal muscle via direct phosphorylation of PGC-1α. *PNAS* 104(29):12017–22, 2007. doi: 10.1073/pnas.0705070104.
38. Akimoto T, Pohnert SC, Li P, Zhang M, Gumbs C, Rosenberg PB, Williams RS, Yan Z. Exercise Stimulates Pgc-1α Transcription in Skeletal Muscle through Activation of the p38 MAPK Pathway. *J Biol Chem* 280:19587–19593, 2005. doi: 10.1074/jbc.M408862200.
39. Pogozelski AR, Geng T, Li P, Yin X, Lira VA, Zhang M, Chi JT, Yan Z. p38gamma mitogen-activated protein kinase is a key regulator in skeletal muscle metabolic adaptation in mice. *PLoS One* 4(11):e7934, 2009. doi: 10.1371/journal.pone.0007934.
40. Wu H, Kanatous SB, Thurmond FA, Gallardo T, Isotani E, Bassel-Duby R, Williams RS. Regulation of mitochondrial biogenesis in skeletal muscle by CaMK. *Science (80-)* 296:349–352, 2002. doi: 10.1126/science.1071163.
41. Rose AJ, Hargreaves M. Exercise increases Ca2+-calmodulin-dependent protein kinase II activity in human skeletal muscle. *J Physiol* 553:303–309, 2003. doi: 10.1113/jphysiol.2003.054171.
42. Memme JM, Oliveira AN, Hood DA. Chronology of UPR activation in skeletal muscle adaptations to chronic contractile activity. *Am J Physiol Cell Physiol* 310(11):C1024-36, 2016. doi: 10.1152/ajpcell.00009.2016.
43. Bohnert KR, McMillan JD, Kumar A. Emerging roles of ER stress and unfolded protein response pathways in skeletal muscle health and disease. *J Cell Physiol* 233(1):67-78, 2018. doi: 10.1002/jcp.25852.
44. Davies KJ, Packer L, Brooks GA. Biochemical adaptation of mitochondria, muscle, and whole-animal respiration to endurance training. *Arch Biochem Biophys* 209(2):539-54, 1981. doi: 10.1016/0003-9861(81)90312-x.
45. Constable SH, Favier RJ, McLane JA, Fell RD, Chen M, Holloszy JO. Energy metabolism in contracting rat skeletal muscle: adaptation to exercise training. *Am J Physiol* 253(2 Pt 1):C316-22, 1987. doi: 10.1152/ajpcell.1987.253.2.C316.
46. Dudley GA, Tullson PC, Terjung RL. Influence of mitochondrial content on the sensitivity of respiratory control. *J Biol Chem* 262(19):9109-14, 1987.
47. Carter HN, Pauly M, Tryon LD, Hood DA. Effect of contractile activity on PGC-1α transcription in young and aged skeletal muscle. *J Appl Physiol* 124(6):1605-1615, 2018. doi: 10.1152/japplphysiol.01110.2017.
48. Kirkwood SP, Packer L, Brooks GA. Effects of endurance training on a mitochondrial reticulum in limb skeletal muscle. *Arch Biochem Biophys* 255(1):80-88, 1987. doi: 10.1016/0003-9861(87)90296-7.

49. Iqbal S, Ostojic O, Singh K, Joseph AM, Hood DA. Expression of mitochondrial fission and fusion regulatory proteins in skeletal muscle during chronic use and disuse. *Muscle Nerve* 48(6):963-70, 2013. doi: 10.1002/mus.23838.
50. Holloway GP. Nutrition and training influences on the regulation of mitochondrial adenosine diphosphate sensitivity and bioenergetics. *Sports Med* 27:13-21, 2017. doi: 10.1007/s40279-017-0693-3.
51. MacIntosh BR, Esau SP, Holash RJ, Fletcher JR. Procedures for rat in situ skeletal muscle contractile properties. *J Vis Exp* (56):e3167, 2011. doi: 10.3791/3167.
52. Ljubicic V, Joseph AM, Adhihetty PJ, Huang JH, Saleem A, Uguccioni G, Hood DA. Molecular basis for an attenuated mitochondrial adaptive plasticity in aged skeletal muscle. *Aging* 1(9):818-30, 2009. doi: 10.18632/aging.
53. Crilly MJ, Tryon LD, Erlich AT, Hood DA. The role of Nrf2 in skeletal muscle contractile and mitochondrial function. *J Appl Physiol* 121(3):730-40, 2016. doi: 10.1152/japplphysiol.00042.2016.
54. Sherwin CM. Voluntary wheel running: a review and novel interpretation. *Anim Behav* 56:11–27, 1998. doi: 10.1006/anbe.1998.0836.
55. Saleem A, Adhihetty PJ, Hood DA. Role of p53 in mitochondrial biogenesis and apoptosis in skeletal muscle. *Physiol Genomics* 37:58–66, 2009. doi: 10.1152/physiolgenomics.90346.2008.
56. Chen CCW, Erlich AT, Hood DA. Role of Parkin and endurance training on mitochondrial turnover in skeletal muscle. *Skeletal Muscle* 8:10, 2018. doi: 10.1186/s13395-018-0157-y.
57. Kim J, Kundu M, Viollet B, Guan KL. AMPK and mTOR regulate autophagy through direct phosphorylation of Ulk1. *Nat Cell Biol* 13(2):132-41, 2011. doi: 10.1038/ncb2152.
58. Han X, Goh KY, Lee WX, Choy SM, Tang H-W. The Importance of mTORC1-Autophagy Axis for Skeletal Muscle Diseases. *International Journal of Molecular Sciences* 24(1):297, 2023. doi.org/10.3390/ijms24010297.
59. Kang R, Zeh HJ, Lotze MT, Tang D. The Beclin 1 network regulates autophagy and apoptosis. *Cell Death Differ* 18:571–580, 2011. doi: 10.1038/cdd.2010.191.
60. Russell RC, Tian Y, Yuan H, Park HW, Chang YY, Kim J et al. ULK1 induces autophagy by phosphorylating Beclin-1 and activating VPS34 lipid kinase. *Nat Cell Biol* 15:741–750, 2013. doi: 10.1038/ncb2757.
61. Park J-M, Seo M, Jung CH, Grunwald D, Stone M, Otto NM et al. ULK1 phosphorylates Ser30 of BECN1 in association with ATG14 to stimulate autophagy induction. *Autophagy* 14:584, 2018. doi: 10.1080/15548627.2017.1422851.
62. Wei Y, Liu M, Li X, Liu J, Li H. Origin of the Autophagosome Membrane in Mammals. *Biomed Res Int* 2018:1012789, 2018. doi: 10.1155/2018/1012789.
63. Kabeya Y, Mizushima N, Ueno T, Yamamoto A, Kirisako T, Noda T, Kominami E, Ohsumi Y, Yoshimori T. LC3, a mammalian homologue of yeast Apg8p, is localized in autophagosome membranes after processing. *EMBO J* 19(21):5720-8, 2000. doi: 10.1093/emboj/19.21.5720.
64. Kabeya Y, Mizushima N, Yamamoto A, Oshitani-Okamoto S, Ohsumi Y, Yoshimori T. LC3, GABARAP and GATE16 localize to autophagosomal membrane depending on form-II formation. *J Cell Sci* 117:2805–2812, 2004. doi: 10.1242/jcs.01131.z
65. Weidberg H, Shvets E, Shpilka T, Shimron F, Shinder V, Elazar Z. LC3 and GATE-16/GABARAP subfamilies are both essential yet act differently in autophagosome biogenesis. *EMBO J* 29:1792–1802, 2010. doi: 10.1038/emboj.2010.74.

66. Orsi A, Razi M, Dooley HC, Robinson D, Weston AE, Collinson LM, Tooze SA. Dynamic and transient interactions of Atg9 with autophagosomes, but not membrane integration, are required for autophagy. *Mol Biol Cell* 23(10):1860-73, 2012. doi: 10.1091/mbc.E11-09-0746.
67. Webb JL, Ravikumar B, Rubinsztein DC. Microtubule disruption inhibits autophagosome–lysosome fusion: implications for studying the roles of aggresomes in polyglutamine diseases. *Int J Biochem Cell Biol* 2004; 36: 2541– 2550. doi: 10.1016/j.biocel.2004.02.003.
68. Yu L, Chen Y, Tooze SA. Autophagy pathway: Cellular and molecular mechanisms. *Autophagy* 14(2):207-215, 2018. doi: 10.1080/15548627.2017.1378838.
69. Eskelinen EL. Roles of LAMP-1 and LAMP-2 in lysosome biogenesis and autophagy. *Mol Aspects Med* 27(5-6):495-502, 2006. doi: 10.1016/j.mam.2006.08.005.
70. Hansen M, Rubinsztein DC, Walker DW. Autophagy as a promoter of longevity: insights from model organisms. *Nat Rev Mol Cell Biol* 19(9):579-593, 2018. doi: 10.1038/s41580-018-0033-y.
71. Carnio S, LoVerso, F., Baraibar, M. A., Longa, E., Khan, M. M., Maffei, M., et al. Autophagy impairment in muscle induces neuromuscular junction degeneration and precocious aging. *Cell Rep.* 8, 1509–1521, 2014. doi: 10.1016/j.celrep.2014.07.061
72. Masiero E, Agatea L, Mammucari C, Blaauw B, Loro E, Komatsu M, Metzger D, Reggiani C, Schiaffino S, Sandri M. Autophagy is required to maintain muscle mass. *Cell Metab* 10(6):507-15, 2009. doi: 10.1016/j.cmet.2009.10.008.
73. Penna F, Costamagna D, Pin F, Camperi A, Fanzani A, Chiarpotto EM, Cavallini G, Bonelli G, Baccino FM, Costelli P. Autophagic degradation contributes to muscle wasting in cancer cachexia. *Am J Pathol* 182(4):1367-78, 2013. doi: 10.1016/j.ajpath.2012.12.023.
74. Pyo JO, Yoo SM, Ahn HH, Nah J, Hong SH, Kam TI, Jung S, Jung YK. Overexpression of Atg5 in mice activates autophagy and extends lifespan. *Nat Commun*. 4:2300, 2013. doi: 10.1038/ncomms3300.
75. Zeng Z, Liang J, Wu L, Zhang H, Lv J, Chen N. Exercise-Induced Autophagy Suppresses Sarcopenia Through Akt/mTOR and Akt/FoxO3a Signal Pathways and AMPK-Mediated Mitochondrial Quality Control. *Front Physiol* 11:583478, 2020. doi: 10.3389/fphys.2020.583478.
76. Coffey JW, de Duve C. Digestive Activity of Lysosomes. *J Biol Chem* 243:3255–3263, 1968. doi.org/10.1016/S0021-9258(18)93301-6.
77. Ohkuma S, Moriyama Y, Takano T. Identification and characterization of a proton pump on lysosomes by fluorescein isothiocyanate-dextran fluorescence. *Proc Natl Acad Sci USA* 1982;79:2758–2762, 1982. doi: 10.1073/pnas.79.9.2758.
78. Mindell JA. Lysosomal Acidification Mechanisms. *Annu Rev Physiol* 74:69–86, 2012. doi: 10.1146/annurev-physiol-012110-142317.
79. Medina, D., Di Paola, S., Peluso, I. et al. Lysosomal calcium signalling regulates autophagy through calcineurin and TFEB. *Nat Cell Biol* 17:288–299, 2015. https://doi.org/10.1038/ncb3114
80. Lawrence RE, Zoncu R. The lysosome as a cellular centre for signalling, metabolism and quality control. *Nat Cell Biol* 21:133–142, 2019. doi: 10.1038/s41556-018-0244-7.
81. Ballabio A, Bonifacino JS. Lysosomes as dynamic regulators of cell and organismal homeostasis. *Nat Rev Mol Cell Biol* 21:101–118, 2020. doi: 10.1038/s41580-019-0185-4.
82. Meena NK, Raben N. Pompe Disease: New Developments in an Old Lysosomal Storage Disorder. Biomolecules 10(9):1339, 2020. doi: 10.3390/biom10091339.

83. Zhai Y, Miao J, Peng Y, Wang Y, Dong J, Zhao X. Clinical features of Danon disease and insights gained from LAMP-2 deficiency models. Trends Cardiovasc Med 33(2):81-89, 2023. doi: 10.1016/j.tcm.2021.10.012.
84. Thomas RE, Andrews LA, Burman JL, Lin W-Y, Pallanck LJ. PINK1-Parkin Pathway Activity Is Regulated by Degradation of PINK1 in the Mitochondrial Matrix. *PLoS Genet* 10:e1004279, 2014. doi: 10.1371/journal.pgen.1004279.
85. Greene AW, Grenier K, Aguileta MA, Muise S, Farazifard R, Haque ME , McBride HM, Park DS, Fon EA. Mitochondrial processing peptidase regulates PINK1 processing, import and Parkin recruitment. *EMBO Rep* 13:378–385, 2012. doi: 10.1038/embor.2012.14.
86. Narendra DP, Jin SM, Tanaka A, Suen D-FF, Gautier CA, Shen J et al. PINK1 is selectively stabilized on impaired mitochondria to activate Parkin. *PLoS Biol* 8:e1000298, 2010. doi: 10.1371/journal.pbio.1000298.
87. Kondapalli C, Kazlauskaite A, Zhang N, Woodroof HI, Campbell DG, Gourlay R, Burchell L, Walden H, Macartney TJ, Deak M, Knebel A, Alessi DR, Muqit MM. PINK1 is activated by mitochondrial membrane potential depolarization and stimulates Parkin E3 ligase activity by phosphorylating Serine 65. *Open Biol* 2:120080, 2012. doi: 10.1098/rsob.120080.
88. Jin SM, Youle RJ. The accumulation of misfolded proteins in the mitochondrial matrix is sensed by PINK1 to induce PARK2/Parkin-mediated mitophagy of polarized mitochondria. *Autophagy* 9:1750–1757, 2013. doi: 10.4161/auto.26122.
89. Okatsu K, Oka T, Iguchi M, Imamura K, Kosako H, Tani N, Kimura M, Go E, Koyano F, Funayama M, Shiba-Fukushima K, Sato S, Shimizu H, Fukunaga Y, Taniguchi H, Komatsu M, Hattori N, Mihara K, Tanaka K, Matsuda N. PINK1 autophosphorylation upon membrane potential dissipation is essential for Parkin recruitment to damaged mitochondria. *Nat Commun* 3:1–10, 2012. doi: 10.1038/ncomms2016.
90. Kazlauskaite A, Kondapalli C, Gourlay R, Campbell DG, Ritorto MS, Hofmann K, Alessi DR, Knebel A, Trost M, Muqit MM. Parkin is activated by PINK1-dependent phosphorylation of ubiquitin at Ser65. Biochem J 460:127–39, 2014. doi: 10.1042/BJ20140334.
91. Lazarou M, Sliter DA, Kane LA, Sarraf SA, Wang C, Burman JL, Sideris DP, Fogel AI, Youle RJ. The ubiquitin kinase PINK1 recruits autophagy receptors to induce mitophagy. *Nat* 5247565 2015;524:309–314, 2015. doi: 10.1038/nature14893.
92. Geisler S, Holmstr.m KM, Skujat D, Fiesel FC, Rothfuss OC, Kahle PJ, Springer W. PINK1/Parkin-mediated mitophagy is dependent on VDAC1 and p62/SQSTM1. *Nat Cell Biol* 12:119–131, 2010. doi: 10.1038/ncb2012.
93. Rikka S, Quinsay MN, Thomas RL, Kubli DA, Zhang X, Murphy AN, Gustafsson ÅB. Bnip3 impairs mitochondrial bioenergetics and stimulates mitochondrial turnover. *Cell Death Differ* 18:721–31, 2011. doi: 10.1038/cdd.2010.146.
94. Novak I, Kirkin V, McEwan DG, Zhang J, Wild P, Rozenknop A, Rogov V, Löhr F, Popovic D, Occhipinti A, Reichert AS, Terzic J, Dötsch V, Ney PA, Dikic I. Nix is a selective autophagy receptor for mitochondrial clearance. *EMBO Rep* 11(1):45-51, 2010. doi: 10.1038/embor.2009.256.
95. Ding WX, Ni HM, Li M, Liao Y, Chen X, Stolz DB, Dorn GW 2nd, Yin XM. Nix is critical to two distinct phases of mitophagy, reactive oxygen species-mediated autophagy induction and Parkin-ubiquitin-p62-mediated mitochondrial priming. *J Biol Chem* 285(36):27879-90, 2010. doi: 10.1074/jbc.M110.119537.

96. Kanki T. Nix, a receptor protein for mitophagy in mammals. *Autophagy* 6:433–5, 2010. doi: 10.4161/auto.6.3.11420.
97. Rogov V V., Suzuki H, Marinković M, Lang V, Kato R, Kawasaki M et al. Phosphorylation of the mitochondrial autophagy receptor Nix enhances its interaction with LC3 proteins. *Sci Reports* 7:1–12, 2017. doi.org/10.1038/s41598-017-01258-6
98. Gao J, Yu L, Wang Z, Wang R, Liu X. Induction of mitophagy in C2C12 cells by electrical pulse stimulation involves increasing the level of the mitochondrial receptor FUNDC1 through the AMPK-ULK1 pathway. *Am J Transl Res* 12:6879–6894, 2020.
99. Liu L, Feng D, Chen G, Chen M, Zheng Q, Song P, Ma Q, Zhu C, Wang R, Qi W, Huang L, Xue P, Li B, Wang X, Jin H, Wang J, Yang F, Liu P, Zhu Y, Sui S, Chen Q. Mitochondrial outer-membrane protein FUNDC1 mediates hypoxia-induced mitophagy in mammalian cells. *Nat Cell Biol* 14(2):177-85, 2012. doi: 10.1038/ncb2422.
100. Wu W, Tian W, Hu Z, Chen G, Huang L, Li W, Zhang X, Xue P, Zhou C, Liu L, Zhu Y, Zhang X, Li L, Zhang L, Sui S, Zhao B, Feng D. ULK1 translocates to mitochondria and phosphorylates FUNDC1 to regulate mitophagy. *EMBO Rep* 15(5):566-75, 2014. doi: 10.1002/embr.201438501
101. Sun N, Youle RJ, Finkel T. The mitochondrial basis of aging. *Mol Cell* 61:654–666, 2016. doi: 10.1016/j.molcel.2016.01.028.
102. Woldt E, Sebti Y, Solt LA, Duhem C, Lancel S, Eeckhoute J, Hesselink MK, Paquet C, Delhaye S, Shin Y, Kamenecka TM, Schaart G, Lefebvre P, Nevière R, Burris TP, Schrauwen P, Staels B, Duez H. Rev-erb-alpha modulates skeletal muscle oxidative capacity by regulating mitochondrial biogenesis and autophagy. *Nat Med* 19, 1039–1046, 2013. doi: 10.1038/nm.3213
103. Laker RC, Drake JC, Wilson RJ, Lira VA, Lewellen BM, Ryall KA, Fisher CC, Zhang M, Saucerman JJ, Goodyear LJ, Kundu M, Yan Z. Ampk phosphorylation of Ulk1 is required for targeting of mitochondria to lysosomes in exercise-induced mitophagy. *Nat Commun* 8(1):548, 2017. doi: 10.1038/s41467-017-00520-9.
104. Vainshtein A, Tryon LD, Pauly M, Hood DA. Role of PGC-1α during acute exercise-induced autophagy and mitophagy in skeletal muscle. *Am J Physiol Cell Physiol* 308(9):C710–19 129, 2015. doi: 10.1152/ajpcell.00380.2014.
105. Chen CCW, Erlich AT, Crilly MJ, Hood DA. Parkin is required for exercise-induced mitophagy in muscle: impact of aging. *Am J Physiol Endocrinol Metab* 315:E404–15, 2018. doi: 10.1152/ajpendo.00391.2017.
106. Dun Y, Liu S, Zhang W, Xie M, Qiu L. Exercise Combined with *Rhodiola sacra* Supplementation Improves Exercise Capacity and Ameliorates Exhaustive Exercise-Induced Muscle Damage through Enhancement of Mitochondrial Quality Control. *Oxid Med Cell Longev* 2017:8024857, 2017. doi: 10.1155/2017/8024857.
107. Lira VA, Okutsu M, Zhang M, Greene NP, Laker RC, Breen DS, Hoehn KL, Yan Z. Autophagy is required for exercise training-induced skeletal muscle adaptation and improvement of physical performance. *FASEB J* 27(10):4184-93, 2013. doi: 10.1096/fj.13-228486.
108. Ju JS, Jeon SI, Park JY, Lee JY, Lee SC, Cho KJ, Jeong JM. Autophagy plays a role in skeletal muscle mitochondrial biogenesis in an endurance exercise-trained condition. *J Physiol Sci* 66(5):417-30, 2016. doi: 10.1007/s12576-016-0440-9.
109. Tarpey MD, Davy KP, McMillan RP, Bowser SM, Halliday TM, Boutagy NE, Davy BM, Frisard MI, Hulver MW. Skeletal muscle autophagy and mitophagy in endurance-trained

runners before and after a high-fat meal. *Mol Metab* 6(12):1597-1609, 2017. doi: 10.1016/j.molmet.2017.10.006.
110. Steingrimsson E, Copeland NG, and Jenkins NA. Melanocytes and the microphthalmia transcription factor network. *Annu Rev Genet* 38, 365–411, 2004. doi: 10.1146/annurev.genet.38.072902.092717.
111. La Spina M, Contreras PS, Rissone A, Meena NK, Jeong E and Martina JA. MiT/TFE Family of Transcription Factors: An Evolutionary Perspective. *Front Cell Dev Biol* 8:609683, 2021. doi: 10.3389/fcell.2020.609683.
112. Martina JA, Diab HI, Lishu L, Jeong AL, Patange S, Raben N, Puertollano R. The nutrient-responsive transcription factor TFE3 promotes autophagy, lysosomal biogenesis, and clearance of cellular debris. *Sci Signal* 7:ra9, 2014. doi: 10.1126/scisignal.2004754.
113. Martina JA, Diab HI, Li H, Puertollano R. Novel roles for the MiTF/TFE family of transcription factors in organelle biogenesis, nutrient sensing, and energy homeostasis. *Cell Mol Life Sci* 71:2483–97, 2014. doi: 10.1007/s00018-014-1565-8.
114. Slade L, Pulinilkunnil T. The MiTF/TFE family of transcription factors: master regulators of organelle signaling, metabolism, and stress adaptation. *Mol Cancer Res* 15:1637–1643, 2017. doi: 10.1158/1541-7786.MCR-17-0320.
115. Hemesath TJ, Steingrimsson E, Mcgill G, Hansen MJ, Vaught J, Hodgkinson CA, Arnheiter H, Copeland NG, Jenkins NA, Fisher DE. Microphthalmia, a critical factor in melanocyte development, defines a discrete transcription factor family. *Genes Dev* 8, 2770–2780, 1994. doi: 10.1101/gad.8.22.2770.
116. Pogenberg V, Ballesteros-Alvarez J, Schober R, Sigvaldadottir I, Obarska Kosinska A, Milewski M, Schindl R, Ögmundsdóttir MH, Steingrímsson E, Wilmanns M. Mechanism of conditional partner selectivity in MITF/TFE family transcription factors with a conserved coiled coil stammer motif. *Nucleic Acids Res* 48, 934–948, 2020. doi: 10.1093/nar/gkz1104.
117. Palmieri M, Impey S, Kang H, Di Ronza A, Pelz C, Sardiello M, Ballabio A. Characterization of the CLEAR network reveals an integrated control of cellular clearance pathways. *Hum Mol Genet* 20, 3852–3866, 2011. doi: 10.1093/hmg/ddr306.
118. Martina JA, Puertollano R. Rag GTPases mediate amino acid-dependent recruitment of TFEB and MITF to lysosomes. *J Cell Biol* 200(4):475-91, 2013. doi: 10.1083/jcb.201209135.
119. Sancak Y, Bar-Peled L, Zoncu R, Markhard AL, Nada S, Sabatini DM. Ragulator-rag complex targets mTORC1 to the lysosomal surface and is necessary for its activation by amino acids. *Cell* 141:290–303, 2010. doi: 10.1016/j.cell.2010.02.024.
120. Sancak Y, Peterson TR, Shaul YD, Lindquist RA, Thoreen CC, Bar-Peled L, Sabatini DM. The Rag GTPases bind raptor and mediate amino acid signaling to mTORC1. *Science* 320(5882):1496-501, 2008. doi: 10.1126/science.1157535.
121. Settembre C, Zoncu R, Medina DL, Vetrini F, Erdin S, Erdin S, Huynh T, Ferron M, Karsenty G, Vellard MC, Facchinetti V, Sabatini DM, Ballabio A. A lysosome-to-nucleus signalling mechanism senses and regulates the lysosome via mTOR and TFEB. *EMBO J* 31(5):1095-108, 2012. doi: 10.1038/emboj.2012.32.
122. Medina DL, Di Paola S, Peluso I, Armani A, De Stefani D, Venditti R, Montefusco S, Scotto-Rosato A, Prezioso C, Forrester A, Settembre C, Wang W, Gao Q, Xu H, Sandri M, Rizzuto R, De Matteis MA, Ballabio A. Lysosomal calcium signalling regulates autophagy through calcineurin and TFEB. *Nat Cell Biol* 17:288–299, 2015. doi: 10.1038/ncb3114.

123. Zhang X, Cheng X, Yu L, Yang J, Calvo R, Patnaik S, Hu X, Gao Q, Yang M, Lawas M, Delling M, Marugan J, Ferrer M, Xu H. MCOLN1 is a ROS sensor in lysosomes that regulates autophagy. *Nat Commun* 7:12109, 2016. doi: 10.1038/ncomms12109.
124. Scotto Rosato A, Montefusco S, Soldati C, Di Paola S, Capuozzo A, Monfregola J, Polishchuk E, Amabile A, Grimm C, Lombardo A, De Matteis MA, Ballabio A, Medina DL. TRPML1 links lysosomal calcium to autophagosome biogenesis through the activation of the CaMKKβ/VPS34 pathway. *Nat Commun* 10:1–16, 2019. doi: 10.1038/s41467-019-13572-w.
125. Martina JA, Diab HI, Brady OA, Puertollano R. TFEB and TFE3 are novel components of the integrated stress response. *EMBO J* 35(5):479-95, 2016. doi: 10.15252/embj.201593428.
126. Andersson DC, Betzenhauser MJ, Reiken S, Meli AC, Umanskaya A, Xie W, Shiomi T, Zalk R, Lacampagne A, Marks AR. Ryanodine receptor oxidation causes intracellular calcium leak and muscle weakness in aging. *Cell Metab* 14:196–207, 2011. doi: 10.1016/j.cmet.2011.05.014.
127. Wang H, Wang N, Xu D, Ma Q, Chen Y, Xu S, Xia Q, Zhang Y, Prehn JHM, Wang G, Ying Z. Oxidation of multiple MiT/TFE transcription factors links oxidative stress to transcriptional control of autophagy and lysosome biogenesis. *Autophagy* 16:1683–1696, 2020. doi: 10.1080/15548627.2019.1704104.
128. Paquette M, El-Houjeiri L, Zirden LC, Puustinen P, Blanchette P, Jeong H, Dejgaard K, Siegel PM, Pause A. AMPK-dependent phosphorylation is required for transcriptional activation of TFEB and TFE3. *Autophagy* Epub:1–19, 2021. doi: 10.1080/15548627.2021.1898748.
129. Nezich CL, Wang C, Fogel AI, Youle RJ. MiT/TFE transcription factors are activated during mitophagy downstream of Parkin and Atg5. *J Cell Biol* 210:435–50, 2015. doi: 10.1083/jcb.201501002.
130. Nakagawa Y, Shimano H, Yoshikawa T, Ide T, Tamura M, Furusawa M, Yamamoto T, Inoue N, Matsuzaka T, Takahashi A, Hasty AH, Suzuki H, Sone H, Toyoshima H, Yahagi N, Yamada N. TFE3 transcriptionally activates hepatic IRS-2, participates in insulin signaling and ameliorates diabetes. *Nat Med* 12: 107–113, 2006. doi: 10.1038/nm1334.
131. Kim MY, Jo SH, Park JM, Kim TH, Im SS, Ahn YH. Adenovirus-mediated overexpression of Tcfe3 ameliorates hyperglycaemia in a mouse model of diabetes by upregulating glucokinase in the liver. *Diabetologia* 56:635–643, 2013. doi: 10.1007/s00125-012-2807-7.
132. Xiong J, Wang K, He J, Zhang G, Zhang D, Chen F. TFE3 alleviates hepatic steatosis through autophagy-induced lipophagy and PGC1alpha-mediated fatty acid beta-oxidation. *Int J Mol Sci* 17: 387, 2016. doi: 10.3390/ijms17030387.
133. Pastore N, Vainshtein A, Klisch TJ, Armani A, Huynh T, Herz NJ, Polishchuk EV, Sandri M, Ballabio A. TFE3 regulates whole-body energy metabolism in cooperation with TFEB. *EMBO Mol Med* 9:605–621, 2017. doi: 10.15252/emmm.201607204.
134. Fujimoto Y, Nakagawa Y, Satoh A, Okuda K, Shingyouchi A, Naka A, Matsuzaka T, Iwasaki H, Kobayashi K, Yahagi N, Shimada M, Yatoh S, Suzuki H, Yogosawa S, Izumi T, Sone H, Urayama O, Yamada N, Shimano H. TFE3 controls lipid metabolism in adipose tissue of male mice by suppressing lipolysis and thermogenesis. *Endocrinology* 154:3577–3588, 2013. doi: 10.1210/en.2013-1203.
135. Salma N, Song JS, Kawakami A, Devi SP. Tfe3 and Tfeb transcriptionally regulate peroxisome proliferator-activated receptor gamma2 expression in adipocytes and mediate

adiponectin and glucose levels in mice. *Mol Cell Biol* 37:1–23, 2017. doi: 10.1128/MCB.00608-16.
136. Iwasaki H, Naka A, Iida KT, Nakagawa Y, Matsuzaka T, Ishii K, Kobayashi K, Takahashi A, Yatoh S, Yahagi N, Sone H, Suzuki H, Yamada N, Shimano H. TFE3 regulates muscle metabolic gene expression, increases glycogen stores, and enhances insulin sensitivity in mice. *Am J Physiol Metab* 302:E896–E902, 2012. doi: 10.1152/ajpendo.00204.2011.
137. Salma N, Song JS, Arany Z, Fisher DE. Transcription factor Tfe3 directly regulates Pgc-1alpha in muscle. *J Cell Physiol* 2015. doi: 10.1002/jcp.24978.
138. Ozturk DG, Kocak M, Akcay A, Kinoglu K, Kara E, Buyuk Y, Kazan H, Gozuacik D. MITF-MIR211 axis is a novel autophagy amplifier system during cellular stress. *Autophagy* 15:375–390, 2019. doi: 10.1080/15548627.2018.1531197.
139. Sardiello M, Palmieri M, di Ronza A, Medina DL, Valenza M, Gennarino VA, Di Malta C, Donaudy F, Embrione V, Polishchuk RS, Banfi S, Parenti G, Cattaneo E, Ballabio A. A gene network regulating lysosomal biogenesis and function. *Science* 325(5939):473-7, 2009. doi: 10.1126/science.1174447.
140. Martina JA, Chen Y, Gucek M, Puertollano R. MTORC1 functions as a transcriptional regulator of autophagy by preventing nuclear transport of TFEB. *Autophagy* 8:904-914, 2012. doi:10.4161/auto.19653.
141. Medina DL, Di Paola S, Peluso I, Armani A, De Stefani D, Venditti R, Montefusco S, Scotto-Rosato A, Prezioso C, Forrester A, Settembre C, Wang W, Gao Q, Xu H, Sandri M, Rizzuto R, De Matteis MA, Ballabio A. Lysosomal calcium signalling regulates autophagy through calcineurin and TFEB. *Nat Cell Biol* 17:288-299, 2015. doi:10.1038/ncb3114.
142. Napolitano G, Ballabio A. TFEB at a glance. *J Cell Sci* 129(13):2475-81, 2016. doi: 10.1242/jcs.146365.
143. Steingrimsson E, Tessarollo L, Reid SW, Jenkins NA, Copeland NG. The bHLH-Zip transcription factor Tfeb is essential for placental vascularization. *Development* 125:4607–4616, 1998. doi: 10.1242/dev.125.23.4607.
144. Mansueto G, Armani A, Viscomi C, D'Orsi L, De Cegli R, Polishchuk EV, Lamperti C, Di Meo I, Romanello V, Marchet S, Saha PK, Zong H, Blaauw B, Solagna F, Tezze C, Grumati P, Bonaldo P, Pessin JE, Zeviani M, Sandri M, Ballabio A. Transcription factor EB controls metabolic flexibility during exercise. *Cell Metab* 25:182-196, 2017. doi:10.1016/j.cmet.2016.11.003.
145. Erlich AT, Brownlee DM, Beyfuss K, Hood DA. Exercise induces TFEB expression and activity in skeletal muscle in a PGC-1α-dependent manner. *Am J Physiol Cell Physiol* 314(1):C62-C72, 2018. doi: 10.1152/ajpcell.00162.2017.
146. Ho H, Kapadia R, Al-Tahan S, Ahmad S, Ganesan AK. WIPI1 coordinates melanogenic gene transcription and melanosome formation via TORC1 inhibition. *J Biol Chem* 286(14):12509–12523, 2011. doi: 10.1074/jbc.M110.200543.
147. Cheli Y, Ohanna M, Ballotti R, Bertolotto C. Fifteen-year quest for microphthalmia-associated transcription factor target genes. *Pigment Cell Melanoma Res* 23(1):27–40, 2010. doi: 10.1111/j.1755-148X.2009.00653.x.
148. Tassabehjil M, Newton VE, Read AP. Waardenburg syndrome type 2 caused by mutations in the human microphthalmia (MITF) gene. *Nat Gen* 8:251–255, 1994. doi: 10.1038/ng1194-251.
149. Rehli M, Den Elzen N, Cassady AI, Ostrowski MC, Hume DA. Cloning and characterization of the murine genes for bHLH-ZIP transcription factors TFEC and TFEB reveal a common

gene organization for all MiT subfamily members. *Genomics* 56(1):111-20, 1999. doi: 10.1006/geno.1998.5588.

150. Zhao GQ, Zhao Q, Zhou X, Mattei MG, de Crombrugghe B. TFEC, a basic helix-loop helix protein, forms heterodimers with TFE3 and inhibits TFE3-dependent transcription activation. *Mol Cell Biol* 13:4505–4512, 2015. doi: 10.1128/mcb.13.8.4505-4512.1993.

CHAPTER 2: MANUSCRIPT

MANUSCRIPT AUTHOR CONTRIBUTIONS

Jenna C. Wong: Performed all surgical procedures, data collection, and data analyses; wrote the manuscript.

Ashley N. Oliveira: Aided in tissue collection and mitochondrial fractions.

Priyanka Khemraj: Aided in tissue collection and mitochondrial fractions.

Dr. David A. Hood: Supervised this project and is the Principal Investigator.

THE ROLE OF TFE3 IN MEDIATING SKELETAL MUSCLE MITOCHONDRIAL ADAPTATIONS TO EXERCISE TRAINING

Jenna C. Wong, Ashley N. Oliveira, Priyanka Khemraj and David A. Hood

Muscle Health Research Centre, School of Kinesiology and Health Science, York University, Toronto, Ontario, M3J 1P3, Canada

To whom correspondence should be addressed: David A. Hood, PhD (dhood@yorku.ca)
Muscle Health Research Centre
School of Kinesiology and Health Science
York University, Toronto, ON
Canada M3J 1P3

ABSTRACT

TFE3 is a transcription factor that activates the expression of lysosomal genes involved in the clearance of dysfunctional mitochondria, termed mitophagy. With exercise, TFE3 is presumed to optimize the mitochondrial pool through the removal of organelles via lysosomes. However, the molecular mechanisms of the involved pathways remain unknown. Wild-type (WT) and TFE3 knockout (KO) mice were subjected to 6 weeks of voluntary wheel running as an endurance training regimen. This was followed by a 45-minute bout of *in situ* stimulation of the sciatic nerve innervating hindlimb muscles to evaluate muscle fatigue and contractile properties. A subset of animals was treated with colchicine to measure autophagy and mitophagy flux. Fatigability during stimulation was reduced with training in WT animals, as seen by a 13% increase in percent of maximum force at 5 minutes of stimulation, and a 30% increase at 30 minutes. Permeabilized fiber oxygen consumption was also improved with training. Concurrent with improved muscle and mitochondrial function, COX activity and COX I protein expression were increased in trained WT animals compared to untrained animals, signifying an increase in mitochondrial content. These training adaptations were abolished with the loss of TFE3. Surprisingly, untrained TFE3 KO animals experienced a greater induction of mitophagy flux with acute stimulation compared to their WT counterparts. Training blunted this mitophagic response in KO mice. Our results suggest that the loss of TFE3 compromises beneficial training adaptations leading to improved muscle endurance and mitochondrial function and may induce a greater sensitivity to mitophagy induction in untrained muscle.

INTRODUCTION

Skeletal muscle comprises approximately 40% of body mass and relies on a highly dynamic pool of mitochondria for metabolic function (1). Mitochondria exist as a reticulum and adapt to various stimuli and conditions, lending to the highly plastic nature of the tissue. One such stimulus is exercise, known to be an effective driver for improved muscle health. Specifically, exercise remodels and optimizes the mitochondrial network via both the production, as well as the clearance of mitochondria to create a set of high-functioning organelles (2, 3). Endurance training has been shown to increase mitochondrial biogenesis and improve muscle metabolism (4-6). In turn, this elevation in mitochondrial content leads to enhanced oxidative capacity and better-quality muscle (7, 8).

In opposition to mitochondrial biogenesis, these organelles are also subject to removal and degradation when their function becomes compromised. Damaged mitochondria, characterized by an increased presence of reactive oxygen species (ROS) and decreased oxidative capacity, are removed from the reticulum via mitochondrial fission to be degraded subsequently by targeted mechanisms (9). Mitochondria are a primary site of reactive oxygen species (ROS) formation, and their accumulation leads to cellular stress and impairment. Therefore, the clearance of dysfunctional mitochondria is an essential cellular process to protect against extensive damage (10). This selective autophagy of mitochondria, termed mitophagy, is a critical regulator of skeletal muscle health, function, and exercise-induced adaptations (11-13). Inhibition of autophagic pathways induces a buildup of mitochondria with impaired morphology and function that causes global cellular detriment (14, 15). Vital to these autophagic processes are lysosomes, ultimately responsible for the breakdown of mitochondria. Their importance has been established in research

on lysosomal storage diseases, which are characterized by an accumulation of dysfunctional mitochondria (16).

The transcription factor E3 (TFE3) belongs to a family of microphthalmia (MiT/TFE) transcription factors containing a basic helix-loop-helix leucine zipper motif. TFE3 is expressed ubiquitously in mammalian cells and has been implicated in the activation of autophagic pathways through the transcription of lysosomal and autophagy-related genes (Fig. 1) (17, 18). During nutrient- and energy-rich conditions, TFE3 is phosphorylated by mammalian target of rapamycin complex 1 (mTORC1) and bound to the chaperone-like protein 14-3-3, remaining inactive in the cytosol. Under cellular stress, such as starvation or exercise, calcineurin and AMP-activated protein kinase (AMPK) activate TFE3, and the transcription factor then translocates to the nucleus and binds to a coordinated lysosomal expression and regulation (CLEAR) element composed of a palindromic 10 base-pair sequence (19-22). These CLEAR sites are present on the promoters of several lysosomal and autophagic genes, and their expression is activated upon TFE3 binding.

In skeletal muscle, TFE3 has demonstrated involvement in metabolic regulation. Overexpression of TFE3 was shown to increase endurance capacity and lysosomal biogenesis (22). Implications of TFE3 in mitochondrial-specific activity have also been suggested. TFE3 likely regulates PGC-1α, a key transcriptional regulator of mitochondrial biogenesis, as shown in a TFE3 knockdown model (23). Additionally, TFE3 knockout mice exhibit morphologically abnormal mitochondria and impaired glucose homeostasis and lipid metabolism (24). The same study also showed that exercise promoted nuclear localization of ectopically expressed TFE3 in mouse skeletal muscle. While literature suggests that TFE3 may be involved in mediating mitochondrial morphology and dynamics, the link between this transcription factor and the molecular mechanisms of mitochondrial turnover remain unknown.

In this study, the objective was to elucidate the role of TFE3 in exercise-mediated adaptations in skeletal muscle mitochondria. Wild-type (WT) and TFE3 knockout (KO) mice were subjected to a 6-week voluntary wheel running regimen to induce an endurance-trained phenotype. An acute bout of *in situ* stimulation of the sciatic nerve following the training program acted as a model of acute exercise and allowed for a measure of muscle function characteristics, including peak force production and fatigability. Further analyses were performed to understand the effect of TFE3 KO on mitochondrial function and content, lysosomal content, and autophagy and mitophagy flux. Our findings indicate that TFE3 KO mice were unable to improve fatigue resistance, enhance mitochondrial function, or increase mitochondrial content with training, as was observed in WT mice. Further, mitophagic responses to acute contractile activity were abolished in the absence of TFE3 with training. Therefore, our study highlights an important role for TFE3 in mitochondrial adaptations to endurance training, and the response to acute exercise.

METHODS

Animals. C57BL/6 and B6.129S1-Tfe3^{tm1Est}/Mmjax (TFE3 whole-body KO) mice were obtained from Jackson Laboratories. Animals were bred in accordance with the guidelines of the York University Animal Care Committee. Animals were genotyped by DNA extraction from ear clippings. DNA extracts were incubated with Jumpstart RED-Taq DNA polymerase (D8187, Sigma), and forward and reverse primers specific to the wild-type littermate control (WT) or mutant nucleotide sequences and were amplified by polymerase chain reaction. The products were separated on a 1.0% agarose gel and visualized with the use of ethidium bromide to distinguish between WT, KO, or heterozygous (HT) animals.

Voluntary wheel running. At 2.5 months of age, WT and TFE3 KO mice were age-matched and assigned to a control or running group. Mice were housed individually and kept on a 12:12-h light-

dark cycle. Food and water were provided ad libitum. Runners had access to a freely rotating wheel, and revolutions were recorded every 24 hours by a magnetic counter. The number of revolutions were converted into distance (kilometers). The training protocol consisted of a 1-week acclimatization period followed by 6 weeks of voluntary running. Animals that did not the running wheel during the acclimatization period were reassigned to the untrained group.

Autophagy and mitophagy pre-lysosomal flux measurements. To determine autophagy and mitophagy flux up to the point of lysosome delivery, mice were administered with sterile colchicine (0.4mg/kg/day; COL; C9754, Sigma) or 0.9% phosphate-buffered saline as vehicle (VEH) via intraperitoneal injections 24, 48, and 72 hours prior to *in situ* stimulation and tissue collection. Animals were randomly assigned to either treatment group. To determine flux, western blotting of p62 and LC3-II was performed in whole muscle and mitochondrial extracts (as described below). Protein abundance was quantified using ImageJ software (Version 1.53, NIH) and values were corrected to the loading controls. To calculate flux, saline values were subtracted from the corresponding colchicine values.

Acute in situ muscle stimulation. The right gastrocnemius muscle was attached to a force transducer via the Achilles tendon and the isolated sciatic nerve innervating the hindlimb muscles was stimulated at 10V. A temperature probe was inserted into the gastrocnemius muscle and a temperature of 37°C was maintained with heat lamps. Three single twitch contractions were analyzed for contractile properties, and maximum tetanic force was measured. To induce severe muscle fatigue, the nerve was stimulated at 0.1 tetanic contractions per second (TPS) for 30 minutes, then 3 minutes each at 0.25 TPS, 0.5 TPS, 1.0 TPS, 2.0 TPS, and 3.0 TPS. Throughout the protocol, PBS was periodically administered to maintain moisture of the muscle. The contractions were expressed as a percent of maximum force. Following the *in situ* stimulation, the

gastrocnemius was weighed and placed into ice-cold mitochondrial isolation buffer, and the tibialis anterior (TA) was quickly excised, weighed, and frozen in liquid nitrogen to be stored at -80°C.

Mitochondrial respiration and ROS. Permeabilized muscle fiber bundles were prepared from the medial portion of the TA. Fibers were mechanically separated on ice in BIOPS buffer (2.77mM CaK_2EGTA, 7.23mM K_2EGTA, 5.77mM Na_2ATP, 6.56mM $MgCl_2$ hexahydrate, 20mM Taurine, 15mM Na_2Phosphocreatine, 20mM Imidazole, 0.5mM Dithiothreitol, 50mM MES Hydrate), permeabilized in BIOPS with 40ug/uL Saponin at 4°C for 30 mins, and subsequently washed in Buffer Z (105mM K-MES, 30mM KCl, 10mM KH_2PO_4, 5mM $MgCl_2$ hexahydrate, 1mM EGTA, 5mg/mL BSA). Bundles were incubated in oxygenated Buffer Z supplemented with 1uM Blebbistatin (B592500, Toronto Research Chemicals) to prevent tetanus, 25U/mL Cu/Zn SOD1 to convert O_2 to H_2O_2, 10uM Amplex-Red (A36006, ThermoFisher) to measure ROS emission and 2mM EGTA. Substrates were then titrated in the following order: pyruvate-malate to assess complex I supported respiration, ADP to assess complex I active respiration, and succinate to assess complex I+II active respiration. Oxygen consumption and ROS emission was measured using high-resolution respirometry (Power Oxygraph 2K-Fluorespirometer, Oroboros Instruments).

Cytochrome C Oxidase (COX) activity. COX activity was used as an indicator of mitochondrial content. Frozen samples of the middle portion of the TA were used for this assay. Briefly, the muscle was lysed in enzyme extraction buffer using the Qiagen TissueLyser II and sonicated (3x3s, at 30% power). A buffered test solution with fully reduced horse heart cytochrome c (C-2506, Sigma) was prepared and combined with enzyme extracts in a 96-well plate. The maximal oxidation rate of fully reduced cytochrome c was measured by the absorbance at 550nm at 30°C using a microplate reader (Cytation 5, BioTek).

Whole muscle protein extracts. Frozen samples of the distal portion of the TA were used for whole muscle extracts. The muscle samples were snap frozen in liquid nitrogen following tissue collection and stored at -80°C. The tissue was lysed in Sakamoto buffer (20mM HEPES, 2 mM EGTA, 1% Triton X-100, 50% glycerol, 50 mM β-glycerophosphate) containing both phosphatase and protease inhibitors (P0044, Sigma; P5726, Sigma; 11-647-498-001, Roche) using metal beads and the Qiagen TissueLyser II at 30 Hz for 1 minute and repeated 3 times. Homogenates were centrifuged at 14,000g for 10 minutes, and supernatant fractions were collected as muscle extracts and stored at -80°C. The Bradford technique was used to determine protein content.

Mitochondrial fraction isolation. The whole gastrocnemius muscle was immediately minced on a glass plate over ice after tissue removal and homogenized. The homogenate was centrifuged at 1,200g for 15 minutes, and the supernate was collected and further centrifuged at 12,000g for 20 minutes. The pellets were resuspended in 100uL of mitochondrial isolation buffer and centrifuged again at 12,000g for 20 minutes. Finally, the mitochondrial pellets were resuspended in 40uL of mitochondrial isolation buffer and stored at -80°C. Protein concentration values of these crude mitochondria fractions was quantified using the Bradford method.

Immunoblotting. Whole muscle and mitochondrial extracts (25 ug) were separated using SDS-PAGE (12-15% polyacrylamide) and transferred to nitrocellulose membranes (Bio-Rad). Membranes were coated in Ponceau stain, imaged, and cut according to the molecular weight of each protein of interest. Blots were blocked in 5% milk at room temperature for an hour, then incubated overnight at 4°C with primary antibodies diluted in 5% skim milk in TBS-T (See Table 1 for a list of antibodies). Following the first incubation period, blots are incubated for 1 hour at room temperature with the appropriate horseradish peroxidase-conjugated secondary antibodies. The membranes are visualized using enhanced chemiluminescence (Clarity ECL Western blotting

substrates, 1705061, Bio-Rad) and an Invitrogen Imaging instrument (iBright CL1500 Imaging System, ThermoFisher). Images are quantified using ImageJ software (Version 1.53, NIH). Values are normalized to each protein's corresponding loading control.

Statistical analysis. All data were analyzed using Prism software (GraphPad 9.3.1) and values are reported as means ± SD. Student's t-tests were used to determine significant differences between genotypes. Two-way ANOVAs with Tukey posttest were conducted to assess effects of genotype and training. Three-way ANOVAs were used to analyze the response to stimulation between genotype and training. Statistical significance was set at $p<0.05$. N values listed represent total animals used per condition.

RESULTS

WT and TFE3 KO mice exhibit no differences in voluntary running behaviour. WT and KO animals were determined by DNA genotyping (Fig. 1A), and the KO model was further confirmed with an abolishment in TFE3 protein expression (Fig 1B, C). To investigate the effects of TFE3 on endurance training-induced adaptations in skeletal muscle, WT and TFE3 KO mice were trained for 6 weeks via voluntary wheel running. WT and TFE3 KO mice ran an average of 183km and 167km, respectively, over 6 weeks (Fig. 1D). There were no significant differences in running distances between WT and KO animals. Total body weight and individual hindlimb weights were measured following the 6 weeks of training. Body weight showed a trending effect of genotype and a significant effect of training, where voluntary wheel running reduced overall body weight (Fig. E). The GA, EDL, SOL, and combined hindlimb weights showed significant effects of genotype and training when corrected for body weight (Fig. 1F, H-J). These results may be attributed to the increased epididymal fat in KOs compared to WT animals and the seeming reduction in fat mass with training (Fig. B1).

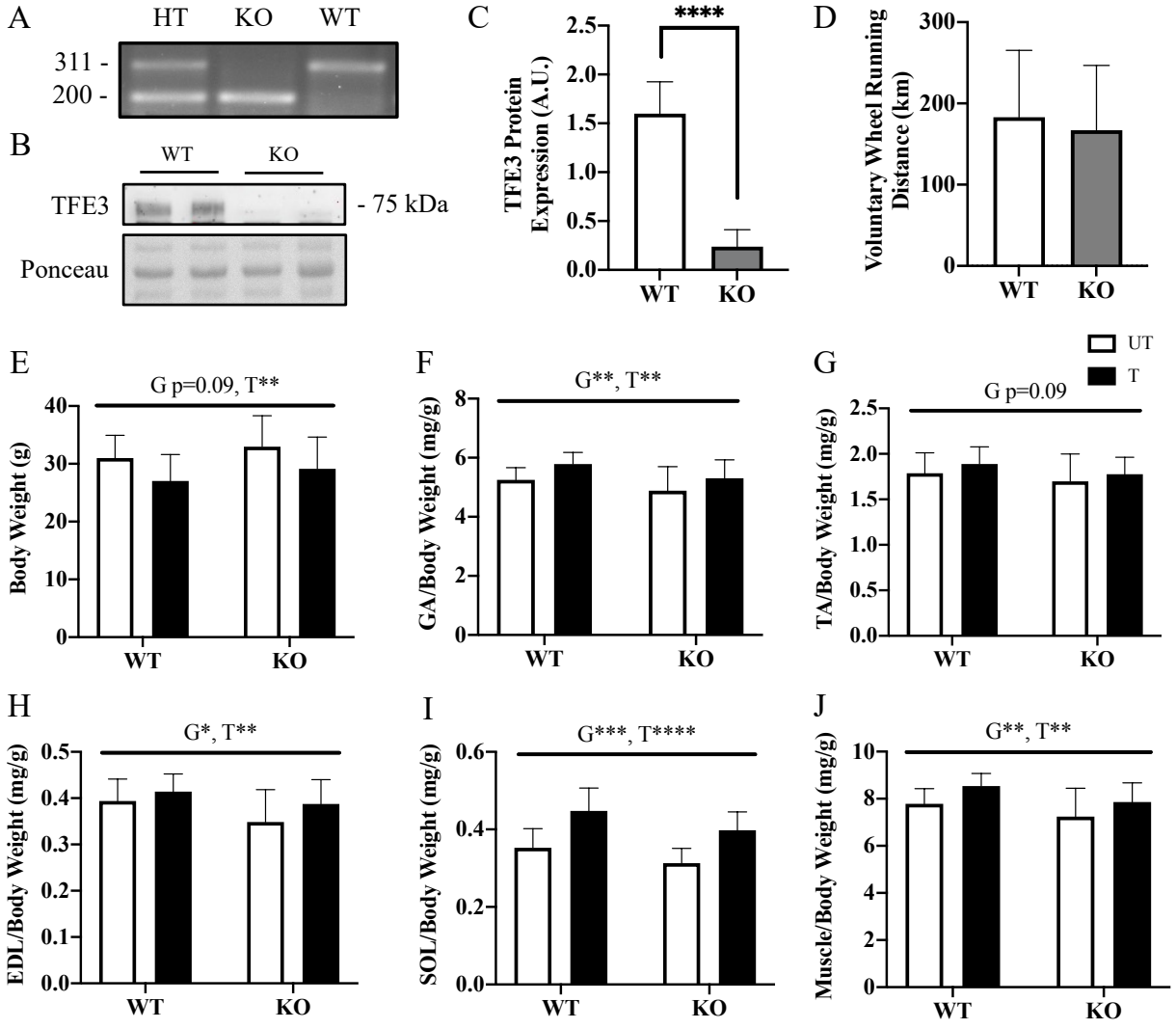

Fig 1. Phenotypic characteristics of WT and TFE3 KO mice. Confirmation of the TFE3 KO mouse model as performed by DNA genotyping targeting the WT and mutant knockout (KO) sequences of the TFE3 gene (A). Representative western blot of TFE3 protein expression (B). Graphical representation of TFE3 protein expression in WT and TFE3 KO animals (C) (n = 3-6). Total voluntary wheel running distances over the 6-week training period (D) (n = 13-14). Total body weight comparison between WT and KO animals with and without endurance training (E) (n = 13-21). Muscle weights of GA (F), TA (G), EDL (H), SOL (I), and hindlimb (J) corrected to body weight (n = 13-21). Weight measurements underwent two-way ANOVA, G, main effect of genotype; T, main effect of training; *, $p<0.05$; **, $p<0.01$; ***, $p<0.001$; ****, $p<0.0001$. GA, gastrocnemius; TA, tibialis anterior; EDL, extensor digitorum longus; SOL, soleus; UT, untrained; T, trained. Values are mean ± SD.

Muscle force production is not altered in the absence of TFE3. Prior to *in situ* stimulation, measurements of 3 twitch contractions and a tetanic contraction were collected to analyze contractile properties. Differences in these kinetic parameters may be indicative of differential muscle fiber type distribution. No significant differences were found for maximum tetanic force or maximum twitch force with training or between WT and KO mice (Fig. 2A). Time to peak tension and half-relaxation time were also unaffected by genotype or training states (Fig. 2B).

Training reduces fatigability in WT mice but not in the absence of TFE3. *In situ* stimulation of the sciatic nerve innervating the hindlimb muscles provided a means for fatigue and force analyses. Force was measured at 0 mins, 1 min, 2 mins, 3 mins, 5 mins, 10 mins, 20 mins, 30 mins, and every minute thereafter for the final 15 minutes of the protocol. Colchicine treatment did not affect force output over the 45 minutes (Fig. B2). Force production at these timepoints were converted to percent force of maximum (force at 0 mins). Trained WT mice better maintained force throughout the protocol compared to untrained WT mice, indicating increased resistance to fatigability with training (Fig. 2C). However, KO mice did not exhibit this same improved endurance with training (Fig. 2D). To further examine fatigue differences with genotype and training status, percent of maximum force was quantified at 5 mins (Fig. E), 10 mins (Fig. F), and 30 mins (Fig. 3G). At all three timepoints, trained WT mice exhibited a better maintenance of force and reduced fatigue not seen with KO animals, exhibited by a significant interaction effect of genotype and training. Trained WT mice presented a 13% increased force at 5 mins, a 19% increased force at 10 mins, and a 30% increased force at 30 mins over untrained mice. In contrast, force output was comparatively unchanged with training in the muscle of TFE3 KO mice.

Enhanced mitochondrial function with training is not observed in the absence of TFE3. Mitochondrial function was analyzed via high resolution respirometry to measure oxygen

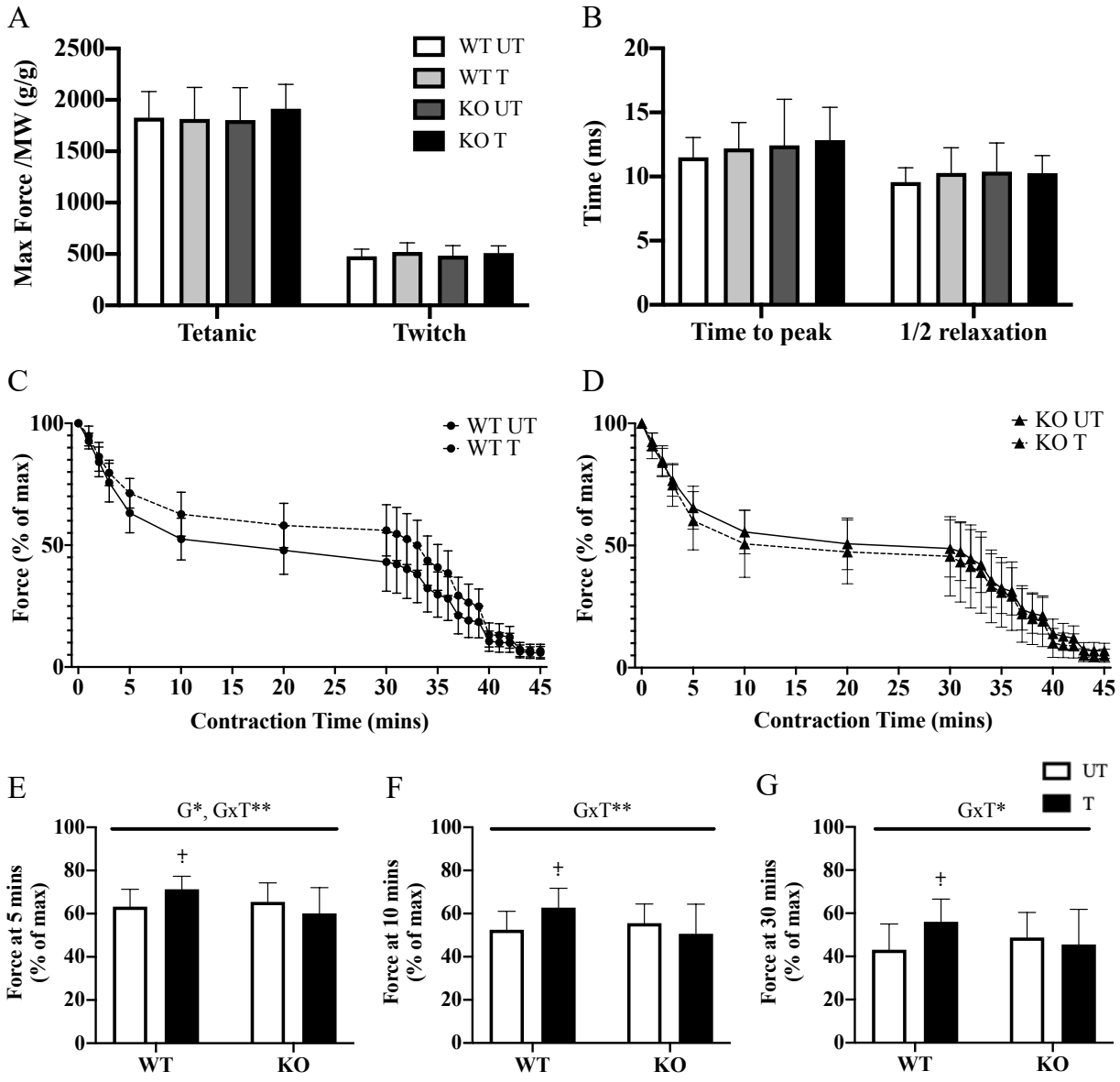

Fig 2. Twitch kinetics and fatigability of hindlimb muscles with acute contractile activity. Maximum tetanic and twitch forces corrected to muscle weight (A). Time to peak tension and ½ relaxation time (B). Force output of untrained and trained WT animals during the 45-minute contractile activity protocol (C). Force output of untrained and trained KO animals over the 45-minute contractile activity protocol (D). Graphical representation of the percent of maximum force at 5 minutes (E), 10 minutes (F), and 30 minutes (G) of electrical stimulation. Force at timepoints underwent two-way ANOVA with Tukey post-hoc tests, G, main effect of genotype; GxT, interaction effect of genotype and training; *, $p<0.05$; **, $p<0.01$; ǂ, $p<0.05$. UT, untrained; T, trained. N = 13-21. Values are mean ± SD.

consumption and ROS production in permeabilized fibers. Oxygen consumption supported by complex I, complex I in the presence of ADP, and complex I and II in the presence of ADP all exhibited a significant interaction effect between genotype and training (Fig. 3A-C). In complex I active and complex I and II active respiratory states, training significantly improved oxidative capacity in WT mice while trained KO mice showed a reduction in mitochondrial respiration compared to untrained animals. ROS emissions were unaffected by genotype and training (Fig. 3D-F).

Mitochondrial content is increased in trained WT mice. As mitochondrial content is known to increase with endurance training, COX enzymatic activity was measured to assess the effects of TFE3 in mediating this adaptation. A main effect of training was observed, where training significantly increased mitochondrial content in WT animals (Fig. 3G). Furthermore, trained WT mice exhibited a significantly higher percent increase above their untrained counterparts compared to KO mice (Fig 3H). Protein expression of mitochondrial markers was also evaluated to corroborate COX activity data (Fig I). An effect of training was seen in COX I protein expression, with a significant increase of this measure in trained WT mice vs. untrained mice (Fig. 3J). Similarly, there was a significantly higher fold change of protein expression of trained over untrained animals in WT mice compared to KO mice (Fig. 3K). Although no trend was detected in UQCRC2 protein expression between genotype or training (Fig. 3L), there was a significantly higher fold change between WT and KO animals with training (Fig. 3M). No differences were observed in VDAC and citrate synthase protein expression.

Training enhances lysosomal and autophagic machinery. Given that TFE3 is implicated in lysosomal regulation, we measured the expression of several lysosomal proteins (Fig. 4A). v-ATPase, a protein responsible for lysosomal acidification, showed a main effect of training (Fig.

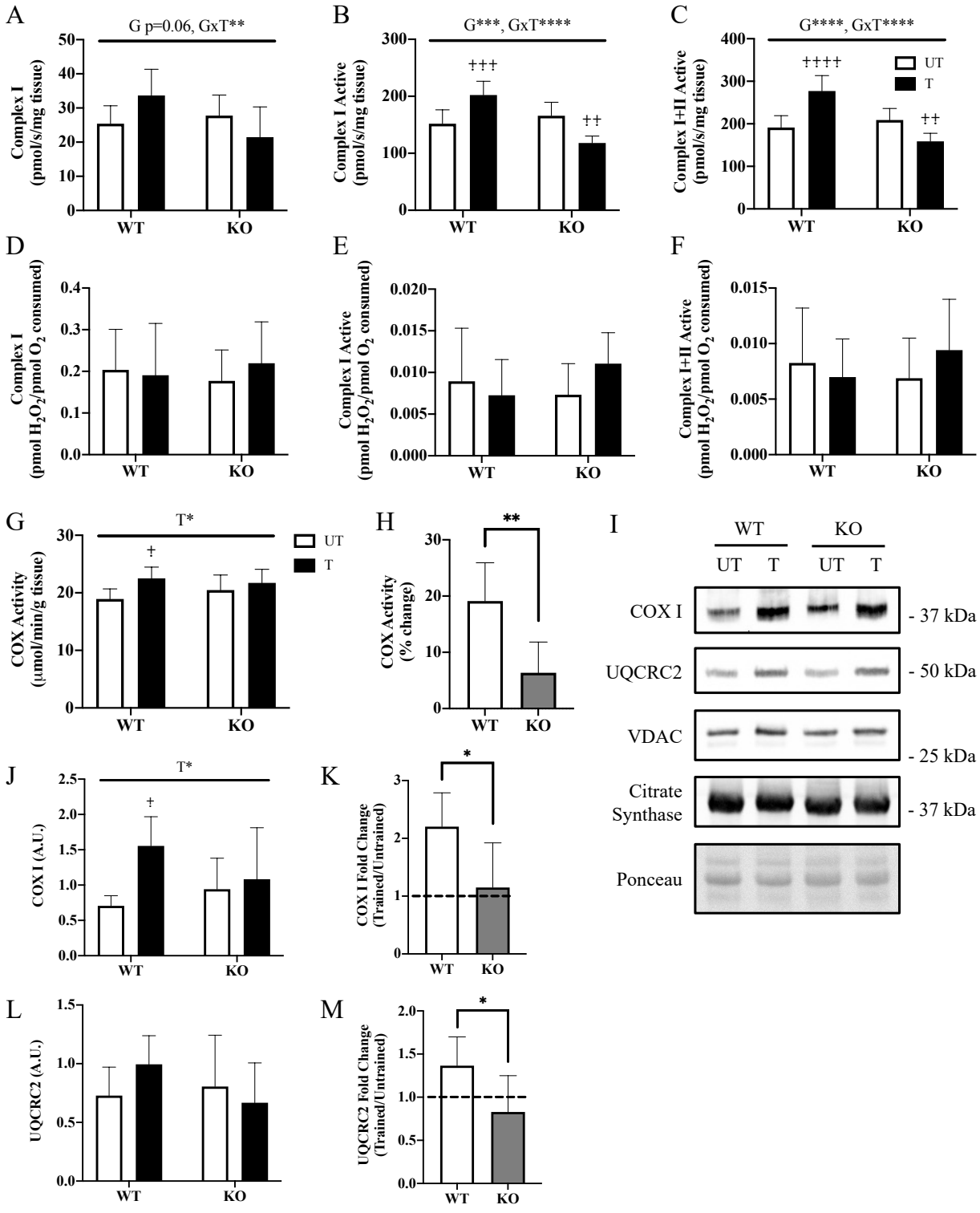
A
G p=0.06, GxT**
Complex I (pmol/s/mg tissue)
B
G***, GxT****
Complex I Active (pmol/s/mg tissue)
C
G****, GxT****
UT
T
Complex I+II Active (pmol/s/mg tissue)
D
Complex I (pmol H2O2/pmol O2 consumed)
E
Complex I Active (pmol H2O2/pmol O2 consumed)
F
Complex I+II Active (pmol H2O2/pmol O2 consumed)
G
T*
UT
T
COX Activity (µmol/min/g tissue)
H
**
COX Activity (% change)
I
WT
KO
UT
T
COX I
- 37 kDa
UQCRC2
- 50 kDa
VDAC
- 25 kDa
Citrate Synthase
- 37 kDa
Ponceau
J
T*
COX I (A.U.)
K
*
COX I Fold Change (Trained/Untrained)
L
UQCRC2 (A.U.)
M
*
UQCRC2 Fold Change (Trained/Untrained)
WT
KO

Fig 3. Mitochondrial adaptations to endurance training in WT and TFE3 KO animals. Oxygen consumption rates under complex I (A), complex I active (B), and complex I+II active (C) respiratory states (n = 7-9). ROS emission under complex I (D), complex I active (E), and complex I+II active (F) respiratory states (n = 6-9). Graphical representation of COX enzyme activity (A-B) (n = 6). Representative western blots of mitochondrial markers (C). Graphical representation of COX I (D-E) and UQCRC2 (F-G) (n.= 6). Two-way ANOVA between genotype and training with Tukey post-hoc tests, G, main effect of genotype; GxT, interaction effect of genotype and training; T, main effect of training; *, $p<0.05$; **, $p<0.01$; ***, $p<0.001$; ****, $p<0.0001$; ┼, $p<0.05$; ┼┼, $p<0.01$; ┼┼┼, $p<0.001$; ┼┼┼┼, $p<0.0001$. UT, untrained; T, trained. Values are mean ± SD.

4B). Cathepsins are ubiquitously distributed in lysosomes and are integral enzymes for lysosomal function. A main effect of training was seen in the presence of the mature and active form of Cathepsin D (Fig. 4D). However, the mature:total ratio of Cathepsin D, an indicator of its function, remained unchanged (Fig. 4E). No trends were observed in Cathepsin B for either mature protein content or mature:total expression (Fig. 4F, G). We also examined autophagy-related proteins (Fig. 4H). TFEB, a transcription factor holding similar functions to TFE3, exhibited a trending effect of training ($p=0.06$, Fig. 4I). Parkin, a key regulator of autophagy, also presented a trending effect of training ($p=0.09$, Fig. 4J). Surprisingly, there were no differences between WT and KO animals. mRNA expression of several lysosomal and autophagic genes were measured for untrained and trained mice of both genotypes (Fig. B3). However, there were no differences between any conditions.

Altered mitophagic response between WT and KO animals with in situ stimulation. To establish the role of TFE3 in mediating training-induced adaptations in exercise-induced mitophagy flux, mice were assigned to 6 weeks of voluntary wheel training followed by a bout of acute *in situ* stimulation. Immunoblots were organized as a full set of experimental conditions of either untrained or trained animals (Fig. 5A). Mitophagy flux was measured through the administration of either saline or colchicine, a microtubule depolarizing agent that inhibits autophagosomes from

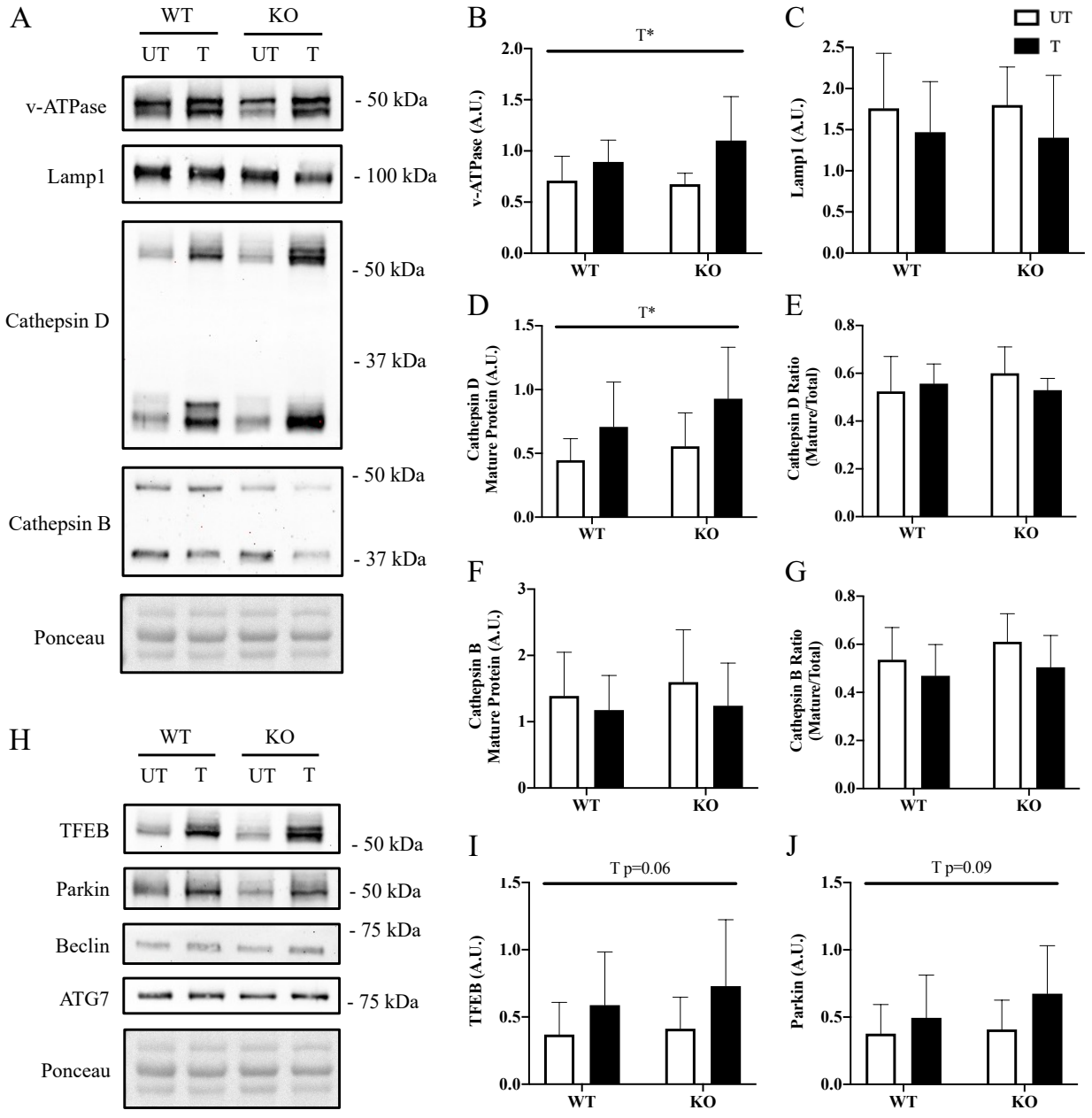

Fig 4. Lysosomal content adaptations to endurance training in WT and TFE3 KO animals. Representative western blots of lysosomal markers (A). Graphical representation of v-ATPase (B), Lamp1 (C), Cathepsin D (D-E), and Cathepsin B (F-G). Representative western blots of autophagy-related proteins (H). Graphical representation of TFEB (I) and Parkin (J). Two-way ANOVA between genotype and training, T, main effect of training; *, $p<0.05$; **, $p<0.01$. UT, untrained; T, trained. N = 6-8. Values are mean ± SD.

reaching lysosomes for contents to be recycled. Colchicine treatment results in a build-up of organelles and autophagy machinery markers, such as p62 and LC3-II, targeted for degradation. The difference in protein content of p62 and LC3-II between colchicine- and vehicle-treated animals in mitochondrial extracts is used to indicate mitophagy flux. In all animals, a main effect of stimulation was observed with p62 and LC3-II, signifying an induction of mitophagy flux with the exhaustive contractile activity (Fig. 5B, C). Additionally, there was a significant interaction effect of genotype and training, as well as an interaction effect between stimulation, genotype, and training. In untrained animals, mitophagy flux was significantly increased between control and stimulated muscle in KO mice indicating increased mitophagy with stimulation compared to WT mice. In trained animals, however, mitophagy was induced to a greater extent in WT mice compared to KO mice. Therefore, training resulted in a differential response to acute stimulation in the presence or absence of TFE3.

***No difference in autophagy flux with acute stimulation*.** Autophagy flux was measured similarly to mitophagy flux, following the 6-week training protocol and *in situ* stimulation. Immunoblots of whole muscle extract samples were organized as a full set of experimental conditions of either untrained or trained animals (Fig. 5D). Once again, flux was calculated as the difference in protein content of p62 and LC3-II between colchicine and vehicle animals. Measurements of p62 expression demonstrated a main effect of *in situ* stimulation, indicating an induction of autophagy (Fig. 5E). However, LC3-II flux data showed only a trending main effect of training and interaction effect of stimulation and genotype (Fig. 5F).

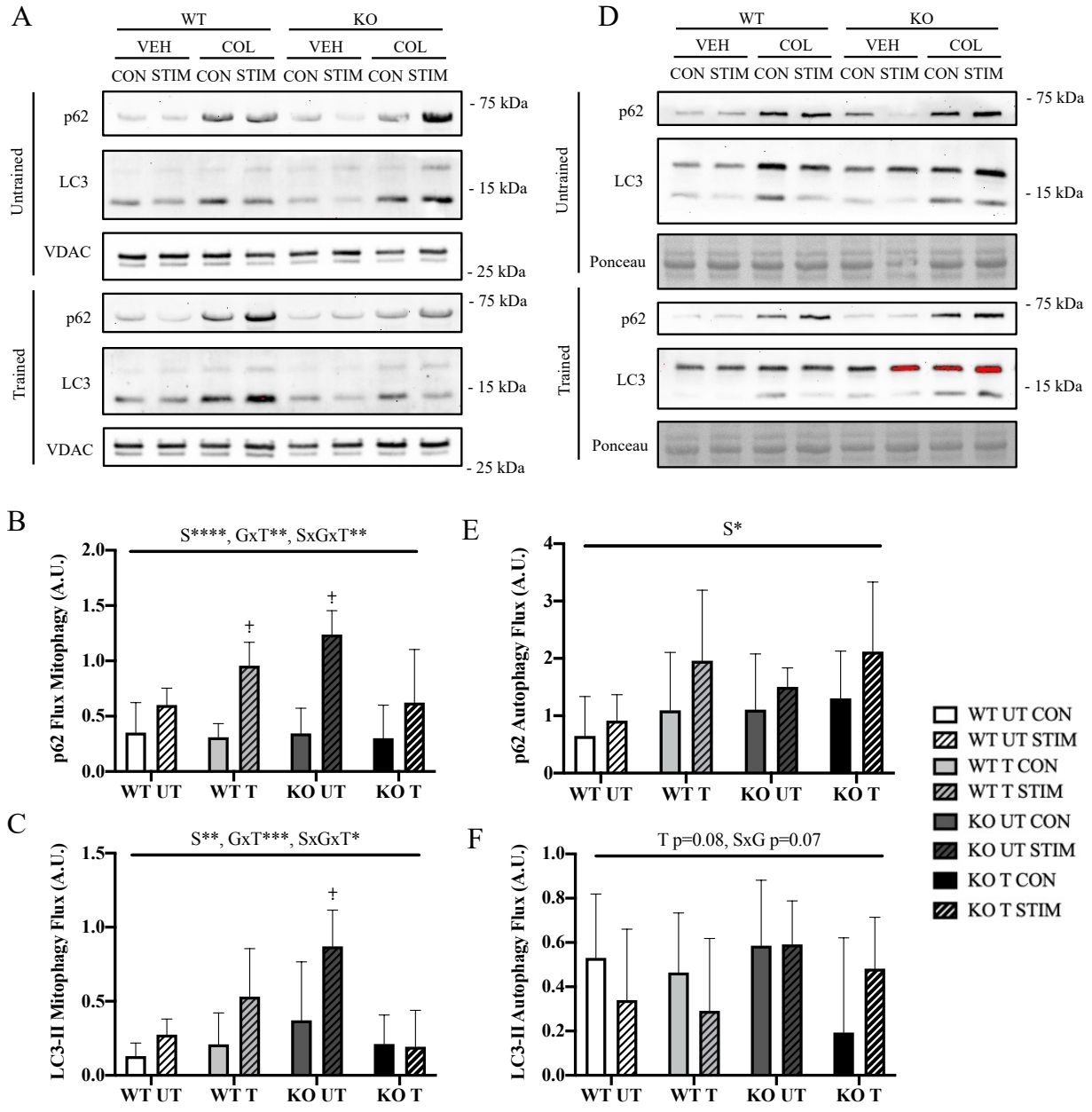

Fig 5. Autophagic adaptations of WT and KO animals with endurance exercise and acute electrical stimulation. Representative western blots of mitophagy flux (D) Graphical representation of p62 (E) and LC3-II (F) mitophagy flux. Representative western blots of autophagy flux (G) Graphical representation of p62 (H) and LC3-II (I) autophagy flux. Autophagic protein markers underwent two-way ANOVA, mitophagy and autophagy flux measurements underwent three-way ANOVA with Tukey posthoc tests, T, main effect of training; S, main effect of stimulation; GxT, interaction effect of genotype and training; SxGxT, interaction effect of stimulation, genotype, and training; SxG, interaction effect of stimulation and genotype; *, $p<0.05$; **, $p<0.01$; ***, $p<0.001$; ****, $p<0.0001$; ┼, $p<0.05$. UT, untrained; T, trained; VEH, saline-treated; COL, colchicine-treated; STIM, acute electrical stimulation. N = 5-6. Values are mean ± SD.

DISCUSSION

Endurance exercise is well known to have beneficial effects on skeletal muscle health, in part by improving mitochondrial content and oxidative capacity. The enhancement of the mitochondrial network is attributable to several transcriptional, translational, and post-translational events. However, details pertaining to the molecular regulation of this pathway remain incomplete. TFE3 is a transcription factor implicated in lysosomal biogenesis and the clearance of organelles through the autophagic pathway. The removal of dysfunctional mitochondria in this pathway has been suggested as an important process for skeletal muscle remodeling, however the specific role of TFE3 in mediating exercise-induced adaptations has not yet been elucidated. To understand the function of TFE3 in the skeletal muscle adaptive response to exercise, we trained WT and TFE3 KO mice for 6 weeks of voluntary wheel running, a stimulus known to induce increases in mitochondrial content (3, 5, 25). The training program was followed by an acute 45-minute *in situ* stimulation of the sciatic nerve to investigate fatigue, force production and contraction-induced mitophagy flux.

Basally, untrained WT and KO mice presented similar muscle characteristics. Contractile properties remained unaffected by genotype, signifying no differences in muscle quality and fiber types between WT and KO animals. We also did not observe differences in muscle fatigability, mitochondrial function, and mitochondrial content. The trending effects of genotype observed in body and muscle weights suggest increased adiposity in KO animals. This is validated by the increase in epididymal fat in TFE3 KO animals, and is consistent with a previous study presenting TFE3 KO mice with impaired lipid metabolism and increased fat mass (26).

As a supposed driver of lysosomal health and function (17), we aimed to better understand the importance of TFE3 in the maintenance of these organelles. Expression of lysosomal markers,

such as Cathepsin D and Lamp1, was unaffected by the absence of TFE3 at the mRNA and protein level. Other regulatory factors, such as TFEB, may therefore be sufficient to maintain baseline lysosomal content. The dynamic process of mitophagy flux was assessed through the injection of a saline control or colchicine, a microtubule destabilizing agent that prevents autophagosome maturation. The difference in protein content localized to mitochondria between colchicine- and saline-treated samples denoted mitophagy flux. Previous studies have shown that acute exercise is sufficient to induce mitophagy (11, 13). In line with the literature, *in situ* stimulation effectively prompted an increase in p62 and LC3-II mitophagic flux for both untrained WT and KO animals. In addition, a greater increase in p62 and LC3-II flux with contractile activity specific to TFE3 KO mice indicates that a greater sensitivity to acute exercise in the absence of TFE3. This challenged our initial hypothesis of reduced autophagy and mitophagy flux in response to exercise in muscle of TFE3 KO animals. It may be that the absence of TFE3 causes an overcompensatory response involving other MiT/TFE members, such as TFEB, to withstand the cellular stress. We did not observe an increase in TFEB protein content, however, an increase in TFEB activation and localization to the nucleus may explain this occurrence, as shown previously (27). Nonetheless, there is an indication that a lack of TFE3 alters normal pathway mechanisms with respect to mitochondrial clearance.

Endurance training is a known stimulus for muscle remodeling and quality improvement. In WT mice, maximum tetanic force and twitch kinetics were not changed with 6 weeks of voluntary wheel running, suggesting no fiber type shift. As expected, trained WT animals were less fatigued than untrained WT animals throughout the acute *in situ* stimulation protocol. Therefore, training successfully improved muscle endurance in WT mice. These results match previous studies that showed increased running distances to exhaustion in mice with endurance

training (3, 13), which is likely attributed to an enhancement of mitochondrial function and content with endurance training (4-8). Correspondingly, both oxygen consumption and markers of mitochondrial content increased with training in WT mice. Body weight was also reduced with training in conjunction with an increase in relative muscle weight. These changes are attributed to a reduction in adiposity as trained animals appear to have less epididymal fat, and muscle mass did not greatly change with training.

Contractile properties were unaltered with training in KO mice, similar to WT animals. However, many measures greatly deviated from the adaptations observed in WT animals. Trained TFE3 KO animals did not show improved endurance capacity compared to their untrained counterparts, as seen in WT mice. Mitochondrial function did not improve with training, and the organelles even demonstrated poorer quality compared to untrained animals as indicated by the significant decrease in oxygen consumption in trained KO animals. Mitochondrial content was also not improved in trained TFE3 KO mice. These results matched fatigue data trends, providing evidence for mitochondrial-driven adaptations to training that are dependent on the presence of TFE3. This signifies an inability of skeletal muscle to adapt to endurance exercise training with the abolition of TFE3 expression.

There is evidence that training may enhance the pool of lysosomal machinery and the cellular capacity to carry out autophagic functions (28, 29). Consistent with these finding, we found an increase in v-ATPase, Cathepsin D, TFEB, and Parkin protein expression in both trained WT and KO animals compared to their untrained counterparts. Literature has also suggested that endurance-trained animals demonstrate reduced mitophagy as training results in improved mitochondrial quality (13, 29). However, our data showed no difference in basal mitophagy levels with training. It is likely that the magnitude of the training-induced improvement in mitochondrial

content and function was insufficient to attenuate mitophagy signaling in resting muscle. Studies have also shown that the trained state also induces an attenuated mitophagic response to acute exercise (13). Unexpectedly, mitophagy was significantly induced in trained WT mice but mitophagy induction with acute stimulation was abolished with training in the absence of TFE3. In response to training, TFE3 must therefore drive an adaptive increase in the expression of lysosomal and mitophagy-related proteins that are critical to increase mitophagy flux in the presence of cellular stress. Although contrary to our initial hypothesis, this indicates a differential response to muscle stimulation in TFE3-null mice.

Both male and female mice were used in the study. Given the limited N of each group, data have not been stratified by sex. However, there is an increasing body of literature that reveals that males and females differentially adapt to stimuli and processes (30, 31). Recent work from our group has been shown that TFE3 plays divergent roles basally and in response to denervation with respect to sex (32). Future research is needed to examine sex differences pertaining to TFE3 and exercise adaptations.

In conclusion, our study suggests that TFE3 is a regulator of the adaptive improvements of skeletal muscle performance and mitochondrial function with endurance training. Basally, WT and TFE3 KO muscle exhibited similar muscle performance and mitochondrial capacity. However, the absence of TFE3 resulted in impaired muscle adaptations to training, characterized by an inability to mitigate fatigue during an acute bout of stimulation-induce contractile activity following 6 weeks of endurance exercise. This was associated with a lack of improvement of both mitochondrial content and oxidative capacity. Surprisingly, TFE3 did not affect the presence of lysosomal and autophagic machinery at a basal level. However, when subjected to acute contractile activity, TFE3 KO animals displayed a differential mitophagic response in the untrained and

trained states. This work will further our understanding of the role of TFE3 in mitochondrial mechanisms underlying training adaptations, and may establish this transcription factor as a potential therapeutic target.

ACKNOWLEDGEMENTS

This work was supported by funding from the Natural Sciences and Engineering Research Council of Canada (NSERC) to D.A. Hood. D.A. Hood is also the holder of a Canada Research Chair in Cell Physiology. J.C. Wong is the recipient of the Ontario Graduate Scholarship.

REFERENCES

1. Hood DA, Memme JM, Oliveira AN, Triolo M. Maintenance of skeletal muscle mitochondrial in health, exercise, and aging. *Annu Rev Physiol* 81: 19-41, 2019. doi: 10.1146/annurev-physiol-020518-114310.
2. Egan B, Zierath JR. Exercise metabolism and the molecular regulation of skeletal muscle adaptation. *Cell Metab* 17(2):162-84, 2013. doi: 10.1016/j.cmet.2012.12.012.
3. Crilly MJ, Tryon LD, Erlich AT, Hood DA. The role of Nrf2 in skeletal muscle contractile and mitochondrial function. *J Appl Physiol* 121(3):730-40, 2016. doi: 10.1152/japplphysiol.00042.2016.
4. Davies KJ, Packer L, Brooks GA. Biochemical adaptation of mitochondria, muscle, and whole-animal respiration to endurance training. *Arch Biochem Biophys* 209(2):539-54, 1981. doi: 10.1016/0003-9861(81)90312-x.
5. Menzies KJ, Singh K, Saleem A, Hood DA. Sirtuin 1-mediated effects of exercise and resveratrol on mitochondrial biogenesis. *J Biol Chem* 288(10):6968-79, 2013. doi: 10.1074/jbc.M112.431155.
6. Carter HN, Pauly M, Tryon LD, Hood DA. Effect of contractile activity on PGC-1α transcription in young and aged skeletal muscle. *J Appl Physiol* 124(6):1605-1615, 2018. doi: 10.1152/japplphysiol.01110.2017.
7. Dudley GA, Tullson PC, Terjung RL. Influence of mitochondrial content on the sensitivity of respiratory control. *J Biol Chem* 262(19):9109-14, 1987.
8. Constable SH, Favier RJ, McLane JA, Fell RD, Chen M, Holloszy JO. Energy metabolism in contracting rat skeletal muscle: adaptation to exercise training. *Am J Physiol* 253(2 Pt 1):C316-22, 1987. doi: 10.1152/ajpcell.1987.253.2.C316.
9. Ashrafi G, Schwarz TL. The pathways of mitophagy for quality control and clearance of mitochondria. *Cell Death Differ* 20(1):31-42, 2013. doi: 10.1038/cdd.2012.81.
10. Quinlan CL, Perevoshchikova IV, Hey-Mogensen M, Orr AL, Brand MD. Sites of reactive oxygen species generation by mitochondria oxidizing different substrates. *Redox Biol* 1(1):304-12, 2013. doi: 10.1016/j.redox.2013.04.005.
11. Vainshtein A, Tryon LD, Pauly M, Hood DA. Role of PGC-1α during acute exercise-induced autophagy and mitophagy in skeletal muscle. *Am J Physiol Cell Physiol* 308(9):C710-9, 2015. doi: 10.1152/ajpcell.00380.2014.
12. Guan Y, Drake JC, Yan Z. Exercise-Induced Mitophagy in Skeletal Muscle and Heart. *Exerc Sport Sci Rev* 47(3):151-156, 2019. doi: 10.1249/JES.0000000000000192.
13. Chen CCW, Erlich AT, Hood DA. Role of Parkin and endurance training on mitochondrial turnover in skeletal muscle. *Skelet Muscle* 8(10) 2018. https://doi.org/10.1186/s13395-018-0157-y.
14. Wu JJ, Quijano C, Chen E, Liu H, Cao L, Fergusson MM, Rovira II, Gutkind S, Daniels MP, Komatsu M, Finkel T. Mitochondrial dysfunction and oxidative stress mediate the physiological impairment induced by the disruption of autophagy. *Aging* 1(4):425-37, 2009. doi: 10.18632/aging.100038.
15. Furuya N, Ikeda S, Sato S, Soma S, Ezaki J, Oliva Trejo JA, Takeda-Ezaki M, Fujimura T, Arikawa-Hirasawa E, Tada N, Komatsu M, Tanaka K, Kominami E, Hattori N, Ueno T. PARK2/Parkin-mediated mitochondrial clearance contributes to proteasome activation during slow-twitch muscle atrophy via NFE2L1 nuclear translocation. *Autophagy* 10(4):631-41, 2014. doi: 10.4161/auto.27785.

16. Raben N, Wong A, Ralston E, Myerowitz R. Autophagy and mitochondria in Pompe disease: nothing is so new as what has long been forgotten. *Am J Med Genet C Semin Med Genet* 160C(1):13-21, 2012. doi: 10.1002/ajmg.c.31317.
17. Martina JA, Diab HI, Lishu L, Jeong-A L, Patange S, Raben N, Puertollano R. The nutrient-responsive transcription factor TFE3 promotes autophagy, lysosomal biogenesis, and clearance of cellular debris. *Sci Signal* 7(309):ra9, 2014. doi: 10.1126/scisignal.2004754.
18. Raben N, Puertollano R. TFEB and TFE3: Linking Lysosomes to Cellular Adaptation to Stress. *Annu Rev Cell Dev Biol* 32:255-278, 2016. doi: 10.1146/annurev-cellbio-111315-125407.
19. Sardiello M, Palmieri M, di Ronza A, Medina DL, Valenza M, Gennarino VA, Di Malta C, Donaudy F, Embrione V, Polishchuk RS, Banfi S, Parenti G, Cattaneo E, Ballabio A. A gene network regulating lysosomal biogenesis and function. *Science* 325(5939):473-7, 2009. doi: 10.1126/science.1174447.
20. Paquette M, El-Houjeiri L, C Zirden L, Puustinen P, Blanchette P, Jeong H, Dejgaard K, Siegel PM, Pause A. AMPK-dependent phosphorylation is required for transcriptional activation of TFEB and TFE3. *Autophagy* 17(12):3957-3975, 2021. doi: 10.1080/15548627.2021.1898748.
21. Markby GR, Sakamoto K. Transcription factor EB and TFE3: new metabolic coordinators mediating adaptive responses to exercise in skeletal muscle? *Am J Physiol Endocrinol Metab* 319(4):E763-E768, 2020. doi: 10.1152/ajpendo.00339.2020.
22. La Spina M, Contreras PS, Rissone A, Meena NK, Jeong E, Martina JA. MiT/TFE Family of Transcription Factors: An Evolutionary Perspective. *Front Cell Dev Biol* 8:609683, 2021. doi: 10.3389/fcell.2020.609683.
23. Iwasaki H, Naka A, Iida KT, Nakagawa Y, Matsuzaka T, Ishii KA, Kobayashi K, Takahashi A, Yatoh S, Yahagi N, Sone H, Suzuki H, Yamada N, Shimano H. TFE3 regulates muscle metabolic gene expression, increases glycogen stores, and enhances insulin sensitivity in mice. *Am J Physiol Endocrinol Metab* 302(7):E896-902, 2012. doi: 10.1152/ajpendo.00204.2011.
24. Salma N, Song JS, Arany Z, Fisher DE. Transcription Factor Tfe3 Directly Regulates Pgc-1alpha in Muscle. *J Cell Physiol* 230(10):2330-6, 2015. doi: 10.1002/jcp.24978.
25. Saleem A, Adhihetty PJ, Hood DA. Role of p53 in mitochondrial biogenesis and apoptosis in skeletal muscle. *Physiol Genomics* 37(1):58-66, 2009. doi: 10.1152/physiolgenomics.90346.2008.
26. Pastore N, Vainshtein A, Klisch TJ, Armani A, Huynh T, Herz NJ, Polishchuk EV, Sandri M, Ballabio A. TFE3 regulates whole-body energy metabolism in cooperation with TFEB. *EMBO Mol Med* 9(5):605-621, 2017. doi: 10.15252/emmm.201607204.
27. Erlich AT, Brownlee DM, Beyfuss K, Hood DA. Exercise induces TFEB expression and activity in skeletal muscle in a PGC-1α-dependent manner. *Am J Physiol Cell Physiol* 314(1):C62-C72, 2018. doi: 10.1152/ajpcell.00162.2017.
28. Kim Y, Hood DA. Regulation of the autophagy system during chronic contractile activity-induced muscle adaptations. *Physiol Rep* 5(14):e13307, 2017. doi: 10.14814/phy2.13307.
29. Carter HN, Kim Y, Erlich AT, Zarrin-Khat D, Hood DA. Autophagy and mitophagy flux in young and aged skeletal muscle following chronic contractile activity. *J Physiol* 596(16):3567-3584, 2018. doi: 10.1113/JP275998.
30. Farhat F, Amérand A, Simon B, Guegueniat N, Moisan C. Gender-dependent differences of mitochondrial function and oxidative stress in rat skeletal muscle at rest and after exercise training. *Redox Rep* 22(6):508-514, 2017. doi: 10.1080/13510002.2017.1296637.

31. Triolo M, Oliveira AN, Kumari R, Hood DA. The influence of age, sex, and exercise on autophagy, mitophagy, and lysosome biogenesis in skeletal muscle. *Skelet Muscle* 12(1):13, 2022. doi: 10.1186/s13395-022-00296-7.
32. Oliveira AN, Memme JM, Wong JC, Hood DA. Dimorphic Effect of TFE3 in Determining Mitochondrial and Lysosomal Content in Muscle Following Denervation. *Submitted to Skeletal Muscle*, 2023.

FUTURE DIRECTIONS

1. Evaluating the role of TFE3 on lysosomal function may resolve the differences seen in mitophagic responses given the absence of discrepancy in lysosomal content.
2. Exploring the interactions of TFE3 and other transcription factors, such as TFEB, with exercise. For example, nuclear localization and homo/heterodimerization of TFE3 and TFEB could be measured to demonstrate the role and cooperation of these transcription factors with this particular stressor.
3. Examining the effects of a muscle-specific TFE3 KO on training adaptations. It is clear from other studies that TFE3 contributes to whole-body effects, influencing lipid and liver metabolism. A muscle-specific KO model would aid in isolating the role of TFE3 in skeletal muscle mitochondrial responses to exercise training.
4. Stratifying the effects of TFE3 on exercise adaptations by sex. The emerging evidence that TFE3 evokes differential responses on mitochondrial and lysosomal function places significance on this area of study. It will be beneficial to further investigate the potential sex differences in TFE3 mechanisms.

APPENDIX A: SAMPLE DATA AND STATISTICAL ANALYSES

Table A1. TFE3 Protein Expression.

	TFE3 Protein (A.U.)	
N	**WT**	**KO**
1	1.99	0.11
2	1.70	0.12
3	2.25	0.66
4	1.52	0.16
5	1.26	0.09
6	1.51	0.24
7	1.58	0.25
8	1.80	0.21
9	1.40	0.30
10	1.79	
11	1.15	
12	1.24	
X	1.60	0.24
SD	0.325305131	0.173956749

UNPAIRED T-TEST: WT vs. KO	
P value	<0.0001
P value summary	****
Significantly different (P < 0.05)?	Yes

Table A2. Voluntary Wheel Running Distances.

	VWR DISTANCE (km)	
N	**WT**	**KO**
1	121.72	134.04
2	189.71	117.10
3	106.06	125.30
4	188.96	159.34
5	118.95	101.73
6	106.30	189.63
7	229.89	156.41
8	285.36	110.34
9	255.13	386.73
10	113.10	203.74
11	308.48	157.90
12	184.66	112.55
13	350.88	
14	151.50	
X	193.62	162.90
SD	81.26330092	77.42793247

UNPAIRED T-TEST: WT vs. KO	
P value	0.3355
P value summary	ns
Significantly different (P < 0.05)?	No

Table A3. Animal Body Weights.

	BODY WEIGHT (g)			
	WT		KO	
N	UT	T	UT	T
1	29.5	30.3	29.9	33.3
2	30.1	33.7	34.2	29.1
3	27.2	28.4	43.4	42.3
4	28	30.5	28.8	31.4
5	35.3	25.4	33.2	31.2
6	33.1	29	27.7	29.7
7	35.2	30.3	26.7	22.7
8	34.3	34.9	30.8	31.2
9	30.5	24.7	42.7	20.5
10	35.3	*21.5*	34.3	23.7
11	32.2	23.4	32.9	26.9
12	30.9	21.8	29.1	27.1
13	37.1	21	32.9	29.8
14	31.8	23.7	30.2	
15	31.5		32.9	
16	34.3		30.6	
17	34.1		*31.5*	
18	22.5		38.9	
19	24		45.3	
20	27		28.8	
21	27.4		27.3	
X	31.014286	27.042857	32.957143	29.146154
SD	3.9174336	4.5763126	5.3505674	5.4751888

2-WAY ANOVA			
Source of Variation	P value	P value summary	Significant?
Interaction	0.9465	ns	No
Genotype	0.0939	ns	No
Training	0.0017	**	Yes

POST-HOC TEST				
Tukey	Mean difference	Significant?	P value summary	Adjusted P value
WT:UT vs. WT:T	3.971	No	ns	0.0897
WT:UT vs. KO:UT	-1.943	No	ns	0.5628
WT:UT vs. KO:T	1.868	No	ns	0.6922
WT:T vs. KO:UT	-5.914	Yes	**	0.0039
WT:T vs. KO:T	-2.103	No	ns	0.671
KO:UT vs. KO:T	3.811	No	ns	0.1235

Table A4. GA/Body Weights.

	GA/BW WEIGHT (mg/g)			
	WT		KO	
N	UT	T	UT	T
1	5.29	5.58	5.34	4.65
2	5.61	5.18	4.95	5.71
3	5.32	5.54	3.80	4.29
4	5.56	5.93	5.16	*5.92*
5	5.57	6.10	5.07	5.42
6	5.28	6.15	6.27	5.65
7	5.03	5.18	5.73	6.18
8	4.81	5.26	4.92	4.69
9	5.12	5.59	4.03	6.02
10	4.76	*5.92*	5.35	5.78
11	5.30	6.24	4.59	4.65
12	5.96	6.25	5.16	5.08
13	4.57	5.85	5.02	4.93
14	4.96	6.22	5.62	
15	5.49		5.93	
16	5.20		5.55	
17	4.33		*3.85*	
18	5.73		3.36	
19	5.77		3.38	
20	5.03		4.73	
21	5.53		4.83	
X	5.2485639	5.7851602	4.887591	5.3046924
SD	0.4135115	0.3942413	0.8075516	0.621347

2-WAY ANOVA			
Source of Variation	P value	P value summary	Significant?
Interaction	0.9465	ns	No
Genotype	0.0939	ns	No
Training	0.0017	**	Yes

POST-HOC TEST				
Tukey	Mean difference	Significant?	P value summary	Adjusted P value
WT:UT vs. WT:T	-0.5366	No	ns	0.0536
WT:UT vs. KO:UT	0.361	No	ns	0.2132
WT:UT vs. KO:T	-0.05616	No	ns	0.9933
WT:T vs. KO:UT	0.8976	Yes	***	0.0003
WT:T vs. KO:T	0.4805	No	ns	0.1666
KO:UT vs. KO:T	-0.4171	No	ns	0.2053

Image A1. Example Force Tracing of the *In Situ* Protocol.

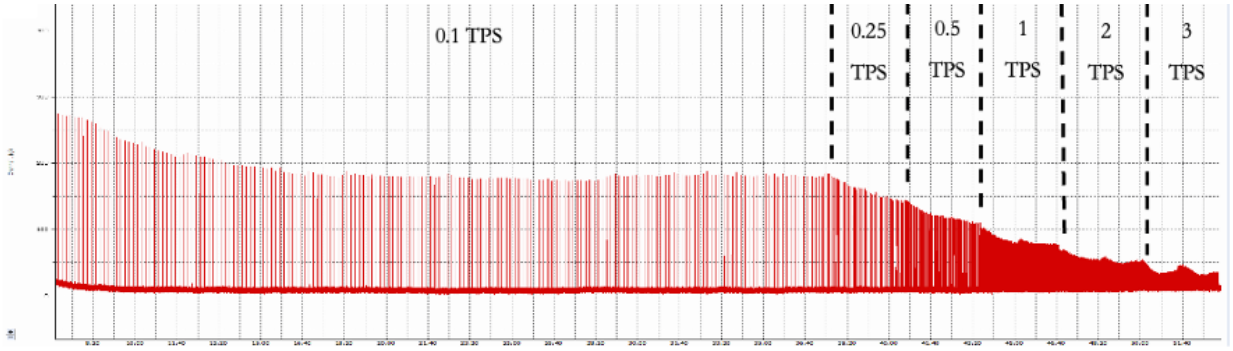

Table A5. Fatigue at 5 mins.

	FORCE AT 5 MINS (% OF MAX)			
	WT		KO	
N	UT	T	UT	T
1	61.08	76.42	66.49	45.31
2	57.29	74.33	55.56	63.15
3	63.08	74.20	57.58	59.92
4	68.11	70.00	61.07	*76.72*
5	70.26	66.87	79.34	57.01
6	69.78	80.85	72.48	68.10
7	71.88	80.14	66.73	48.51
8	54.69	69.29	66.01	60.45
9	65.56	70.04	59.67	36.24
10	62.31	60.63	61.32	73.95
11	67.67	68.41	59.00	57.55
12	57.99	61.91	60.88	75.08
13	62.75	75.95	73.47	59.74
14	54.98	68.91	60.08	
15	63.61		55.30	
16	64.50		66.32	
17	78.25		68.09	
18	42.66		80.54	
19	50.99		84.95	
20	70.96		54.53	
21	69.22		59.63	
X	63.2221323	71.2806902	65.1920177	60.1330316
SD	8.12869036	6.06241891	8.6625872	11.9184688

2-WAY ANOVA			
Source of Variation	P value	P value summary	Significant?
Interaction	0.0035	**	Yes
Genotype	0.0379	*	Yes
Training	0.491	ns	No

POST-HOC TEST				
Tukey	Mean difference	Significant?	P value summary	Adjusted P value
WT:UT vs. WT:T	-8.059	Yes	*	0.047
WT:UT vs. KO:UT	-1.97	No	ns	0.8858
WT:UT vs. KO:T	3.089	No	ns	0.7513
WT:T vs. KO:UT	6.089	No	ns	0.1945
WT:T vs. KO:T	11.15	Yes	**	0.0084
KO:UT vs. KO:T	5.059	No	ns	0.3672

Table A6. Fatigue at 10 mins.

	FORCE AT 10 MINS (% OF MAX)			
	WT		KO	
N	UT	T	UT	T
1	46.53	65.55	64.86	38.98
2	51.62	63.12	36.93	54.78
3	58.94	69.58	46.73	51.16
4	52.09	51.35	58.48	69.93
5	58.91	64.20	70.14	49.09
6	49.06	76.29	59.45	57.37
7	62.95	72.79	62.43	31.69
8	38.77	58.82	64.66	51.77
9	49.12	59.21	48.53	24.61
10	47.71	57.04	54.95	66.67
11	58.59	57.72	51.78	44.93
12	44.48	49.33	51.64	69.36
13	49.76	78.50	64.23	48.45
14	46.17	54.52	44.95	
15	55.71		47.61	
16	58.98		60.15	
17	73.11		53.23	
18	40.75		68.83	
19	40.61		55.84	
20	57.15		45.31	
21	61.20		50.76	
X	52.4862632	62.7155744	55.3090956	50.6761866
SD	8.56014665	8.99797722	8.76750175	13.7097415

2-WAY ANOVA			
Source of Variation	P value	P value summary	Significant?
Interaction	0.0033	**	Yes
Genotype	0.0625	ns	No
Training	0.254	ns	No

POST-HOC TEST				
Tukey	Mean difference	Significant?	P value summary	Adjusted P value
WT:UT vs. WT:T	-10.23	Yes	*	0.0191
WT:UT vs. KO:UT	-2.823	No	ns	0.7898
WT:UT vs. KO:T	1.81	No	ns	0.9539
WT:T vs. KO:UT	7.406	No	ns	0.1401
WT:T vs. KO:T	12.04	Yes	*	0.0121
KO:UT vs. KO:T	4.633	No	ns	0.546

Table A7. Fatigue at 30 mins.

	FORCE AT 30 MINS (% OF MAX)			
	WT		KO	
N	UT	T	UT	T
1	20.64	60.09	42.46	21.45
2	57.42	60.92	34.51	49.45
3	33.56	49.60	29.53	50.61
4	44.62	44.13	59.16	56.38
5	43.81	60.15	66.66	46.42
6	45.64	66.75	53.33	45.28
7	54.74	63.52	59.78	24.29
8	30.07	59.13	48.88	49.07
9	45.07	59.12	45.31	17.88
10	39.99	*50.26*	53.35	60.53
11	51.82	53.11	48.28	37.81
12	27.36	31.65	43.96	64.27
13	48.49	74.82	63.49	69.14
14	39.36	51.92	43.51	
15	53.95		35.86	
16	50.17		51.16	
17	61.32		*59.09*	
18	18.14		67.55	
19	37.81		28.80	
20	58.08		40.65	
21	42.89		46.21	
X	43.0925141	56.0837701	48.6435348	45.5833625
SD	11.9792128	10.5106091	11.3717891	16.2279344

2-WAY ANOVA			
Source of Variation	P value	P value summary	Significant?
Interaction	0.0111	*	Yes
Genotype	0.423	ns	No
Training	0.1105	ns	No

POST-HOC TEST				
Tukey	Mean difference	Significant?	P value summary	Adjusted P value
WT:UT vs. WT:T	-12.99	Yes	*	0.0181
WT:UT vs. KO:UT	-5.551	No	ns	0.4756
WT:UT vs. KO:T	-2.491	No	ns	0.9414
WT:T vs. KO:UT	7.44	No	ns	0.3147
WT:T vs. KO:T	10.5	No	ns	0.1362
KO:UT vs. KO:T	3.06	No	ns	0.8978

Table A8. Complex I+II Active Oxygen Consumption.

	COMPLEX I+II ACTIVE O_2 CONSUMPTION			
	WT		KO	
N	UT	T	UT	T
1	229.3268	318.7664	219.3208	135.8302
2	222.1376	336.9656	241.572	135.1833
3	200.9642	258.387	229.7678	162.0799
4	201.6289	273.512	227.1992	164.7463
5	185.0951	250.1532	197.1094	177.0259
6	177.2322	256.361	225.4407	184.2743
7	167.653	246.1603	153.9824	151.5381
8	139.3889		197.5865	
9	198.2145		187.42412	
X	191.29347	277.1865	208.82255	158.66829
SD	27.693038	36.047371	27.30405	18.996551

2-WAY ANOVA			
Source of Variation	P value	P value summary	Significant?
Interaction	<0.0001	****	Yes
Genotype	<0.0001	****	Yes
Training	0.0849	ns	No

POST-HOC TEST				
Tukey	Mean difference	Significant?	P value summary	Adjusted P value
WT:UT vs. WT:T	-85.89	Yes	****	<0.0001
WT:UT vs. KO:UT	-17.53	No	ns	0.5554
WT:UT vs. KO:T	32.63	No	ns	0.1207
WT:T vs. KO:UT	68.36	Yes	***	0.0002
WT:T vs. KO:T	118.5	Yes	****	<0.0001
KO:UT vs. KO:T	50.15	Yes	**	0.0072

Table A9. Complex I+II Active ROS Consumption.

	COMPLEX I+II ACTIVE ROS EMISSION			
	WT		KO	
N	UT	T	UT	T
1	0.009657	0.011921	0.005938	0.011446
2	0.002632	0.00735	0.003439	0.016907
3	0.008166	0.002876	0.0098803	0.005361
4	0.003832	0.009824	0.010509	0.012424
5	0.002822	0.004201	0.00218	0.005752
6	0.005495	0.005733	0.011125	0.004317
7	0.016072		0.0051551	0.009697
8	0.011449			
9	0.0141395			
X	0.0082516	0.0069842	0.0068895	0.0094149
SD	0.0049526	0.0034281	0.0036052	0.0045686

2-WAY ANOVA			
Source of Variation	P value	P value summary	Significant?
Interaction	0.249	ns	No
Genotype	0.7423	ns	No
Training	0.6988	ns	No

POST-HOC TEST				
Tukey	Mean difference	Significant?	P value summary	Adjusted P value
WT:UT vs. WT:T	0.001267	No	ns	0.9424
WT:UT vs. KO:UT	0.001362	No	ns	0.9209
WT:UT vs. KO:T	-0.001163	No	ns	0.9486
WT:T vs. KO:UT	0.00009468	No	ns	>0.9999
WT:T vs. KO:T	-0.002431	No	ns	0.7391
KO:UT vs. KO:T	-0.002525	No	ns	0.6907

Table A10. COX Activity.

	COX ACTIVITY			
	WT		KO	
N	UT	T	UT	T
1	19.58	24.79	19.96	19.69
2	20.85	23.76	22.84	24.32
3	17.63	22.68	19.99	22.21
4	17.15	19.81	17.28	19.55
5	20.95	23.57	24.28	24.71
6	17.49	20.54	18.58	19.90
X	18.940555	22.522993	20.48767	21.729467
SD	1.7421727	1.9523878	2.6214092	2.369205

2-WAY ANOVA			
Source of Variation	P value	P value summary	Significant?
Interaction	0.207	ns	No
Genotype	0.6791	ns	No
Training	0.0142	*	Yes

POST-HOC TEST				
Tukey	Mean difference	Significant?	P value summary	Adjusted P value
WT:UT vs. WT:T	-3.582	Yes	*	0.0476
WT:UT vs. KO:UT	-1.547	No	ns	0.6225
WT:UT vs. KO:T	-2.789	No	ns	0.1581
WT:T vs. KO:UT	2.035	No	ns	0.3991
WT:T vs. KO:T	0.7935	No	ns	0.9228
KO:UT vs. KO:T	-1.242	No	ns	0.7631

Table A11. Corresponding Fold-Above-Control for COX Activity.

	COX ACTIVITY (% change)	
N	**WT**	**KO**
1	26.56	-1.36
2	13.92	6.46
3	28.67	11.08
4	15.52	13.14
5	12.49	1.79
6	17.47	7.11
X	19.11	6.37
SD	6.829848461	5.464467037

UNPAIRED T-TEST: WT vs. KO	
P value	0.0051
P value summary	**
Significantly different (P < 0.05)?	Yes

Table A12. COX I Protein Expression.

	COX I (A.U.)			
	WT		KO	
N	**UT**	**T**	**UT**	**T**
1	0.57	0.94	1.25	0.41
2	0.81	0.63	1.75	1.22
3	0.94	1.31	2.31	2.23
4	0.57	1.07	1.31	0.39
5	0.65	1.44	1.42	1.57
6	0.70	0.26	1.28	0.69
X	0.705936	0.9424172	1.5548683	1.083488
SD	0.1438813	0.4372882	0.4131381	0.7279901

2-WAY ANOVA			
Source of Variation	P value	P value summary	Significant?
Interaction	0.0845	ns	No
Training	0.0196	*	Yes
Genotype	0.5537	ns	No

POST-HOC TEST				
Tukey	Mean difference	Significant?	P value summary	Adjusted P value
UT:WT vs. UT:KO	-0.2365	No	ns	0.8263
UT:WT vs. T:WT	-0.8489	Yes	*	0.0279
UT:WT vs. T:KO	-0.3776	No	ns	0.5321
UT:KO vs. T:WT	-0.6125	No	ns	0.1517
UT:KO vs. T:KO	-0.1411	No	ns	0.9554
T:WT vs. T:KO	0.4714	No	ns	0.3451

Table A13. Corresponding Fold-Above-Control for COX I Protein Expression.

	COX I (fold change)	
N	**WT**	**KO**
1	1.77	0.44
2	2.49	1.29
3	3.27	2.36
4	1.86	0.41
5	2.01	1.66
6	1.82	0.73
X	2.20	1.15
SD	0.584796261	0.770958278

UNPAIRED T-TEST: WT vs. KO	
P value	0.0235
P value summary	*
Significantly different (P < 0.05)?	Yes

Table A14. v-ATPase Protein Expression.

	v-ATPase (A.U.)			
	WT		KO	
N	UT	T	UT	T
1	0.6110064	0.5419351	0.6805517	0.6908345
2	0.5674744	0.7274827	1.2002787	0.5447864
3	0.4073012	0.8000496	0.9598989	1.424211
4	1.0925535	0.5443563	0.858753	1.673063
5	0.8306563	0.7371321	1.022642	1.0754459
6	0.750521	0.6972711	0.6371888	1.2020149
X	0.7099188	0.6747045	0.8932188	1.101726
SD	0.2384478	0.1072584	0.2132834	0.4289952

2-WAY ANOVA			
Source of Variation	P value	P value summary	Significant?
Interaction	0.287	ns	No
Training	0.0126	*	Yes
Genotype	0.4458	ns	No

POST-HOC TEST				
Tukey	Mean difference	Significant?	P value summary	Adjusted P value
UT:WT vs. UT:KO	0.03521	No	ns	>0.9999
UT:WT vs. T:WT	-0.1833	No	ns	>0.9999
UT:WT vs. T:KO	-0.3918	No	ns	0.131
UT:KO vs. T:WT	-0.2185	No	ns	>0.9999
UT:KO vs. T:KO	-0.427	No	ns	0.0808
T:WT vs. T:KO	-0.2085	No	ns	>0.9999

Table A15. TFEB Protein Expression.

	TFEB (A.U.)			
	WT		KO	
N	UT	T	UT	T
1	0.0776842	0.1074657	0.1347333	0.3089434
2	0.3390221	0.8815187	0.289222	0.2227172
3	0.4692757	0.1820606	0.5857889	0.6666278
4	0.7828267	0.421171	1.0348709	1.6119287
5	0.2487975	0.427419	1.0900927	0.7518239
6	0.296413	0.5264626	0.3895956	0.8113411
7		0.3989755		
8		0.3575317		
X	0.3690032	0.4128256	0.5873839	0.728897
SD	0.2394948	0.2337934	0.3964534	0.4946765

2-WAY ANOVA			
Source of Variation	P value	P value summary	Significant?
Interaction	0.7266	ns	No
Training	0.0656	ns	No
Genotype	0.5087	ns	No

POST-HOC TEST				
Tukey	Mean difference	Significant?	P value summary	Adjusted P value
UT:WT vs. UT:KO	-0.04382	No	ns	0.9954
UT:WT vs. T:WT	-0.2184	No	ns	0.7027
UT:WT vs. T:KO	-0.3599	No	ns	0.3062
UT:KO vs. T:WT	-0.1746	No	ns	0.7912
UT:KO vs. T:KO	-0.3161	No	ns	0.3589
T:WT vs. T:KO	-0.1415	No	ns	0.895

Table A16. Mitophagy Flux Data for p62.

	p62 MITOPHAGY FLUX (A.U.)							
	WT				KO			
	UT		T		UT		T	
N	CON	STIM	CON	STIM	CON	STIM	CON	STIM
1	0.254	0.541	0.155	0.860	0.405	1.187	0.304	0.693
2	0.268	0.647	0.261	1.104	0.712	1.570	0.133	0.380
3	0.827	0.874	0.469	1.263	0.270	1.139	0.043	0.287
4	0.042	0.607	0.419	0.943	0.142	0.995	0.805	1.433
5	0.485	0.452	0.210	0.646	0.191	1.301	0.223	0.321
6	0.230	0.489	0.345	0.924				
X	0.351041	0.601533	0.309929	0.956727	0.343855	1.238486	0.301564	0.622936
SD	0.272454	0.151544	0.122311	0.211071	0.228322	0.215446	0.297888	0.480636

3-WAY ANOVA			
Source of Variation	P value	P value summary	Significant?
Stim	<0.0001	****	Yes
Genotype	0.3693	ns	No
Training	0.2844	ns	No
Stim x Genotype	0.3205	ns	No
Stim x Training	0.5794	ns	No
Genotype x Training	0.004	**	Yes
Stim x Genotype x Training	0.0041	**	Yes

POST-HOC TEST				
Tukey	Mean difference	Significant?	P value summary	Adjusted P value
CON:WT UT vs. CON:WT T	0.04111	No	ns	>0.9999
CON:WT UT vs. CON:KO UT	0.007186	No	ns	>0.9999
CON:WT UT vs. CON:KO T	0.04948	No	ns	>0.9999
CON:WT UT vs. STIM:WT UT	-0.2505	No	ns	0.7111
CON:WT UT vs. STIM:WT T	-0.6057	Yes	**	0.0063
CON:WT UT vs. STIM:KO UT	-0.8874	Yes	****	<0.0001
CON:WT UT vs. STIM:KO T	-0.2719	No	ns	0.6755
CON:WT T vs. CON:KO UT	-0.03393	No	ns	>0.9999
CON:WT T vs. CON:KO T	0.008365	No	ns	>0.9999
CON:WT T vs. STIM:WT UT	-0.2916	No	ns	0.5383
CON:WT T vs. STIM:WT T	-0.6468	Yes	**	0.0029
CON:WT T vs. STIM:KO UT	-0.9286	Yes	****	<0.0001
CON:WT T vs. STIM:KO T	-0.313	No	ns	0.5093
CON:KO UT vs. CON:KO T	0.04229	No	ns	>0.9999
CON:KO UT vs. STIM:WT UT	-0.2577	No	ns	0.7302
CON:KO UT vs. STIM:WT T	-0.6129	Yes	**	0.0093
CON:KO UT vs. STIM:KO UT	-0.8946	Yes	***	0.0001
CON:KO UT vs. STIM:KO T	-0.2791	No	ns	0.6938
CON:KO T vs. STIM:WT UT	-0.3	No	ns	0.5621
CON:KO T vs. STIM:WT T	-0.6552	Yes	**	0.0044
CON:KO T vs. STIM:KO UT	-0.9369	Yes	****	<0.0001
CON:KO T vs. STIM:KO T	-0.3214	No	ns	0.5308
STIM:WT UT vs. STIM:WT T	-0.3552	No	ns	0.2935
STIM:WT UT vs. STIM:KO UT	-0.637	Yes	**	0.0061
STIM:WT UT vs. STIM:KO T	-0.0214	No	ns	>0.9999
STIM:WT T vs. STIM:KO UT	-0.2818	No	ns	0.6361
STIM:WT T vs. STIM:KO T	0.3338	No	ns	0.428
STIM:KO UT vs. STIM:KO T	0.6155	Yes	*	0.0138

Table A17. Mitophagy Flux Data for LC3-II.

	LC3-II MITOPHAGY FLUX (A.U.)							
	WT				KO			
	UT		T		UT		T	
N	CON	STIM	CON	STIM	CON	STIM	CON	STIM
1	0.023	0.327	0.222	0.443	0.180	0.931	0.324	0.112
2	0.065	0.358	0.314	0.586	0.725	1.230	-0.107	0.144
3	0.266	0.366	0.457	1.080	-0.202	0.739	0.153	0.133
4	0.193	0.313	0.330	0.563	0.736	0.569	0.340	0.613
5	0.121	0.122	-0.131	0.081	0.416	0.883	0.349	-0.034
6	0.116	0.160	0.067	0.436				
X	0.130427	0.27429	0.209856	0.531649	0.371194	0.870405	0.211785	0.193368
SD	0.087681	0.105786	0.21133	0.323991	0.39549	0.245523	0.19577	0.245099

3-WAY ANOVA			
Source of Variation	P value	P value summary	Significant?
Stim	0.0026	**	Yes
Genotype	0.0959	ns	No
Training	0.0964	ns	No
Stim x Genotype	0.959	ns	No
Stim x Training	0.2535	ns	No
Genotype x Training	0.0003	***	Yes
Stim x Genotype x Training	0.0229	*	Yes

POST-HOC TEST				
Tukey	Mean difference	Significant?	P value summary	Adjusted P value
CON:WT UT vs. CON:WT T	-0.07943	No	ns	0.999
CON:WT UT vs. CON:KO UT	-0.2408	No	ns	0.7206
CON:WT UT vs. CON:KO T	-0.08136	No	ns	0.9992
CON:WT UT vs. STIM:WT UT	-0.1439	No	ns	0.9664
CON:WT UT vs. STIM:WT T	-0.4012	No	ns	0.1081
CON:WT UT vs. STIM:KO UT	-0.74	Yes	***	0.0003
CON:WT UT vs. STIM:KO T	-0.06294	No	ns	0.9998
CON:WT T vs. CON:KO UT	-0.1613	No	ns	0.9521
CON:WT T vs. CON:KO T	-0.001929	No	ns	>0.9999
CON:WT T vs. STIM:WT UT	-0.06443	No	ns	0.9998
CON:WT T vs. STIM:WT T	-0.3218	No	ns	0.3182
CON:WT T vs. STIM:KO UT	-0.6605	Yes	**	0.0015
CON:WT T vs. STIM:KO T	0.01649	No	ns	>0.9999
CON:KO UT vs. CON:KO T	0.1594	No	ns	0.9642
CON:KO UT vs. STIM:WT UT	0.0969	No	ns	0.9975
CON:KO UT vs. STIM:WT T	-0.1605	No	ns	0.9535
CON:KO UT vs. STIM:KO UT	-0.4992	Yes	*	0.0443
CON:KO UT vs. STIM:KO T	0.1778	No	ns	0.9371
CON:KO T vs. STIM:WT UT	-0.06251	No	ns	0.9999
CON:KO T vs. STIM:WT T	-0.3199	No	ns	0.3837
CON:KO T vs. STIM:KO UT	-0.6586	Yes	**	0.0028
CON:KO T vs. STIM:KO T	0.01842	No	ns	>0.9999
STIM:WT UT vs. STIM:WT T	-0.2574	No	ns	0.5956
STIM:WT UT vs. STIM:KO UT	-0.5961	Yes	**	0.0054
STIM:WT UT vs. STIM:KO T	0.08092	No	ns	0.9992
STIM:WT T vs. STIM:KO UT	-0.3388	No	ns	0.3138
STIM:WT T vs. STIM:KO T	0.3383	No	ns	0.3154
STIM:KO UT vs. STIM:KO T	0.677	Yes	**	0.002

APPENDIX B: SUPPLEMENTAL DATA

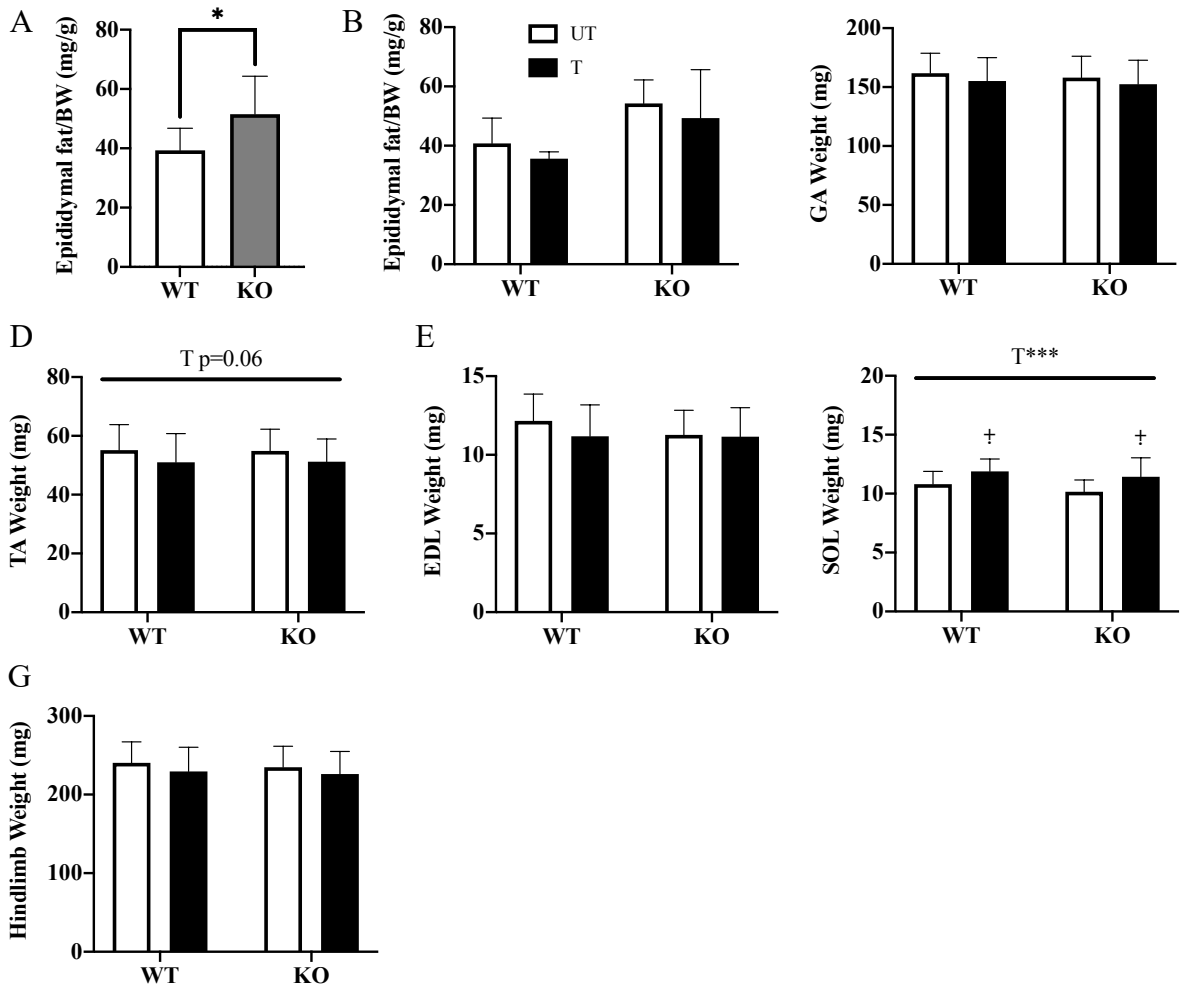

Fig B1. Epididymal fat and raw muscle weights. Fat mass differences between WT and KO animals (A). Fat mass comparison between all groups, (WT trained n = 2, no statistical tests were run; B). Uncorrected muscle weights for GA (C), TA (D), EDL (E), SOL (F), and combined hindlimb (G). Student's t-test and two-way ANOVA between genotype and training with Tukey post-hoc tests, T, main effect of training; *, $p<0.05$; ***, $p<0.001$; ┼, $p<0.05$. GA, gastrocnemius; TA, tibialis anterior; EDL, extensor digitorum longus; SOL, soleus. UT, untrained; T, trained. Values are mean ± SD.

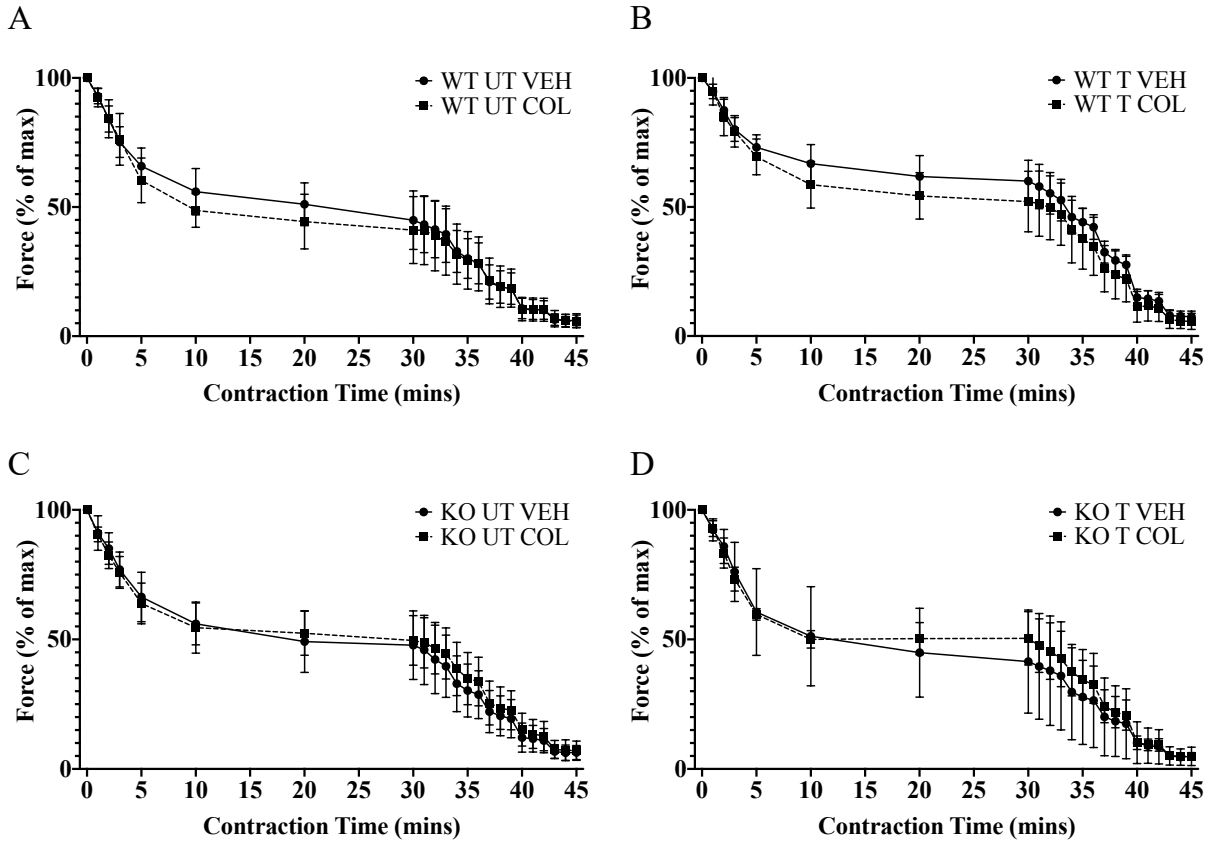

Fig B2. Effects of colchicine on muscle performance in situ. Force output of vehicle- and colchicine- treated WT untrained (A), WT trained (B), KO untrained (C), and KO trained (D) animals during the 45-minute contractile activity protocol. UT, untrained; T, trained. Values are mean ± SD.

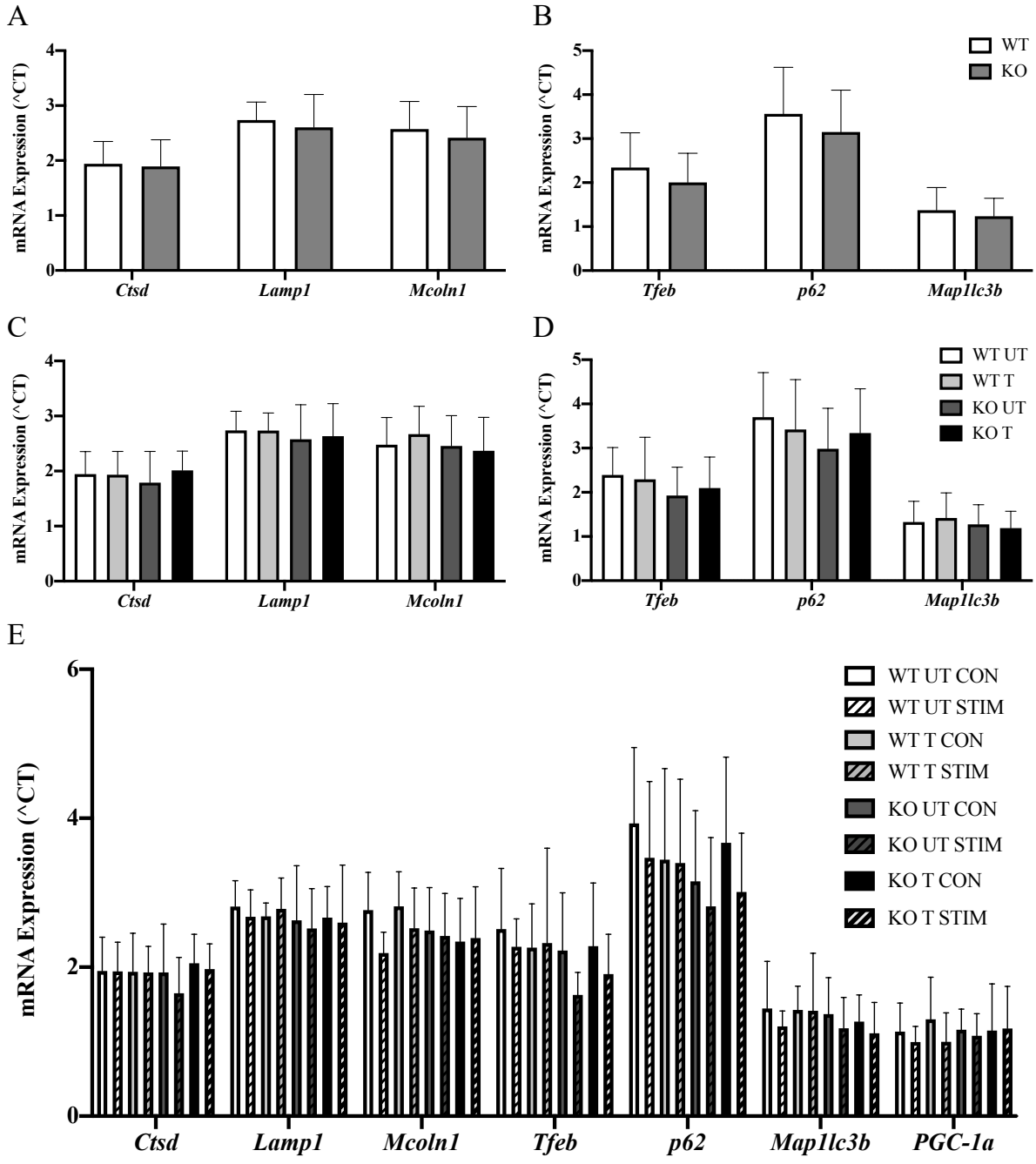

Fig B3. mRNA analysis of WT and TFE3 KO animals with endurance exercise and acute electrical stimulation. mRNA expression of lysosomal (A, C) and autophagic (B, D) genes. Graphical representation of mRNA expression of all conditions (E). UT, untrained; T, trained; STIM, acute electrical stimulation. Values are mean ± SD.

Table B1. List of antibodies used for western blotting

Protein	Concentration	Company	Catalogue Number
ATG7	1:1000	Sigma-Aldrich	A2856
Beclin1	1:1000	Cell Signaling Technology	3738S
Citrate Synthase	1:1000	Abcam	ab96600
COX I	1:500	Abcam	ab14705
Cathepsin B	1:1000	Cell Signaling Technology	31718S
Cathepsin D	1:1000	Santa Cruz Biotechnology	sc-377299
Lamp1	1:1000	Abcam	ab24170
LC3	1:500	Cell Signaling Technology	4108S
P62	1:1000	Cell Signaling Technology	5114S
Parkin	1:1000	Cell Signaling Technology	4211S
TFEB	1:500	MyBioSource	MBS120432
TFE3	1:500	Sigma-Aldrich	HPA023881
UQCRC2	1:500	Abcam	ab14745
v-ATPase	1:1000	Santa Cruz Biotechnology	sc-55544
VDAC	1:1000	Abcam	ab14734
HRP-linked Anti-mouse	As per manufacturer's suggestions	Cell Signaling Technology	7074S
HRP-linked Anti-rabbit	As per manufacturer's suggestions	Cell Signaling Technology	7076S

Table B2. List of primer oligonucleotide sequences in real-time qPCR analysis for *Mus musculus*

Gene	Forward Primer	Reverse Primer
TFE3 WT	5'-CAGGCTCAGGAACAGGAGAG-3'	5'-CATACAGATCCTGTCCAAAAGC-3'
TFE3 Mutant	5'-CAGGCTCAGGAACAGGAGAG-3'	5'-TGGGAAGACAATAGCAGGCA-3'
Ctsd	5'-TTTGCCAATGCTGTCGTACT-3'	5'-AGCGAGTGTGACTATGTGTGA-3'
Lamp1	5'-CTAGTGGGAGTTGCGGTATCA-3'	5'-AGGGCATCAGGAAGAGTCATAT-3'
Mcoln1	5'-TTGCAGCCTACACACAGGAG-3'	5'-AGAGAGCCAAAGCTGATCCA-3'
Tfeb	5'-AGCTCCAACCCGAGAAAGAGTTTG-3'	5'-CGTTCAGGTGGCTGCTAGAC-3'
Sqstm1	5'-TGTGGTGGGAACTCGCTATAA-3'	5'-CAGCGGCTATGAGAGAAGCTAT-3'
Map1lc3b	5'-GCTTGCAGCTCAATGCTAAC-3'	5'-CCTGCGAGGCATAAACCATGTA-3'
PGC-1a	5'-TTCCACCAAGAGCAAGTAT-3'	5'-CGCTGTCCCATGAGGTATT-3'
B2MG	5'-GGTCTTTCTGGTGCTTGTCT-3'	5'-TATGTTCGGCTTCCCATTCT-3'
Gapdh	5'-AACACTGAGCATCTCCCTCA-3'	5'-GTGGGTGCAGCGAACTTTAT-3'

APPENDIX C: LABORATORY METHODS AND PROTOCOLS

DNA GENOTYPING

Reagents:

1. Lysis Buffer with Proteinase K
    a. 900ul Lysis Buffer
        i. Store at RT
    b. 100ul Proteinase K
        i. 1mg/ml in sterile ddH_2O
        ii. Store at -20°C
2. Master Mix (MM), for each sample:
    a. 25ul Jumpstart (D8187, Sigma)
        i. Store at -20°C
    b. 2ul Common Forward Primer
    c. 1ul WT Reverse Primer
    d. 1ul MUT Reverse Primer
    e. 1ul sterile ddH_2O
3. Agarose
4. 50x TAE, autoclaved
    a. 242g Tris
    b. 500ml ddH_2O
    c. 57.1ml acetic acid
    d. 100ml 0.5M EDTA, pH 8.0
        i. 96.96g EDTA
        ii. Volume up to 500ml
5. Ethidium Bromide
    a. Store at 4°C
6. 1x TAE
    a. 80ml 50x TAE
    b. 3920ml ddH_2O

Procedure:

1. Turn on water bath to 55°C
2. Add 20ul Lysis Buffer with Proteinase K to each Eppendorf with an ear clipping
3. Vortex samples and ensure ear clippings are at the bottom of the tube
4. Incubate in water bath for 15 mins
5. Vortex and incubate in water bath again for 15 mins
6. Add 180ul sterile ddH_2O to each Eppendorf
7. Boil samples for 5 mins at 95°C
8. Store samples at -20°C until ready for PCR
9. Add 30ul MM to sterile 0.7ml Eppendorf tubes
10. Add 20ul of sample to corresponding Eppendorf tubes

11. Centrifuge at maximum speed at RT to ensure samples are at the bottom of the Eppendorf
12. Add 2-3 drops of mineral oil to each Eppendorf
13. Load samples into the thermal cycler are run program as follows:
    a. 94°C for 3 mins, 1 cycle
    b. 94°C for 30s
       56°C for 1 min
       72°C for 1 min, repeat for 38 cycles
    c. 72°C for 2 mins, 1 cycle
    d. Store at 4°C
14. Make 1% Agarose gel
    a. 1.5g Agarose
    b. 3ml 50x TAE
    c. 150ml ddH_2O
    d. Microwave for 2 mins until dissolved
    e. Place on stir plate with stir bar until cool to touch
    f. Add 25ul EtBr and pour gel into caster, adding appropriate well combs
7. Load 40ul of each sample into the gel mold
8. Fill caster with 1x TAE
9. Run at 180mV for ~1h
10. Visualize in Invitrogen Imaging instrument (iBright CL1500 Imaging System, ThermoFisher)

ISOLATING WHOLE MUSCLE PROTEIN EXTRACTS

Reagents:

1. Muscle Extraction Buffer (Sakamoto et al., JBC 277:11910, 2002)
    a. 20mM Hepes (ph 7.4) 2.383g/500ml
    b. 2mM EGTA 0.3804g/500ml
    c. 1% Trition-X100 5ml/500ml
    d. 50% Glycerol 10ml/500ml
    e. 50mM β-Glycerophosphate 5.4g/500ml

    Volume up to 500ml with double distilled water (ddH_2O)
    pH to 7.4
2. Make up buffer with Protease and phosphatase inhibitors:
    In a 15ml tube, mix the following at the appropriate ratio as outlined below and keep on ice:
    a. 1 ml Sakamoto Muscle Extraction Buffer
    b. 10 ul Protease Inhibitor Stock (1 tablet in 500uL ddH20)
    c. 10 ul Cocktail 2 Phosphatase Inhibitor
    d. 10 ul Cocktail 3 Phosphatase Inhibitor

Procedure:

1. Add 100µl of Sakamoto Muscle Extraction Buffer to a set of Eppendorf tubes
2. Weigh out 15-20mg of tissue into the first set of Eppendorf tubes and record the exact weight of each sample in a table
3. Add the appropriate volume of buffer solution to each Eppendorf to produce 10x volume

4. Insert a metal bead into each Eppendorf
5. Place Eppendorfs in balanced manner in metal brackets (kept in freezer)
6. Insert brackets into TissueLyser and homogenize (shake) at 30 Hz for 1 min at a time
7. Remove blocks, check for homogeneity and repeat if necessary (flip orientation of blocks for each cycle)
8. Remove beads with magnet and centrifuge at 14000g for 10 minutes at 4°C
9. Completely withdraw the supernatant and pipette the solution into the new pre-labeled Eppendorf tubes
10. Store at -80°C

ISOLATING MITOCHONDRIAL FRACTIONS

Reagents:

2. Mitochondrial Isolation Buffer (MIB)
    a. 64mM Sucrose (323.3g/mol) 22.93g
    b. 50mM Tris (121.14g/mol) 6.06g
    c. 50mm KCl (74.55g/mol) 3.73g
    d. 10mM EDTA (292.24g/mol) 2.92g
    e. 0.2% BSA 2.0g

    Volume up to 1L with double distilled water (ddH_2O)
    pH to 7.4
2. Make up buffer with Protease and phosphatase inhibitors:
    In a 15ml tube, mix the following at the appropriate ratio as outlined below and keep on ice:
    a. 1 ml Mitochondrial Isolation Buffer
    b. 10 ul Protease Inhibitor Stock (1 tablet in 500uL ddH_2O)
    c. 10 ul Cocktail 2 Phosphatase Inhibitor
    d. 10 ul Cocktail 3 Phosphatase Inhibitor

Procedure:

2. Collect gastrocnemius into a labeled tube with 1ml MIB
3. Mince on glass plate over ice
4. Add minced tissue to Dounce Homogenizer tube with 1ml of MIB with inhibitors
5. Homogenize muscle
6. Centrifuge the sample at 1,200g for 15 mins at 4°C
7. Transfer the supernate to a new Eppendorf and centrifuge at 12,000g for 20 mins at 4°C
8. Resuspend the pellet in 100ul MIB with inhibitors
9. Centrifuge the sample at 12,000g for 20 mins at 4°C
10. Resuspend the pellet in 30-50ul of MIC with inhibitors
11. Store at -80°C

SDS Polyacrylamide Gel Electrophoresis (SDS-PAGE) Protean Biorad System

Reagents:

1. Acrylamide/Bis-Acrylamide, 30% Solution 37.5:1 (BioShop 10.502)
    a. Store at 4°C
2. Under Tris Buffer
    a. 1M Tris, pH 8.8 (60.5g/500ml)
    b. Store at 4°C
3. Over Tris Buffer
    a. 1M Tris, pH 6.8 (12.1g/100ml)
    b. Bromophenol Blue (for colour)
    c. Store at 4°C
4. Ammonium Persulfate (APS)
    a. 10% (w/v) APS in ddH_20 (1g/10ml)
    b. Stored at 4°C
5. Sodium Dodecyl Sulfate (SDS)
    a. 10% (w/v) in ddH_20 (1g/10ml)
    b. Store at room temperature
6. TEMED (Sigma T-9281)
7. Electrophoresis Buffer, pH 8.3 (10L)
    a. 25mM Tris 30.34g, 192mM Glycine 144g, 0.1% SDS 10g
    b. Volume to 10L with ddH_20
    c. Store at room temperature
8. 6X SDS
    a. Warm 100% glycerol in water bath at 65°C for 30 minutes
    b. Combine 1.2g SDS, 0.06g Bromophenol Blue, 3mls of 1M Tris, pH 6.8 and 1ml of ddH_20 and stir at 4°C for 5 minutes
    c. Add 3mls of 100% glycerol, stir and aliquot mixture.
    d. Store at -20°C
    e. Add 5% (v/v) ß-mercaptoethanol (Sigma M6250) to 6X SDS <u>just prior</u> to use
9. *tetra*-Amyl alcohol ReagentPlus, 99% (Sigma 152463)

Procedure:

1. Prepare electrophoresis rack:
    a. Clean glass plates thoroughly with soap followed by 95% ethanol then ddH_20.
    b. Dry carefully with a kimwipe.
    c. Assemble glass plates as shown:
    d. Check the seal by adding a small volume of ddH_20 then pour off and let dry.

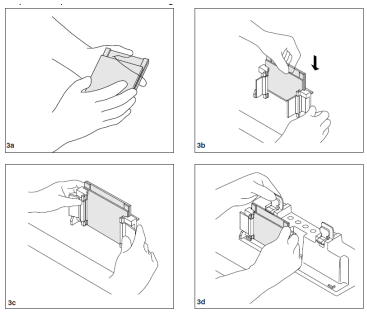

2. Prepare separating gels:
    a. Mini Protean 3 Bio-Rad System volumes:

	8%	10%	12%	15%	18%
Acrylamide	2.7 ml	3.3 ml	4.0 ml	5.0 ml	6.0 ml
ddH_20	4.1 ml	3.5 ml	2.8 ml	1.8 ml	0.8 ml
Under Tris	3.0 ml	3.0 ml	3.0 ml	3.0 ml	3.0 ml
SDS	100µl	100µl	100µl	100µl	100µl
APS	100µl	100µl	100µl	100µl	100µl
TEMED	10µl	10µl	10µl	10µl	10µl

   b. Mix the contents of the separating gel without adding APS or TEMED. Stir.
   c. Add APS and TEMED. Stir.
   d. Slowly pour the entire volume of the solution into the space between the two plates while keeping plates tilted to prevent bubble formation.
   e. Add *tert*-Amyl alcohol to coat top surface of gel solution.
   f. Allow 30 minutes for gel polymerization.
   g. Remove *tert*-Amyl alcohol by pouring it off and remove any remainder with a kimwipe. Rinse with ddH_20.

3. Prepare stacking gel:
   a. For a single mini gel use the following volumes:

Acrylamide	500 µl
Over Tris	625 µl
ddH_20	3.75 ml
SDS	50 µl
APS	50 µl
TEMED	7.5 µl

   b. Mix the contents of the stacking gel without adding APS or TEMED. Stir.
   c. Add APS and TEMED. Stir.
   d. Using a Pasteur pipette slowly add the entire volume from the beaker in between the plates.
   e. Add comb for desired number of wells.
   f. Allow 30 minutes for gel polymerization.

4. Prepare samples:
   a. Turn on the block heater to 95ºC.
   b. Pipette required volume of sample into new eppendorf with same amount of lysis buffer and 5 µl of sample dye. Keep samples on ice until all samples are prepared (use pipette plan).
   c. Briefly spin each sample to bring volume to the bottom of the eppendorf.
   d. Incubate each sample at 95 ºC for 5 minutes in the heating block to denature the proteins.
   e. Briefly spin again to return volume to the bottom of the eppendorf.

5. Assemble Mini-PROTEAN gel caster system:
    a. See images.
    b. If you are only running one gel a plastic rectangular pseudo plate must be clamped on the other side of the caster.
    c. Fill with electrophoresis buffer between the plates and outside of the plates in the chamber.
    d. Slowly remove the comb using both hands (one on each side) by pulling the comb straight upwards.
    e. Fix any wells that are deformed using a small spatula.
    f. Clean out the wells using a syringe filled with electrophoresis buffer.
    g. Withdraw the entire volume of the sample using a Hamilton syringe. Inject volume slowly into the bottom of the well.

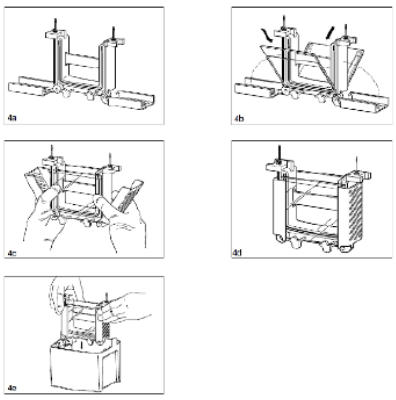

6. Gel electrophoresis
    a. Immediately after all samples are loaded place the lid on the gel chamber.
    b. Place positive and negative plugs into the power supply and turn on power supply.
    c. Set power supply to 120V. Gel will run for ~2 hours depending on percent gel made.
    d. When the bromophenol blue has run off the bottom of the gel (or when gel has separated the desire amount) turn off the power supply. Remove plugs from power supply and remove lid.
    e. Prepare for electrotransfer of proteins from the gel to nitrocellulose membrane.

Western Blotting Transfer and Immunodetection

Reagents:

1. Transfer Buffer
    a. 0.025M Tris-HCl pH 8.3 12.14g
    b. 0.15M Glycine 45.05g
    c. 20% Methanol 800ml
    d. make up to 4L with ddH_20
    e. Store at 4°C
2. Ponceau S stain
    a. 0.1% (w/v) Ponceau S
    b. 0.5% (v/v) Acetic Acid
    c. Store at room temperature
3. Wash Buffer
    a. Tris-HCl pH 7.5 12g
    b. NaCl 58.5g
    c. 0.1% Tween 10ml
    d. Store at room temperature
4. Blocking Solution
    a. 5% (w/v) skim milk power in wash buffer OR
    b. 5% (w/v) BSA in wash buffer

5. Enhanced Chemiluminescence Fluid (ECL; Santa Cruz sc-2048)

Procedure:

1. Transfer Procedure
   a. Remove electrophoresis plates from chamber and separate the plates.
   b. Cut away unnecessary parts of the gel using a spatula and measure remaining gel size.
   c. Using a paper cutter cut 6 pieces of Whatman paper per gel to the same size as the gel. Wearing gloves cut nitrocellulose membrane (GE Healthcare RPN303D) to the dimensions of the gel.
   d. Assemble Whatman paper, nitrocellulose memebrane and gel as shown:
   e. Close the cassette and place in the transfer chamber with the black side of the cassette facing the back side of the chamber.
   f. Place ice pack in the chamber.
   g. Place lid on the chamber and connect the leads to the power supply.
   h. Turn on the power supply and run at 120V for 2 hours. This can vary depending on the size of the protein of interest.

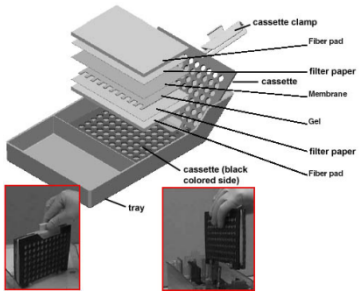

2. Removal of transfer membrane:
   a. Turn off the power supply and disconnect leads from the power supply then remove the lid from the chamber.
   b. Remove the cassette from the chamber.
   c. With gloves on, remove the Whatman paper and gel and place the nitrocellulose membrane in a plastic dish.
   d. Add Ponceau S stain on the membrane and gently swirl.
   e. Drain off the remaining Ponceau S and save for reuse.
   f. Rinse the membrane with ddH_20 to reduce the red background. Wrap membrane in saran wrap and scan image.
   g. Cut the membrane while protein bands are still visible at the desired molecular weight.
   h. Rotate membrane at room temperature in wash buffer until remaining Ponceau S has been removed.
   i. Incubate membrane for 1 hour with rotation in blocking solution.
   j. Incubate membrane with desired antibody diluted in blocking solution overnight at 4ºC. Membrane is placed face up into the solution on a glass plate covered in parafilm. To maintain a moist environment overnight, wet a small kimwipe and form it into a ball and place in each corner of the dish. Cover the dish with saran wrap.

3. Immunodetection
   a. Wash the blots in wash buffer with gentle rotation for 5 minutes 3X.
   b. Incubate the blots for 1 hour in room temperature with the appropriate secondary antibody diluted in blocking solution.
   c. Membrane is placed face up in solution on a glass plate covered with parafilm. Place moist kimwipes in each corner of the dish and cover the dish with saran wrap.
   d. Following the incubation, wash the membrane 3X for 5 minutes with wash buffer.

4. Enhanced Chemiluminescence Detection
   a. Mix ECL fluids "A" and "B" in a 1:1 ratio in a disposable Rohr tube.
   b. Place blots on saran wrap face up and apply ECL solution for 2 minutes.
   c. Dab off excess ECL on a kimwipe and place blots in Imager
   d. Expose blot (time will vary depending on protein and antibody).

MITOCHONDRIAL RESPIRATION AND ROS EMISSION IN PERMEABILIZED FIBERS

Reagents:

1. Buffer Z, for 500ml:
   a. 105mM K-MES 12.26g
   b. 30mM KCl 1.12g
   c. 10mM KH_2PO4 0.7g
   d. 5mM $MgCl_2•6H_2O$ 0.51g
   e. 1mM EGTA 0.19g
   f. 5mg/ml BSA 2.5g
   g. pH 7.4
   h. Store at -20°C
2. BIOPS Buffer, for 1L:
   a. 2.77mM CaK_2EGTA 27.7ml
   b. 7.23mM K_2EGTA 72,3ml
   c. 5.77mM Na_2ATP 3.14g
   d. 6.56mM $MgCl_2•6H_2O$ 1.335g
   e. 20mM Taurine 2.51g
   f. 15mM Na_2Phosphocreatine 3.825g
   g. 20mM Imidazole 1.36g
   h. 0.5mM Dithiothreitol (DTT) 0.077g
   i. 50mM MES Hydrate 9.76g
   j. pH 7.1
   k. Store at -20°C
3. Permeabilization Buffer
   a. BIOPS Buffer 1.5ml
   b. Saponin (10mg/ml) 6ul
   c. 10.5mM CDNB 5ul
4. Amplex Ultra Red Buffer
   a. Buffer Z 321.2ml
   b. 5mM AUR 650ul
      i. 666.6ul DMSO
      ii. 1mg AUR
   c. 5000IU/ml SOD1 1625ul
      i. pH 7.0
   d. 10mM BLEB 32.5ul
   e. 0.5M EGTA 650ul
      i. pH 7.5-8.0
   f. Store in black 5mL tubes at -20°C

5. Horseradish peroxidase (HRP)
    a. Store at -20°C
6. 0.1uM H_2O_2
7. Pyruvate (P2256, Sigma)
    a. 27.5mg/125ul
    b. Store at -20°C
8. Malate (M1000, Sigma), for 10ml stock:
    a. 1.073g
    b. pH 7.1
    c. Store at -20°C
9. ADP (A2754, Sigma), for 10ml stock:
    a. 2.13g
    b. pH 7.1
    c. Store at -20°C
10. Succinate (S2378, Sigma), for 10ml stock:
    a. 2.7014g
    b. pH 7.1
    c. Store at -20°C
11. Cytochrome c
    a. Store at -20°C

Procedure:

1. Collect medial portion of the TA and store in ice cold BIOPS Buffer
2. Gently tease apart muscle fibers with fine-tip forceps in BIOPS Buffer over ice
3. Place bundles in Permeabilization Buffer and permeabilize on orbital for 30 mins at 4°C
4. Transfer bundles to Eppendorf with Buffer Z and wash for 7.5mins
5. Transfer bundles to another Eppendorf with Buffer Z and was for 7.5 mins
6. Measure wet weight muscle bundle (~2-5mg)
7. Set up experiment using O2K
    a. Set up chamber by rinsing with 3x ddH_2O then 1x 70% EtOH. Repeat 3 times ending with ddH_2O. Remove all liquid with suction
    b. Add 3x710ul AUR Buffer into the chamber and close part-way
    c. Wait for oxygen reading to level out and adjust for background detection
    d. Add 1ul BLEB to chamber with p10
    e. Stop stir bar and add muscle bundle
    f. Close chamber part-way and start stir bar
    g. Add 50ml O_2 and close chamber fully for an O_2 reading of ~380
    h. Once O_2 stabilizes, turn on fluorescence
    i. Add 4ul HRP
    j. Calibrate ROS signal
8. Run experiment
    a. Add 5ul pyruvate and 5ul malate to the chamber and wait until O_2 levels stabilize
    b. Add 20ul ADP to the chamber and wait until O_2 levels stabilize
    c. Add 20ul succinate to the chamber and wait until O_2 levels stabilize
    d. Add 5ul Cytochrome c

COX ENZYME ACTIVITY ASSAY

Reagents:

1. 100 mM K-Phosphate Buffer:
    e. make up 0.1 M KH_2PO_4; MW = 136.09
    = 13.6g/1000ml
    pH ~ 5.0, Room Temperature
    b. make up 0.1 M $K_2HPO_4.3H_2O$ MW = 174.18
    = 17.4g/1000ml
    pH ~ 8.0, Room Temperature
    c. Mix in equal proportions, pH to 7.0
2. 10 Mm K-Phosphate Buffer:
    b. dilute 0.1 M KPO_4 Buffer prepared above 1:10 with dH_2O
    (e.g. 10 ml Buffer and 90 ml H_2O)

3. Extraction Buffer (100 mM Na-K Phosphate, 2 mM EDTA; pH 7.2)
    a. 500ml 0.1 M Na_2HPO_4. $2H_20$
    Combine 8.9g Sodium Phosphate with 0.372g EDTA up to 500ml
    b. 200ml 0.1M KH2PO4
    Combine 2.7g Potassium Phosphate with 0.149g EDTA up to 200ml
    c. Mix both solutions, pH to 7.2
4. Test Solution (reduced cytochrome c, 1mg/ml), for 10ml:
    a. Weight out 10mg of horse heart cytochrome c (Sigma, C-2506) in a scintillation vial
    b. Add 1ml of 10 mM KPO_4 buffer and dissolve the cytochrome c
    c. Make up a small volume of 10mg/ml sodium dithionite-10 mM KPO_4 stock solution
    d. Add 40µl of sodium dithionite stock solution to the vial with the test solution and observe red-orange colour change
    e. Add 8ml of ddH_20
    f. Add 1ml of 100mM KPO_4 Buffer
    g. Wrap it up in foil and put in oven at 30°C

Procedure:

1. Add 200µl of Extraction Buffer to a 2.0ml eppendorf on the scale
2. Add the liquid nitrogen flash frozen muscle tissue to the Eppendorf and add the volume of Extraction Buffer required to obtain a 40-fold dilution
3. Homogenize samples using a TissueLyser and metal beads.
4. Remove beads and sonicate each tube 3 x 3 seconds, cleaning the probe between samples
5. Add 200µl of sample to eppendorfs containing 200µl Extraction Buffer
6. In a 96-well plate, pipette 50 µl of sample into wells
7. Open COX Activity plate reader program on plate reader (Cytation 5, BioTek) and start
    a. Set temperature at 30°C
    b. Dispense 240ul of test solution
    c. Absorbance at 550nm
    d. 3s intervals, 21 reads

RNA ISOLATION

Reagents:

1. Tri-reagent (Trizol poly-phenol)
    a. Store at 4°C
2. Chloroform
    a. Store at RT
3. Isopropanol
    a. Store at RT
4. 75% Ethanol
    a. 75 mL of Anhydrous Ethanol (-20°C)
    b. 25 mL sterile ddH_2O

Procedure:

1. In fume hood, pipette 1 mL of Tri-reagent into each pre-labeled 2ml Eppendorf with proximal portion of the TA. Keep on ice
2. Homogenize in TissueLyser with sterile metal beads at 30 Hz for 1 min at a time
3. Remove blocks, check for homogeneity and repeat if necessary (flip orientation of blocks for each cycle)
4. Remove beads with magnet and let stand at RT for 5 mins
5. Add 200ul chloroform to each Eppendorf
6. Shake vigourously for 15s under fumehood and observe colour change
7. Let stand at RT for 2-3 mins
8. Centrifuge at 16,000g for 15 mins at 4°C
9. Transfer upper aqueous phase (clear) to 1.5ml Eppendorf tubes
10. Add 500ul isopropanol to each Eppendorf
11. Shake vigourously for 15s and store at -20°C overnight
12. Let stand at room temperature for 10 minutes
13. Spin at max speed (16,000g) for 10 minutes at 4°C
14. Discard Supernate by pouring into waste container, remover the remaining volume using a p200
15. Add 700 uL of 75% Ethanol to each sample. Wash by lightly pipetting along the wall to lift the pellet, take extra precaution to NOT resuspend the pellet
16. Spin at max speed (16,000g) for 10 min at 4°C
17. Discard Supernate and remove excess liquid with p200 pipette
18. Carefully leave pellets to air dry for 25-40 minutes.
    a. Place Eppendorfs with their lids open facing upside down on Kim-wipe
    b. Cover with top with Kim-wipe
19. Dissolve pellet in 10-30 uL st. dd H_20, by gently pipetting up and down
20. Measure RNA concentration using Nano Drop

FIRST-STRAND CDNA SYNTHESIS (REVERSE TRANSCRIPTION)

Reagents:

1. Master Mix 1 (MM1), for each sample:
    a. 1ul Oligo(dt) 20
    b. 1ul 10mM dNTP
    c. Keep on ice
2. Master Mix 2 (MM2), for each sample:
    a. 4ul 5x first-strand buffer
    b. 1ul 0.1M DTT
    c. Keep on ice
3. RNase OUT
    a. Store at -20°C
4. SuperScript III RT
    a. Store at -20°C

Procedure:

1. Place all reagents related to cDNA preparation to thaw on ice, except for the temperature sensitive 'RNase OUT' and 'SuperScript III RT' reagents
2. Prepare your working cDNA samples (pipette plan) by following the order of sterile water, then your extracted RNA, and finally the correct volume of MM1 and mix well
3. Keep samples on ice and migrate to the thermal cycler to initiating the amplification stage of the procedure
    a. 65°C for 5 mins
4. Let samples stand on ice for 1 min
5. Add the 5ul of MM2 to each tube and transfer to the thermal cycler
6. Work with the temperature-sensitive reagents one at a time
    a. Add 1ul RNase OUT to each Eppendorf
    b. Add 1ul SuperScript III RT to each Eppendorf
7. Run the appropriate file in the thermal cycler
    a. 50°C for 50 mins
    b. 72°C for 20 mins
8. Dilute samples (in new tubes) to a 1:40 concentration
    a. 1 µL cDNA stock
    b. 39 µL sterile water
9. Store both stock and working concentrations at -20°C until ready for qPCR.

APPENDIX D: OTHER CONTRIBUTIONS TO THE LITERATURE

PEER-REVIEWED PUBLICATIONS

1. Oliveira AN, Memme JM, **Wong JC**, Hood DA. (2023). Dimorphic Effect of TFE3 in Determining Mitochondrial and Lysosomal Content in Muscle Following Denervation. *Skeletal Muscle*. (Under review).

ORAL PRESENTATIONS AND PUBLISHED ABSTRACTS

1. **Wong JC**, Oliveira AN, Khemraj P, Hood DA. (2023). The Role of TFE3 in Mediating Skeletal Muscle Mitochondrial Adaptations to Exercise Training. *Muscle Health Awareness Day*, Toronto, Canada. (Abstract).
2. **Wong JC**, Oliveira AN, Hood DA. (2022). The role of TFE3 in endurance training-induced skeletal muscle adaptations. *KAHS Graduate Seminar 2022*. York University, Toronto, ON, Canada. (Oral presentation).
3. **Wong JC**, Oliveira AN, Hood DA. (2022). The role of TFE3 in endurance training-induced skeletal muscle adaptations. *Canadian Society for Exercise Physiology Conference*. International (Poster presentation).
4. Oliveira AN, Memme JM, **Wong JC**, Hood DA. (2022). Intersection of TFE3 and sex in mediating disuse-induced muscle atrophy. *International Biochemistry of Exercise Conference.* International. (Poster presentation – presented by Oliveira).
5. Oliveira AN, Memme JM, **Wong JC**, Hood DA. (2022). Role of TFE3 in Mitochondrial Adaptations to Skeletal Muscle Disuse. *Experimental Biology*. International. (Poster presentation – presented by Oliveira).